

**Structure-function relationship of Strong Metal-Support Interaction  
studied on supported Pd reference catalysts**

vorgelegt von  
Diplom-Chemiker  
Patrick Kast  
aus Füssen

Von der Fakultät II – Mathematik und Naturwissenschaften  
der Technischen Universität Berlin  
zur Erlangung des akademischen Grades  
Doktor der Naturwissenschaften  
Dr. rer. nat.

genehmigte Dissertation

Promotionsausschuss:

Vorsitzender: Prof. Dr. Reinhard Schomäcker

Berichter/Gutachter: Prof. Dr. Robert Schlögl

Berichter/Gutachter: Prof. Dr. Thorsten Ressler

Berichter/Gutachter: Prof. Dr. Martin Muhler

Tag der wissenschaftlichen Aussprache: 13.05.2015

Berlin 2015



## **Danksagung**

Gerne möchte ich mich bei allen Personen bedanken, die mich fachlich und/oder moralisch unterstützt haben, dazu gehören Prof. Dr. Robert Schlögl, unter dessen Leitung diese Arbeit am Fritz-Haber-Institut der Max-Planck-Gesellschaft zwischen Februar 2011 und Februar 2015 entstand, Prof. Dr. Malte Behrens, der mir als Gruppenleiter stets fachlich behilflich war und mich auch häufig motiviert hat, Dr. Raoul Naumann d'Alnoncourt, der mich in den ersten Monaten mit vielen technischen Ratschlägen bei der Konstruktion der CO-oxidations-Anlage unterstützt hat, Dr. Matthias Friedrich, Dr. Stefan Zander, Thomas Homburg, Leon Zwiener und Daniel Brennecke, für fachlichen Diskurs bzw. das angenehme Büro-Klima, Martin Kuhn von der TU Darmstadt, für die Selektivitätsmessungen bei der Acetylenhydrierung, Dr. Elias Frei, für das Gegenlesen der Einleitung, Dr. Edward Kunkes, für seine große Hilfsbereitschaft, Dr. Frank Girgsdies, für seine fachliche Kompetenz und seine Effizienz bei den XRD-Messungen, Dr. Dirk Rosenthal, für die Vermittlung wichtiger Kenntnisse im Bereich der Chemisorption, Dr. Steffi Kühl, für ihre Hilfsbereitschaft, Dr. Detre Teschner, für die Hilfe und die fachlichen Diskussionen bei XPS, Jutta Kröhnert, für den angenehmen fachlichen Umgang, Dr. Andrey Tarasov für die TG-Messungen, Maike Hashagen für die BET-Messungen, die Mitglieder der Elektronen-Mikroskopie-Gruppe für SEM/TEM Messungen, Dr. Olaf Timpe für die interessanten philosophischen und stoffchemischen Diskussionen, all die Kollegen, mit denen man gerne auch mal nach der Arbeit Zeit verbracht hat, meine Freunde und politischen Mitstreiter in Berlin, meine Familienangehörigen im Ostallgäu und mein bester Freund Johannes.

## Abstract

Transition metal oxide supported, nano-scaled noble metal catalysts are known to show a variety of surface modifications when they are being reduced at increasing temperatures. Such processes involve for example (surface) alloying and the formation of partially reduced oxidic support overlayers that are both induced by the so-called strong metal-support interaction (SMSI). The present work investigated a series of oxide supported Palladium powder catalysts with a loading variation between 1-5 wt.-% on their structure-function relationship after reduction in different media and at different temperatures to create a reference system and explore the nature of SMSI. Hereby surface and bulk sensitive techniques like XPS, chemisorption, TEM, DRIFTS or XRD were applied to study the influence of electronic and structural modifications on the activity in catalytic oxidation of carbon monoxide which served as the main test reaction and was conducted at ambient pressure. The catalysts were synthesized reproducibly by a controlled co-precipitation approach and by impregnation.

The investigated Pd/iron oxide system shows palladium surface decoration at comparably low reduction temperatures. The surface cover was found to be volatile in oxygen containing atmosphere and formed reversibly. Dependent on the Pd particle size it increases the CO oxidation activity. Alloy formation occurs at higher reduction temperatures. In case of the Pd/zinc oxide system reversible surface alloying takes place during reduction that is also beneficial for CO oxidation, but again deactivates fast. When being reduced at even higher temperatures the additional formation of an oxidic overlayer could be observed that does not further activate the system but leads to an overall reduction of active sites. Due to alloy formation, the zinc oxide system at higher conversions shows a different selectivity behavior in acetylene hydrogenation, compared to the iron oxide system. Also in case of the Pd/titania system, reversible surface decoration by partially reduced support happens during reduction. Different to the other investigated systems the surface-cover reversibly decreases CO oxidation activity however. The Pd/alumina system was studied as a less reducible reference. As expected, it does not show SMSI-induced modifications.

In the end the work clearly shows that CO oxidation is a convenient method to study activity and stability of SMSI and decouple it from other involved processes. The effects of surface modification on the catalytic activity in this test reaction however strongly depend on the specific system and pre-conditioning and can either be of activating or deactivating nature. The basic principles involved in case of SMSI seem to apply both in UHV model systems and at powder systems at ambient pressure as found by the catalytic measurements.

## Zusammenfassung

Übergangsmetalloxid geträgerte, nano-skalige Edelmetall-Katalysatoren sind bekannt dafür, eine Reihe von Oberflächen-Veränderungen zu erfahren, wenn sie bei erhöhter Temperatur reduziert werden. Diese Prozesse beinhalten beispielsweise (Oberflächen-) Legierungsbildung und die Ausblidung von teilweise reduzierten, oxidischen Träger-Schichten, in beiden Fällen hervorgerufen durch Starke Metall-Träger Wechselwirkung (Strong Metal-Support Interaction, SMSI). Die vorliegende Arbeit untersuchte eine Reihe von oxid-geträgerten Palladium Pulverkatalysatoren mit einer Variation der Beladung von 1-5 Gewichts-% auf ihre Struktur-Eigenschafts Beziehungen nach Reduktion in verschiedenen Medien und bei verschiedenen Temperaturen, um ein Referenzsystem zu entwickeln und der Natur von SMSI auf den Grund zu gehen. Dabei kamen oberflächen- und volumensensitive Methoden wie XPS, Chemisorption, TEM, DRIFTS oder XRD zum Einsatz, um den Einfluss von elektronischen und strukturellen Veränderungen auf die Aktivität bei katalytischer Oxidation von Kohlenmonoxid zu untersuchen, welche als wichtigste Testreaktion bei Normaldruck durchgeführt wurde. Die Katalysatoren wurden auf reproduzierbare Weise durch kontrollierte Ko-Fällung und durch Imprägnierung hergestellt.

Das untersuchte Pd/Eisenoxid System zeigt Bedeckung der Pd Oberfläche nach Reduktion bei vergleichsweise niedrigen Temperaturen. Diese Bedeckung war instabil in sauerstoffhaltiger Umgebung und bildete sich reversibel aus. Abhängig von der Pd Partikelgröße erhöht sie die Aktivität bei der CO-Oxidation. Legierungsbildung findet bei höheren Reduktionstemperaturen statt. Im Falle von Pd/Zinkoxid findet reversible Legierungsbildung an der Oberfläche statt, die ebenfalls die CO-Oxidation begünstigt, aber ebenfalls schnell deaktiviert. Nach Reduktion bei noch höheren Temperaturen konnte die zusätzliche Ausbildung einer oxidischen Überschicht beobachtet werden, die das System nicht weiter aktivierte, sondern insgesamt die Zahl der aktiven Plätze reduzierte. Wegen Legierungsbildung zeigt das Zinkoxid-System bei höheren Umsätzen in der Acetylenhydrierung ein anderes Selektivitätsverhalten als das Eisenoxid-System. Im Fall von Pd/Titanoxid kommt es während der Reduktion ebenfalls zu reversibler Oberflächen-Bedeckung durch teilweise reduzierten Träger. Anders als in den beiden anderen Fällen verringert diese Schicht hier jedoch die Aktivität in der CO-Oxidation. Pd/Aluminiumoxid wurde als schwer reduzierbares Referenz-System untersucht. Wie erwartet zeigt es keine durch SMSI hervorgerufenen Veränderungen.

Schlussendlich konnte in dieser Arbeit gezeigt werden, dass CO-Oxidation eine einfache und geeignete Methode ist, SMSI zu untersuchen und ihren Einfluss auf Aktivität und Stabilität von dem anderer Prozesse zu trennen. Die Effekte von Oberflächenveränderungen auf die katalytische Aktivität dieser Test-Reaktion hängen jedoch stark vom entsprechenden System und der Vorbehandlung ab und können sowohl aktivierender als auch deaktivierender Natur sein. Die Grundlegenden Prinzipien, die bei SMSI eine Rolle spielen, scheinen sowohl im Fall von Modell-Systemen unter UHV-Bedingungen als auch bei Pulver-Systemen bei Normaldruck zu gelten, wie durch die katalytischen Messungen gezeigt wurde.

## Table of contents

Danksagung	3
Abstract	4
Zusammenfassung	5
<b>Chapter 1: Introduction and outline</b>	<b>9</b>
1.1. Palladium: from the element to catalysis	9
1.2. Strong Metal-Support Interaction	11
1.2.1. Structure	11
1.2.2. Reactivity	13
1.3. Outline of the present work	14
1.3.1. Motivation and objectives	14
1.3.2. Synthesis and characterization of the catalysts	15
1.3.3. Catalytic reactor set-up	17
1.3.4. CO-oxidation	19
1.3.5. Selective hydrogenation of acetylene	19
1.5. References	20
<b>Chapter 2: CO-oxidation as a test reaction for strong metal-support interaction on nano-structured Pd/FeO<sub>x</sub> powder catalysts</b>	<b>25</b>
2.1. Introduction	25
2.2. Experimental	27
2.2.1. Catalyst synthesis	27
2.2.2. Catalyst characterization	27
2.2.3. Catalytic testing	28
2.3. Results and Discussion	29
2.3.1. Synthesis and characterization of calcined pre-catalysts	29

2.3.2. Reduction of the calcined pre-catalysts – bulk effects	30
2.3.3. DRIFTS surface investigation	38
2.3.4. CO chemisorption measurements	41
2.3.5. CO oxidation experiments	42
2.3.6. XPS investigation before and after CO oxidation	46
2.4. Summary and Discussion	48
2.5. Conclusion	50
2.6. References	51

Supplementary Information	54
---------------------------	----

### **Chapter 3: Strong Metal-Support Interaction and alloying of Pd/ZnO catalysts**

#### **for CO-oxidation 70**

3.1. Introduction	70
3.2. Experimental	72
3.2.1. Catalyst synthesis	72
3.2.2. Catalyst characterization	73
3.2.3. Catalytic testing	75
3.3. Results and Discussion	76
3.3.1. Synthesis and characterization of the pre-catalysts	76
3.3.2. Chemical and structural behavior of the system during reduction, illustrated for the 2.5 and 5 wt.-% Pd sample	76
3.3.3. Influence of reductive treatments on the activity in CO-oxidation	80
3.3.4. Electron microscopy study of the 0.75 wt.-% Pd sample in different states	83
3.3.5. Electronic and structural surface investigations: reversible formation of SMSI versus alloying	84
a) DRIFTS	84
b) XPS	87
c) CO-chemisorption	91
3.4. Summary and Conclusion	93

3.5. References	95
Supplementary Information	98
<b>Chapter 4: Supported Palladium catalysts in CO-oxidation and Acetylene Hydrogenation: on the role of SMSI</b>	<b>104</b>
4.1. Introduction	104
4.2. Experimental	107
4.2.1. Catalyst synthesis	107
4.2.2. Catalyst characterization	107
4.2.3. Catalytic testing	108
4.3. Results and Discussion	109
4.3.1. Comparison of the samples	109
4.3.2. Reduction behavior of the 1% Pd/TiO <sub>2</sub> catalyst	111
4.3.3. Influence of SMSI on CO-oxidation	113
4.3.4. Influence of SMSI on selective hydrogenation of acetylene to ethylene	119
4.4. Summary and Conclusion	123
4.5. References	124
Supplementary Information	129
<b>Chapter 5: Summary and Conclusion of the thesis</b>	<b>134</b>
<b>Appendix:</b>	<b>138</b>
List of abbreviations	138
List of publications	140
List of poster presentations	141
CV	142
Erklärung	143



## Chapter 1: Introduction and outline

### 1.1. Palladium: from the element to catalysis

The element palladium (Pd, atomic number 46, fcc, electron configuration [Kr] 4d<sup>10</sup>5s<sup>0</sup>) was first discovered in 1803 by William Hyde Wollaston, as he investigated platinum-containing ore from mines in South Africa.<sup>1</sup> Nowadays, South Africa is one of the most important Pd producing countries, besides Russia (Ural area) and Northern America (Great Lakes area).<sup>2</sup> The worldwide production doubled from 100 t/a in 1995 to about 200 t/a in the year 2010.<sup>2,3</sup>

As a member of the platinum-group metals (see table 1), palladium shows only moderate chemical reactivity, though being more active than the considerably heavier platinum.<sup>4,5</sup>

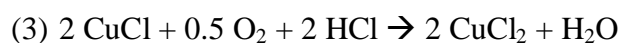
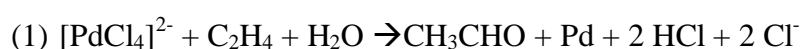
Table 1: light and heavy platinum-group metals

	group			
period	8	9	10	
5	Ru	Rh	<b>Pd</b>	→light
6	Os	Ir	Pt	→heavy

One important property of palladium is its outstanding affinity to hydrogen. The H<sub>2</sub> adsorption capacity is higher than for any other metal and was first reported by T. Graham (1869). He discovered that the metal, after being red-heated,<sup>4,6</sup> could take up 935 times its volume of hydrogen. This corresponds to the hydrogen concentration in liquid H<sub>2</sub> and represents a formal composition of Pd<sub>4</sub>H<sub>3</sub>. A colloidal solution of Pd is even capable of absorbing 3000 times its volume of hydrogen.<sup>7</sup> According to the phase diagram,<sup>8</sup>  $\alpha$  and  $\beta$  hydride phases, PdH<sub>x</sub> exist, while the  $\alpha$ -phase shows low hydrogen content ( $x < 0.017$ ) and the latter is formed at higher hydrogen concentrations ( $x > 0.6$ ) and exhibits volume expansion of about 10%. For technical gas cleaning processes, the temperature is kept above 573 K to keep the alpha phase stable and avoid volume expansion. Since gaseous hydrogen is the only gas capable of passing the palladium lattice, it is used for its purification.<sup>4</sup> The production of highly pure hydrogen is important in fuel cell applications, where Pd is also used as an electrode material.

Since hydrogen leaves the palladium lattice in atomic state ('in status nascendi') at 323 K, it is widely used as a high capacity hydrogenation catalyst, especially in petro-chemistry for cracking and fuel reforming processes. One example is the Lindlar-Catalyst where it is poisoned with lead to reduce its activity and thus permitting the partial reduction of alkynes to alkenes.<sup>9</sup> Another example for the selective hydrogenation on palladium is the reaction of 1,3-butadiene to Z/E- butene or the hydrogenation of unsaturated aldehydes.<sup>10,11</sup>

An important industrial product obtained using palladium as a catalyst is acetaldehyde. This occurs via hydro-formylation of ethene in the Wacker-Process, applying Cu as a co-catalyst, as described by the following formal equations:<sup>3,5</sup>



Another important application of Pd is the catalytic synthesis of organic fine-chemicals by C-C-(cross) coupling reactions like the Stille-coupling, Sonogashira-coupling, Heck-reaction, Suzuki-coupling or Negishi-coupling.<sup>12</sup> The latter three scientists were honored for their work in 2010 with the noble prize, which led to public attention to the element palladium and showed the importance of this kind of reaction. One example for the wide range of pharmaceuticals produced by Pd catalyzed C-C-coupling is the antifungal medication 'Terbinafin' from Sandoz (Novartis).<sup>11</sup>

Palladium is used as well, together with rhodium and platinum, in three-way catalysts for purification (e.g. oxidation of CO) of automobile exhaust fumes.<sup>13</sup>

## 1.2. Strong Metal-Support Interaction

### 1.2.1. Structure

In heterogeneous catalysis, small particles of the catalytic active component (in many cases noble metals, like Pd) are usually supported by metal - or semimetal oxides or by inert carbon nanotubes.<sup>14</sup> The subsequent thermal treatment in a reducing atmosphere induces several processes, depending on the nature of the metal and the support: if the metal is mobile and strong cohesive interactions are operative, sintering of the particles is energetically favored, whereas the metal particles may spread out and form flat islands ('pill-box', see figure 1) if the interactions are adhesive. However, in case of a mobile support and strong adhesive interactions, the metal particles can become encapsulated, induced by the so-called strong metal-support interaction (SMSI). It is evident that wetting and spreading phenomena are significantly involved in all steps of solid-solid catalyst treatment:<sup>14</sup>

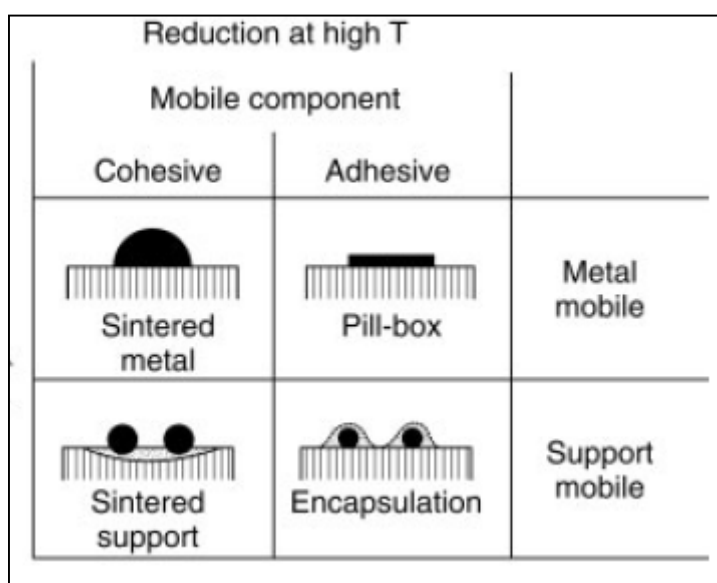


Fig. 1: metal-support-interactions induced by reduction.<sup>15</sup>

The encapsulation or decoration of (high-melting) metal particles by an over-layer of reducible oxide support, like the Rh/TiO<sub>2</sub> system (see figure 2) after reductive treatment (inducing SMSI at around 770 K) can be described as spreading:<sup>16</sup>

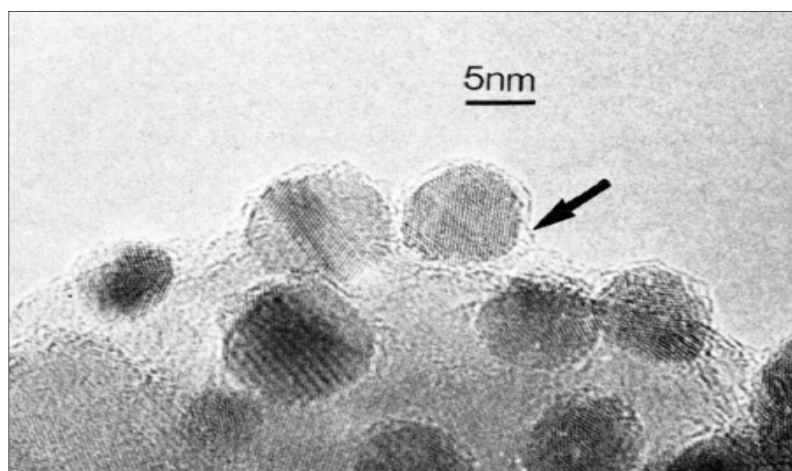


Fig. 2: Micrograph of Rh/TiO<sub>2</sub> after high-temperature-reduction (HTR) at 773 K.<sup>17</sup>

The first observations of the SMSI-phenomenon were made by Tauster et al. in 1978 when TiO<sub>2</sub> supports (P25/Degussa; Cab-O-Ti/Cabot Corp.) were impregnated with group VIII metal salt solutions.<sup>18</sup> After HTR at 773 K they observed almost no more CO or hydrogen adsorption (H/M-ratio reduced to 5%), without loss of BET surface area and with no signs for agglomeration of the metal particles. The effect was completely reversible by re-oxidation followed by low-temperature-reduction (LTR) at 473 K. The authors assumed two possible explanations for this behavior: firstly an overlap of the occupied d-orbitals of the noble metal with the vacant d-orbitals of Ti<sup>4+</sup> and secondly the formation of intermetallic compounds, for example Pt<sub>3</sub>Ti.

The discussion, whether the SMSI-effect could involve alloy/IMC formation, for example PdTi or PdTi<sub>2</sub> in the Pd/TiO<sub>2</sub> system and Pt<sub>3</sub>Ti in the Pt/TiO<sub>2</sub> system continued in the following decades.<sup>19,20</sup>

Since the first reports there is ongoing debate on the contribution of morphological effects (encapsulation leads to loss of active sites; metal-support-interface is reduced) and electronic effects (charging of the nanoparticles, ligand effects).<sup>21</sup> Besides microscopy (HR-TEM), encapsulation could be confirmed by other methods like low energy ion scattering (LEIS): Taglauer and Knözinger<sup>22</sup> and also Linsmeier et al.<sup>23</sup> for instance observed a clear maximum in the I<sub>A</sub>/I<sub>S</sub>-ratio with regard to the rhodium-content after H<sub>2</sub>-treatment of Rh/TiO<sub>2</sub> at 773 K. It was shown that non-reducible (or better: hard-to-reduce) oxides like Al<sub>2</sub>O<sub>3</sub>, SiO<sub>2</sub>, ZrO<sub>2</sub>, Y<sub>2</sub>O<sub>3</sub>, Sc<sub>2</sub>O<sub>3</sub>, HfO<sub>2</sub> or MgO are not subject to the SMSI-effect, whereas easy-to-reduce oxides like CeO<sub>2</sub>, MnO, TiO<sub>2</sub>, V<sub>2</sub>O<sub>3</sub> or Nb<sub>2</sub>O<sub>3</sub> show encapsulation after being reduced.<sup>18</sup> Covering of the metal particles is induced by reduction of the surface free energy and higher interaction

energy between the metal and the support.<sup>14</sup> Nevertheless, alumina-based systems were reported to behave differently:<sup>24</sup> in contrast to the systems Ni/Al<sub>2</sub>O<sub>3</sub> and Rh/Al<sub>2</sub>O<sub>3</sub>, the system Pt/Al<sub>2</sub>O<sub>3</sub> showed reduced hydrogen chemisorption capacity after a HTR between 773 and 1273 K which could be restored by re-oxidation. Agglomeration of metal particles was excluded.

It could be shown that for CVD-produced anatase, impregnated with Pd(NO<sub>3</sub>)<sub>2</sub>, SMSI already occurred at temperatures between 473-623 K.<sup>25</sup> The authors described the migration of partially reduced, stable titania species with the formal composition Ti<sub>4</sub>O<sub>7</sub>. These results are comparable to the reports from Li et al.<sup>26</sup> who also investigated TiO<sub>2</sub> (anatase phase) and TiO<sub>2</sub> (rutile phase), produced with a TiCl<sub>4</sub> precursor and impregnated with PdCl<sub>2</sub>: in EPR-experiments, reduced titanium species could be observed already after LTR in case of the anatase and after HTR for the rutile.

Similar results were obtained after HTR of Pd/CeO<sub>2</sub> samples.<sup>27</sup> The chemisorption capacity was reversibly reduced without sintering of the Pd particles and thin layers of reduced ceria (Ce<sub>2</sub>O<sub>3</sub>) on the surface of Pd particles could be detected by TEM and XPS.

### 1.2.2. Reactivity

The encapsulation does not necessarily have to reduce the catalytic activity: the CO-oxidation reaction showed an increased activity in the SMSI-state for example when covered by FeO<sub>x</sub>-species after HTR of the corresponding Pd/iron oxide system.<sup>28</sup> The instability of this cover will be matter of subsequent discussion. Referring to literature, in general, Pd/FeO<sub>x</sub> systems show high CO-oxidation activities.<sup>29,30</sup>

According to literature, also C=O-bond hydrogenations showed higher activity in the SMSI-state of the systems Pt/TiO<sub>2</sub> and Ni/TiO<sub>2</sub>.<sup>31,32</sup> When reduced at 773 K (encapsulated state) the alcohol formed, whereas decarbonylation occurred if reduction was performed at only 573 K (non-encapsulated state). The authors discussed possible coordination of the oxygen of the C=O group by Ti<sup>3+</sup> or Ti<sup>2+</sup> sites.<sup>33,34</sup> Enhanced selectivity for C=O-bond hydrogenations on the Ru/ZrO<sub>2</sub> system could also be observed<sup>35</sup> and was attributed to the formation of Ru-Zr<sup>n+</sup> active sites, which might decrease the strength of the CO-bond.

Further examples for SMSI dependent selectivity changes are reported in literature for hydrogenation reactions (CO<sub>2</sub>+H<sub>2</sub>) over Pd/CeO<sub>2</sub> catalysts:<sup>27,36</sup> the product selectivity for the methanation reaction changed from 70% methane formation towards 90% methanol

formation after HTR (773 K) of the catalyst. This influence of SMSI on selectivity has been intensively studied with regard to methanol synthesis or methanol steam reforming on supported Cu/ZnO catalysts.<sup>37–41</sup>

Since the influence of SMSI on the catalyst activity was suspected to depend on the grade of structure-sensitivity of the respective reaction investigated, various structure-sensitive and structure-insensitive reactions have been studied in the last decades.<sup>16,42–44</sup> For Rh/Nb<sub>2</sub>O<sub>5</sub> or Rh/TiO<sub>2</sub> catalysts for example, it was observed that, in accordance with a geometric (ensemble) effect (surface decoration), catalytic activities of structure-sensitive reactions like hydrogenolysis of hydrocarbons are strongly suppressed by SMSI, whereas structure-insensitive reactions like hydrogenation or dehydrogenation reactions were not suppressed, or even enhanced, associated with electronic (ligand) effects.

### **1.3. Outline of the present work**

#### **1.3.1. Motivation and objectives**

The present work comprises systematic studies on the structure-function relationship of the strong metal-support interaction (SMSI) effect in Pd-based catalysts. The aim is to create a reference system that provides a more unifying picture as well as quantitative information for the future design of supported nanoparticle catalysts for a certain reaction and beyond, to develop an experimental basis ('benchmark') for theoretical calculations. Therefore it is necessary to explore reliable, reproducible recipes for the synthesis of uniformly sized and homogeneously distributed, supported palladium nano-catalysts. Since it is known from literature that the over-growth mechanism is dependent on the character of reducibility of the support, it is necessary to study a series of metal oxide supports with different grades of reducibility and their influence on SMSI. The study of the impact of the Pd-loading (which determines the size of Pd nano-particles) as well as the dependence of the over-growth of the composition of the reducing atmosphere and the reduction temperature are further goals of the work. The latter is determined by TPR experiments. Detailed characterization by a series of (in- and ex-situ) methods like XPS, XAS, CO-chemisorption, HR-TEM or DRIFTS aims at a better understanding of the process of SMSI-formation by geometric as well as electronic changes directly at the surface while the simultaneous monitoring of the bulk structure for example by XRD should reveal the influence of phase transformation or alloying on the

SMSI phenomenon. The influence of any kind of reduced or encapsulated state on the activity in catalytic CO-oxidation is studied and compared as well as the stability and reproducibility of the SMSI-state. It is explored whether CO-oxidation is a suitable probe reaction for the assumed decoration processes occurring in the co-precipitated systems in general.

Besides this main catalytic test reaction, the influence of strong metal-support interaction on the selectivity of a structure-sensitive reaction, the acetylene hydrogenation, is studied.

### 1.3.2. Synthesis and characterization of the catalysts

In order to assure reliable, reproducible synthesis of phase pure supports and homogeneous palladium particle distribution, the chemical potential during the precursor synthesis and during calcination must be kept constant. For the precursor synthesis, the method of co-precipitation of the respective metal nitrates by sodium hydroxide or sodium carbonate solution in an automated synthesis reactor ('Labmax', Mettler Toledo) was chosen (see figure 3). The synthesis parameters like stirring rate, concentration of the metal salt solution and the base, the rate of their addition and the temperature were controlled and optimized. During the addition of acid and base, the pH-value for the precipitation was kept constant. The appropriate pH-value for a complete precipitation of the respective system was determined by

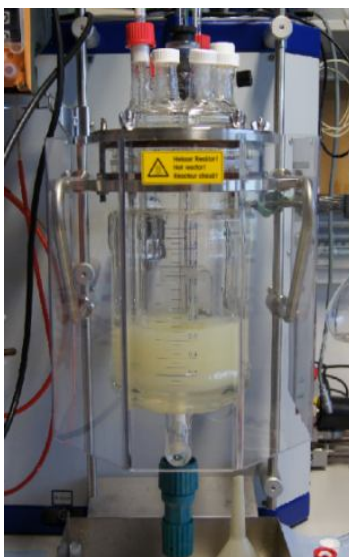


Fig. 3: automated laboratory reactor system

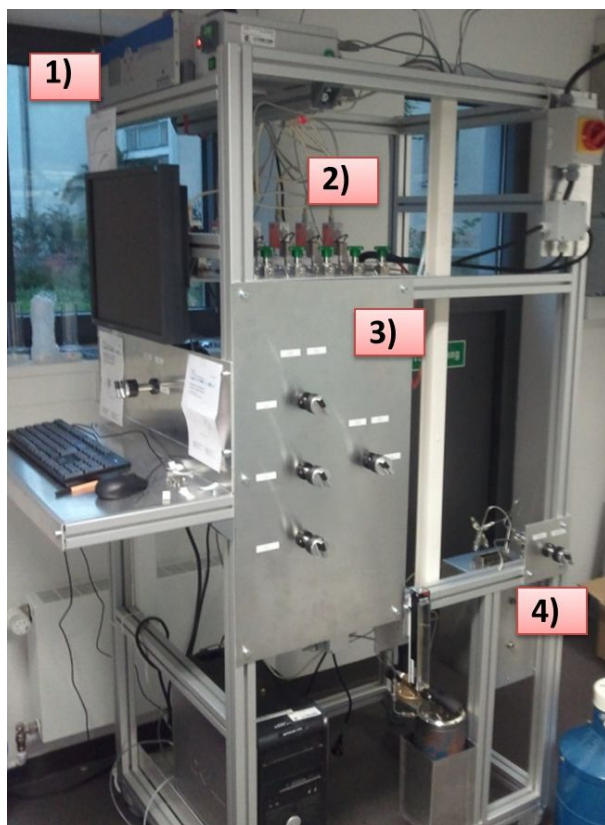
previous titration experiments. After complete addition of the metal salt solutions, the pH-change was further monitored for a certain time period (ageing period). Afterwards the product was washed three times and the conductivity of the filtrate solution was checked. The precursor was dried under air flow before being calcined under controlled conditions (20% O<sub>2</sub>-Ar, 5 Kpm heating rate), determined by TG-DSC-measurements, to yield the pre-catalyst consisting of PdO on the respective metal oxide support. With the developed synthesis routine, catalysts with varied palladium loading on Fe<sub>2</sub>O<sub>3</sub>, ZnO and Al<sub>2</sub>O<sub>3</sub> were synthesized for the studies in this work. Additionally, Pd on TiO<sub>2</sub> (P25) was prepared by impregnation, as will be described in chapter 4. Phase composition, morphology and specific surface area of the pre-catalysts were determined by XRD, SEM and BET measurements. The actual palladium content of the catalysts was verified by XRF and ICP-OES measurements.

The reduction temperature to activate the Pd/MO<sub>x</sub> catalysts was determined by TPR and TG-DSC measurements. STEM, TEM as well as CO-chemisorption measurements were performed to control the Pd particle distribution and to quantify the active surface area.



### 1.3.3. Catalytic reactor-setup

The catalytic CO-oxidation measurements, the reduction of the pre-catalysts to obtain the active catalysts and the TPR experiments in hydrogen and carbon monoxide containing atmosphere to determine the temperature for SMSI formation were conducted in the self-constructed catalytic reactor setup "Pallas" (Fig. 4). CO (3.7), O<sub>2</sub> (5.0), H<sub>2</sub> (5.0) as well as a calibration gas line (for calibration gas with a composition of 1% CO, 1% CO<sub>2</sub>, 1% O<sub>2</sub>, balance He) were connected to the He (5.0) carrier gas line by 6-port or 4-port valves (Valco, Vici) that were mounted on the switchboard. The carrier gas line was equipped with an oxygen and water filter patron (Air Liquide). The gas-mixture was connected to the reactor via a 4-port valve for switching between reactor and bypass. Each gas line was equipped with filters (2µm, Swagelok), mass-flow controllers (Bronkhorst) with gas flows of 20-200 ml/min (3 bar inlet pressure, 1 bar outlet pressure) as well as bellows lock valves and back pressure valves (SS-2C-1/3, Swagelok). The CO-gas line was equipped with a carbonyl trap, consisting of a tube filled with inert SiC and heated to 573 K. One special, customer-designed 6-port valve equipped with a sample loop was interconnected for optional pulse-gas measurements. The samples were filled in a stainless-steel plug-flow U-tube reactor with an inner diameter of 6 mm and covered with an inert inner layer (glass lined tubing, SGA analytical). Heating was performed by a copper-block oven controlled by a Watlow thermo-controller unit. A maximum operation temperature of about 773 K and an isothermal zone ( $\pm$  1 K) of about 4 cm was realized. Product detection was carried out by an on-line gas-analyzer (X-stream XE, Emerson/Rosemount, time resolution of 1 sec.), equipped with an infrared sensor and a paramagnetic sensor, for the simultaneous quantification of O<sub>2</sub>, CO, CO<sub>2</sub> and H<sub>2</sub>O. The sample temperature inside the reactor was directly monitored by the gas-analyzer via an analog connection to a Ni-CrNi (type K) thermocouple. The Cu-block was equipped with a pressured-air connection to allow faster cooling. Sealing of the reactor was performed by copper sealing shims (VCR). All gas lines consisted of 1/8 " stainless-steel tubing, connected by Swagelok connections.



- 1) Gas Analyzer
- 2) Gas-lines with MFCs
- 3) Switch-board
- 4) Cu-block oven with reactor

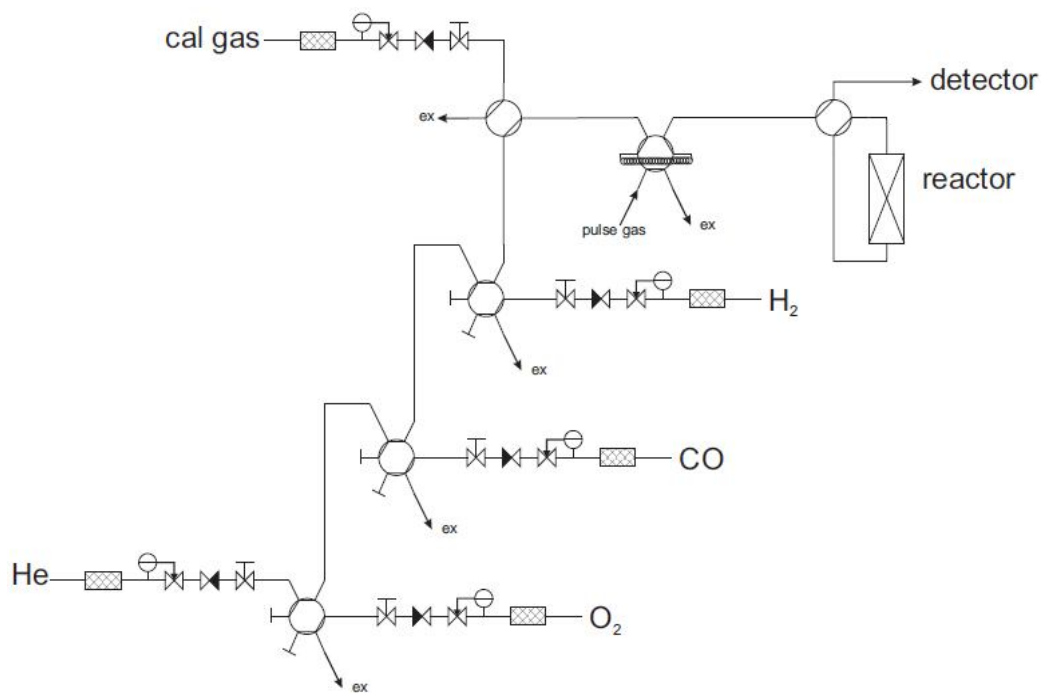


Fig. 4: catalytic reactor setup "Pallas" and flow schematics

#### 1.3.4. CO-oxidation

The CO-oxidation reaction was applied as the main test-reaction for all catalysts. Catalytic CO-oxidation has been intensively studied using palladium and other Pt-group metals during the last decades<sup>45</sup> because it is a comparably simple reaction that can serve as a model reaction for more complex systems. Furthermore, the reaction is of high importance due to its role in automotive exhaust gas purification (three-way catalyst). The reaction was performed in the self-constructed reactor-setup “Pallas”. The comparative measurements of activity and stability of all the different catalysts after different pre-treatments (LTR, HTR, reconditioning) can help to understand the nature of the active sites and the nature of the SMSI effect. Several authors were able to show an enhanced activity for CO-oxidation in case of existing SMSI on iron oxide involving model-systems<sup>46-49</sup> like Pd/Fe<sub>3</sub>O<sub>4</sub>(111)/Pt(111) or Pt/Fe<sub>3</sub>O<sub>4</sub>(111)/Pt(111): the effect of SMSI was dependent on the noble metal in that case. For example, thin, iron oxide film-covered Pt(111) was shown to exhibit a characteristic Moiré pattern in STM investigations and a much higher activity for CO-oxidation, compared to pure platinum. As mentioned before, a recent study in our department was able to show an enhancement of CO-oxidation activity in the HTR-state of co-precipitated Pd/FeO<sub>x</sub> catalysts which the authors attributed to an over-growth of the iron oxide support onto the noble metal.<sup>28</sup> For a more detailed description of fundamental, mechanistic studies of CO-oxidation on Pt-group metals, it is referred to the introduction of chapter 4.

#### 1.3.5. Selective hydrogenation of acetylene

Catalytic hydrogenation of acetylene to ethylene is of industrial importance since both gases are products of the steam-cracking process, acetylene however poisons the catalyst used for ethylene polymerization and thus has to be limited below a concentration of 1 ppm.<sup>50</sup> Hydrogenation of acetylene to ethylene can be used in general to investigate structural and electronic properties of catalysts that influence not only on the conversion, but also on the selectivity of the reaction. It has been applied to study for example the intermetallic compounds PdZn,<sup>51</sup> Pd<sub>2</sub>Ga and other Pd-Ga compounds.<sup>52,53</sup> There exist also several studies where this reaction was used to investigate strong metal-support interaction, for example on the Pd/TiO<sub>2</sub> system.<sup>54-56</sup> Thanks to these investigations, it is well known that both, alloy formation and SMSI can increase the selectivity for ethylene formation. This is due to the fact that the distance between two accessible palladium surface atoms increases in both cases,

leading to a decrease of by-product and follow-up product formation, like butadiene, for which at least two neighbored adsorption sites must exist.<sup>57,58</sup> For the present work, selectivity changes for some catalytic systems after different reduction temperatures will be monitored in order to gain additional experimental evidence on the SMSI formation and/or to distinguish from other processes like alloying.

## 1.5. References

1. Wollaston, W. H. On a New Metal, Found in Crude Platina. *Philos. Trans. R. Soc. Lond.* **94**, 419–430 (1804).
2. U. S. Department of the Interior. *U. S. Geological Survey, Mineral Commodity Summaries*. (2012).
3. Falbe, J., Regitz, M. & Römpp, H. *Römpp Chemie Lexikon*. (Thieme Georg Verlag, 1996).
4. Greenwood, N. N. & Earnshaw, A. *Chemie der Elemente*. (Wiley-VCH).
5. Holleman, A. F. & Wiberg, E. *Lehrbuch der Anorganischen Chemie*. (Gruyter, 1995).
6. Graham, T. *Additional Observations on Hydrogenium*. (Royal Society of London, 1868). at <<http://archive.org/details/philtrans00487974>>
7. *Concise Encyclopedia Chemistry*. (Walter de Gruyter, 1994).
8. Manchester, F. D., San-Martin, A. & Pitre, J. M. The H-Pd (hydrogen-palladium) System. *J. Phase Equilibria* **15**, 62–83 (1994).
9. Lindlar, H. & Dubuis, R. Process For Selective Hydrogenation. (1973). at <<http://www.freepatentsonline.com/3715404.html>>
10. Souza, P. R. N., Pereira, M. M., Antunes, O. A. C., Aranda, D. A. G. & Carneiro, J. W. M. 1, 3-Butadiene hydrogenation on pd-supported systems: geometric effects. *Braz. J. Chem. Eng.* **19**, 187–194 (2002).
11. Baerns, M. *Basic Principles in Applied Catalysis*. (Springer, 2004).
12. Clayden, J., Greeves, N., Warren, S. & Wothers, P. *Organic Chemistry*. (Oxford University Press, 2001).
13. Heck, R. M., Farrauto, R. J. & Gulati, S. T. *Catalytic Air Pollution Control: Commercial Technology*. (Wiley, J, 2009).

14. Ertl, G., Knözinger, H., Schüth, F. & Weitkamp, J. *Handbook of Heterogeneous Catalysis: 8 Volumes*. (Wiley-VCH Verlag GmbH & Co. KGaA, 2008).
15. Van Delft, F. C. M. J. M. & Nieuwenhuys, B. E. Correlation of nucleation- and growth modes with wetting, alloy segregation, catalyst preparation and strong-metal support interaction. *Solid State Ion.* **16**, 233–240 (1985).
16. Stevenson, S. A. & Dumesic, J. A. *Metal Support Interactions in Catalysis, Sintering, and Redispersion*. (Van Nostrand Reinhold, 1987).
17. Logan, A. D., Braunschweig, E. J., Datye, A. K. & Smith, D. J. Direct observation of the surfaces of small metal crystallites: rhodium supported on titania. *Langmuir* **4**, 827–830 (1988).
18. Tauster, S. J., Fung, S. C. & Garten, R. L. Strong metal-support interactions. Group 8 noble metals supported on titanium dioxide. *J. Am. Chem. Soc.* **100**, 170–175 (1978).
19. Bowker, M. *et al.* Model catalyst studies of the strong metal–support interaction: Surface structure identified by STM on Pd nanoparticles on TiO<sub>2</sub>(110). *J. Catal.* **234**, 172–181 (2005).
20. Lamber, R. & Schulz-Ekloff, G. Metal-Support Interaction in a Pt-TiO<sub>2</sub> Thin Film System: Observation of the Pt<sub>3</sub>Ti Phase at 823 K. *Berichte Bunsenges. Für Phys. Chem.* **95**, 1479–1481 (1991).
21. Chung, Y. W. & Zhao, Y. B. in *Strong Metal-Support Interactions* (eds. Baker, R. T. K., Tauster, S. J. & Dumesic, J. A.) **298**, 54–59 (American Chemical Society, 1986).
22. Taglauer, E. & Knözinger, H. Characterization of Supported Catalyst Systems with Surface Spectroscopies. *Phys. Status Solidi B* **192**, 465–475 (1995).
23. Linsmeier, C. & Taglauer, E. Strong metal–support interactions on rhodium model catalysts. *Appl. Catal. Gen.* **391**, 175–186 (2011).
24. Den Otter, G. J. & Dautzenberg, F. M. Metal-support interaction in Pt-Al<sub>2</sub>O<sub>3</sub> catalysts. *J. Catal.* **53**, 116–125 (1978).
25. Sá, J., Bernardi, J. & Anderson, J. A. Imaging of low temperature induced SMSI on Pd/TiO<sub>2</sub> catalysts. *Catal. Lett.* **114**, 91–95 (2007).
26. Li, Y. *et al.* Strong metal-support interaction and catalytic properties of anatase and rutile supported palladium catalyst Pd/TiO<sub>2</sub>. *Chem. Phys. Lett.* **372**, 160–165 (2003).
27. Naito, S., Kasahara, T. & Miyao, T. Transformation of methane formation sites into methanol formation ones during CO-H<sub>2</sub> reaction over Pd/CeO<sub>2</sub> in its SMSI state. *Catal. Today* **74**, 201–206 (2002).

28. Naumann d'Alnoncourt, R. *et al.* Strong metal–support interactions between palladium and iron oxide and their effect on CO oxidation. *J. Catal.* **317**, 220–228 (2014).
29. Kalinkin, A. V., Savchenko, V. I. & Pashis, A. V. Mechanism of low-temperature CO oxidation on a model Pd/Fe<sub>2</sub>O<sub>3</sub> catalyst. *Catal. Lett.* **59**, 115–119 (1999).
30. Gadgil, M. M. & Kulshreshtha, S. K. CO oxidation over Pd/FeSbO<sub>4</sub> catalyst. *J. Mol. Catal. Chem.* **95**, 211–222 (1995).
31. Sen, B. & Vannice, M. A. Metal-support effects on acetone hydrogenation over platinum catalysts. *J. Catal.* **113**, 52–71 (1988).
32. Dandekar, A. & Vannice, M. A. Crotonaldehyde Hydrogenation on Pt/TiO<sub>2</sub> and Ni/TiO<sub>2</sub> SMSI Catalysts. *J. Catal.* **183**, 344–354 (1999).
33. Vannice, M. A. Hydrogenation of CO and carbonyl functional groups. *Catal. Today* **12**, 255–267 (1992).
34. Vannice, M. A. & Sudhakar, C. A model for the metal-support effect enhancing carbon monoxide hydrogenation rates over platinum-titania catalysts. *J. Phys. Chem.* **88**, 2429–2432 (1984).
35. Coq, B., Kumbhar, P. S., Moreau, C., Moreau, P. & Figueras, F. Zirconia-Supported Monometallic Ru and Bimetallic Ru-Sn, Ru-Fe Catalysts: Role of Metal Support Interaction in the Hydrogenation of Cinnamaldehyde. *J. Phys. Chem.* **98**, 10180–10188 (1994).
36. Tsubaki, N. & Fujimoto, K. Promotional SMSI effect on supported palladium catalysts for methanol synthesis. *Top. Catal.* **22**, 325–335 (2003).
37. Zander, S. *Preparation and Characterization of Cu-ZnO Catalysts for Methanol Synthesis [Elektronische Ressource] / Stefan Zander. Betreuer: Robert Schlögl.* (Universitätsbibliothek der Technischen Universität Berlin, 2013). at <<http://nbn-resolving.de/urn:nbn:de:kobv:83-opus-38160>>
38. Zander, S. *et al.* The Role of the Oxide Component in the Development of Copper Composite Catalysts for Methanol Synthesis. *Angew. Chem. Int. Ed.* **52**, 6536–6540 (2013).
39. Behrens, M., Kasatkin, I., Kühl, S. & Weinberg, G. Phase-Pure Cu,Zn,Al Hydrotalcite-like Materials as Precursors for Copper rich Cu/ZnO/Al<sub>2</sub>O<sub>3</sub> Catalysts. *Chem. Mater.* **22**, 386–397 (2010).
40. Behrens, M. & Armbrüster, M. in *Catalysis for Alternative Energy Generation* (eds. Guzzi, L. & Erdöhelyi, A.) 175–235 (Springer New York, 2012). at <[http://link.springer.com/chapter/10.1007/978-1-4614-0344-9\\_5](http://link.springer.com/chapter/10.1007/978-1-4614-0344-9_5)>

41. Behrens, M. *et al.* The Active Site of Methanol Synthesis over Cu/ZnO/Al<sub>2</sub>O<sub>3</sub> Industrial Catalysts. *Science* **336**, 893–897 (2012).
42. Uchijima, T. SMSI effect in some reducible oxides including niobia. *Catal. Today* **28**, 105–117 (1996).
43. Haller, G. L. & Resasco, D. E. in *Advances in Catalysis* (ed. D.D. Eley, H. P. and P. B. W.) **36**, 173–235 (Academic Press, 1989).
44. Kunimori, K., Ito, K., Iwai, K. & Uchijima, T. Strong Metal-Support Interaction (SMSI) Behavior of Rh/Nb<sub>2</sub>O<sub>5</sub> Catalyst Studied By Ethane Hydrogenolysis And Hydrogen Chemisorption. *Chem. Lett.* (1986).
45. Freund, H.-J., Meijer, G., Scheffler, M., Schlögl, R. & Wolf, M. Die CO-Oxidation als Modellreaktion für heterogene Prozesse. *Angew. Chem.* **123**, 10242–10275 (2011).
46. Liu, L. *et al.* Low-temperature CO oxidation over supported Pt, Pd catalysts: Particular role of FeO<sub>x</sub> support for oxygen supply during reactions. *J. Catal.* **274**, 1–10 (2010).
47. Schalow, T. *et al.* CO oxidation on partially oxidized Pd nanoparticles. *J. Catal.* **242**, 58–70 (2006).
48. Lewandowski, M., Sun, Y. N., Qin, Z.-H., Shaikhutdinov, S. & Freund, H.-J. Promotional effect of metal encapsulation on reactivity of iron oxide supported Pt catalysts. *Appl. Catal. Gen.* **391**, 407–410 (2011).
49. Lewandowski, M. Scanning Tunneling Microscopy Study of Iron Oxide based Model Catalysts. (Technische Universität Berlin, 2011). at <<http://opus4.kobv.de/opus4-tuberlin/frontdoor/index/index/docId/3060>>
50. Herrmann, T. Selektivhydrierung von Acetylen unter industriellen tail-end Bedingungen. (TU Darmstadt, 2014). at <<http://tuprints.ulb.tu-darmstadt.de/3951/>>
51. Crespo-Quesada, M. *et al.* Size and Shape-controlled Pd Nanocrystals on ZnO and SiO<sub>2</sub>: When the Nature of the Support Determines the Active Phase. *ChemCatChem* **6**, 767–771 (2014).
52. Ota, A. *et al.* Intermetallic Compound Pd<sub>2</sub>Ga as a Selective Catalyst for the Semi-Hydrogenation of Acetylene: From Model to High Performance Systems†. *J. Phys. Chem. C* **115**, 1368–1374 (2011).
53. Armbrüster, M. *et al.* Pd–Ga Intermetallic Compounds as Highly Selective Semihydrogenation Catalysts. *J. Am. Chem. Soc.* **132**, 14745–14747 (2010).
54. Kang, J. H., Shin, E. W., Kim, W. J., Park, J. D. & Moon, S. H. Selective Hydrogenation of Acetylene on TiO<sub>2</sub>-Added Pd Catalysts. *J. Catal.* **208**, 310–320 (2002).

55. Kim, W. Effect of potassium addition on the properties of a TiO<sub>2</sub>-modified Pd catalyst for the selective hydrogenation of acetylene. *Appl. Catal. Gen.* **268**, 77–82 (2004).
56. Kim, W.-J. & Moon, S. H. Modified Pd catalysts for the selective hydrogenation of acetylene. *Catal. Today* **185**, 2–16 (2012).
57. Tauster, S. J. Strong metal-support interactions. *Acc. Chem. Res.* **20**, 389–394 (1987).
58. Borodziński, A. & Cybulski, A. The kinetic model of hydrogenation of acetylene–ethylene mixtures over palladium surface covered by carbonaceous deposits. *Appl. Catal. Gen.* **198**, 51–66 (2000).



## **Chapter 2: CO-oxidation as a test reaction for strong metal-support interaction on nano-structured Pd/FeO<sub>x</sub> powder catalysts**

Patrick Kast, Matthias Friedrich, Detre Teschner, Frank Girgsdies, Thomas Lunkenbein, Raoul Naumann d'Alnoncourt, Malte Behrens, Robert Schlögl.

### **Abstract:**

A series of differently loaded palladium-iron catalysts was prepared by a controlled co-precipitation method of the nitrate precursors, in order to ensure homogeneous Pd particle size-distribution. After characterization of the pre-catalysts by various techniques, different controlled reduction conditions were applied to investigate the interactions within the Pd/Fe system, containing reversible and irreversible processes like phase transformations, SMSI, sintering and alloying. Strong indications for the reversible surface decoration of the Pd nanoparticles with iron oxide species via strong metal-support interaction were found by the combined results of DRIFTS, CO-chemisorption, TEM and XPS measurements. This SMSI state was found to be unstable. It was observed independent of bulk phase or palladium particle size. Catalytic CO-oxidation was found to be a suitable test reaction for the study of the phenomenon: higher activity as well as oxidative deactivation of the SMSI state was observed by investigating the light-off behavior in repeated, temperature-programmed cycles as well as by isothermal measurements. The instability was found to be higher in case of higher Pd dispersion. In addition, bulk properties of the Pd/Fe system, like alloying, were investigated by detailed XRD measurements.

### **2.1. Introduction**

Recently, iron oxide supported noble metal catalysts have been intensively studied as model systems for the effect of strong metal-support interaction (SMSI) in CO oxidation. For example, the group of Freund studied well-defined Pt-nanoparticles on Fe<sub>3</sub>O<sub>4</sub>(111)/Pt(111).<sup>1-3</sup> The authors were able to generate SMSI (encapsulation) at elevated temperatures and to study its structure-function relationship. The support overlayer wetting the Pt-particles was identified by STM as a FeO (111) monolayer, because of a characteristic Moiré superstructure. In that state, a strongly enhanced CO oxidation activity was observed that was attributed by the authors to an oxygen-induced formation of a catalytically active O-Fe-O trilayer (Mars-van Krevelen type reaction mechanism). No such effect was observed so far for Pd/FeO<sub>x</sub> model systems. Schalow et al.<sup>4-7</sup> studied the surface chemistry and reported the

formation of different oxygen species on Pd/Fe<sub>3</sub>O<sub>4</sub>/Pt(111) model catalysts as well as their influence on CO-oxidation activity. By combining surface sensitive IR-spectroscopy, XPS and molecular beam experiments, they found a reversible formation of Pd-oxide species at T > 500 K. It was dependent on the metal-support interface and occurred preferentially on Pd particles of about 7 nm in diameter. With regard to CO-oxidation kinetics, the Pd-oxides were found to suppress the reaction rate, when compared to adsorbed oxygen species. At T > 450 K the oxidation state of the Pd-species was found to be subject to dynamic changes, in dependence of the reaction gas composition. Wang et al.<sup>8</sup> reduced Pd/Fe<sub>3</sub>O<sub>4</sub> with different reagents (H<sub>2</sub> or CO) and did not find any hints for encapsulation, but for the formation of bimetallic PdFe alloys, which have been characterized earlier by Felicissimo et al.<sup>9</sup>

These UHV-studies have been recently complemented by investigations in our group on more realistic catalysts.<sup>10,11</sup> Post-synthesis treatment of co-precipitated Pd/iron oxide catalysts was found to be crucial for the induction of phase-transition in the supporting iron oxide (from Fe<sub>2</sub>O<sub>3</sub> to Fe<sub>3</sub>O<sub>4</sub> polymorph). We were able to evidence the decoration of the palladium particles via SMSI upon reduction at 523 K by different techniques. The CO-chemisorption capacity of Pd in that decorated state was reduced and the reversibility of the overlayer formation was confirmed by in-situ XPS experiments. Activity studies of CO revealed an enhanced CO-oxidation rate in the state of decoration of the noble metal particles (E<sub>a</sub> determined to 33 kJ/mol), as well as the instability of this SMSI state leading to fast deactivation during reaction (E<sub>a</sub> = 70 kJ/mol).<sup>11</sup> A possible explanation for the different behavior of the co-precipitated Pd/Fe<sub>2</sub>O<sub>3</sub> catalysts, compared to the Pd/Fe<sub>3</sub>O<sub>4</sub> model system could be release of oxygen during the phase transformation of the iron oxide support, which might facilitate the palladium encapsulation, as proposed by Wang et al.<sup>8</sup>

Other CO-oxidation studies on Pd/Fe systems like Pd/Fe<sub>3</sub>O<sub>4</sub> core-shell particles,<sup>12</sup> Pd/ $\alpha$ -Fe<sub>2</sub>O<sub>3</sub><sup>13</sup> or evaporated model system<sup>14</sup> showed moderate catalytic activity with T<sub>50</sub> values between 363 K<sup>12</sup> and 453 K<sup>13</sup> as well as a change of the crystal structure during reaction. The model system showed an E<sub>a</sub> of 136 kJ/mol, decreasing with increasing reduction temperature. Much lower E<sub>a</sub> (about 34 kJ/mol) and full conversion already at around 273 K was reported in studies using uncalcined, co-precipitated Pd/Fe(OH)<sub>x</sub> systems.<sup>15-19</sup>

The target of the present work was to get a deeper understanding of the formation, the reversibility and the stability of the decorated SMSI state during CO oxidation reaction, with a focus on the influence of the gas composition during reduction and during reaction. For this purpose, the analytical methods described previously<sup>11</sup> were applied and complemented by additional CO- infrared studies (DRIFTS) to probe the surface properties in different

reduction states.

We present a multi-technique analysis to better understand the interaction of bulk and surface chemistry with the catalytic behavior in this complex catalytic system. We focus on the prehistory of the system that determines the nature of the active sites (chemical memory). Besides SMSI and PdFe alloy formation, processes like Pd particle sintering, Pd restructuring (by reversible hydride formation), Pd re-oxidation or poisoning by carbon species might play a role.

## **2.2. Experimental**

### **2.2.1. Catalyst synthesis**

The catalyst precursors were synthesized by co-precipitation from Fe- and Pd-nitrate solutions in an automated laboratory reactor and under controlled conditions. The details of the synthesis are presented as supporting information (SI). The precipitate precursor was dried in air for 24 h, mortared and calcined in 20% O<sub>2</sub>/Ar atmosphere (2 h at 823 K, 2 Kpm heating rate). The product consists of PdO supported on  $\alpha$ -Fe<sub>2</sub>O<sub>3</sub> (hematite). The palladium loading was varied to yield 1, 2 and 5 wt.-% Pd/Fe<sub>2</sub>O<sub>3</sub> catalysts. The calcined samples were reduced for microscopy studies with the help of a reduction tube, in 5% H<sub>2</sub>-Ar (100 ml/min) at different temperatures and with a heating rate of 2 Kpm and 30 min of holding time.

### **2.2.2. Catalyst characterization**

Elemental composition of the samples was verified by optical emission spectroscopy (ICP-OES) and energy-dispersive x-ray spectroscopy (EDX). The specific surface area was investigated by nitrogen physisorption (BET). Scanning electron microscopy (SEM) was used to check the morphology, whereas transmission electron microscopy (TEM) was used to investigate the Pd particle distribution and monitor structural changes after treatments or reactions. The reduced samples were transferred to the microscope without air contact. X-ray diffraction (XRD) was used for analysis of the bulk structure/phase analysis. CO-chemisorption was performed to measure the active surface area. CO-IR measurements (diffuse reflectance infrared fourier-transform spectroscopy, DRIFTS), X-ray photoelectron spectroscopy (XPS) and thermogravimetry coupled with differential scanning calorimetry (TG-DSC) were applied to investigate surface and bulk properties during reduction and/or CO-oxidation. The equipment used and the detailed procedures are described in the SI.

### 2.2.3. Catalytic testing

The CO-oxidation as catalytic test reaction was carried out in a self-constructed catalytic reactor setup which is equipped with an on-line gas analyzer (X-Stream, Emerson/Rosemount), consisting of a paramagnetic sensor and an infrared detector to quantify O<sub>2</sub>, CO, CO<sub>2</sub> and H<sub>2</sub>O. The temperature in the catalyst bed can be directly monitored by an analog connection to the gas analyzer. The setup is equipped with a switch-board for mixing the carrier gas (He 5.0) with CO (3.7), O<sub>2</sub> (5.0) or H<sub>2</sub> (5.0) with the help of 6-port switching valves (Valco, Vici). Every gas line is equipped with a filter, a mass-flow controller (E1-flow, Bronkhorst), a check valve and a shut-off valve. The CO-gas line is equipped with a carbonyl remover, consisting of a tube filled with inert SiC and heated to 573 K. The carrier gas line is equipped with a water and oxygen filter. The reactor itself is a U-tube reactor with an inner diameter of 5 mm, made of glass-lined steel (SGE). It is put inside a Cu-block oven for a maximum temperature of about 773 K, controlled by a Watlow thermo-controller unit and offering an isothermal zone of about 4 cm (+/- 1 K). The oven is equipped with a pressured-air connection to make faster cooling possible. Usually, 25 mg of the catalyst, diluted by 250 mg of inert SiC (particle diameter: 250-355 μm) were weighed out and reduced in 5% H<sub>2</sub>-He or in 2% CO-He (100 ml/min) at different temperatures (2 Kpm, holding time 30 min.). For the subsequent CO-oxidation, normally three repeated light-off conversion cycles were measured (100 ml/min, 0.5% O<sub>2</sub>, 1% CO, 98.5 % He) from 323 to 523 K (2 Kpm heating rate, 15 min. holding). The TPR experiments were performed in the same setup using 5% H<sub>2</sub>-He and a heating rate of max. 5 Kpm. About 150 mg of undiluted catalyst were used for TPR.

## 2.3. Results and Discussion

### 2.3.1. Synthesis and characterization of calcined pre-catalysts

Table 2.1: selected physical and chemical properties of the calcined pre-catalysts

#	Catalyst	Pd-loading (wt.-%)	BET surface area (m <sup>2</sup> /g)	Average Pd particle diameter* (CO-chem.; nm)	Active surface area (m <sup>2</sup> /g)*	TEM particle size (aver.) (nm)
14889	1% Pd/Fe <sub>2</sub> O <sub>3</sub>	0.95	35	1-2	2.6	≤ 1 nm
17233	2% Pd/Fe <sub>2</sub> O <sub>3</sub>	1.9	36	3-4	2.6	2 nm**
13757	5% Pd/Fe <sub>2</sub> O <sub>3</sub>	4.7	61	5-6	4.0	4 nm

\*after RT-red.

\*\* after 473 K-red.

Three Pd/Fe<sub>2</sub>O<sub>3</sub> catalysts have been prepared by co-precipitation in the described synthesis reactor. For the surface study of SMSI, lower Pd loaded samples (1 and 2 wt.-%) were favored due to a more narrow Pd particle size distribution and to exclude particle size effects. A higher loaded 5 wt.-% sample was prepared in order to better investigate structural-chemical bulk effects during temperature programmed reduction.

Table 2.1 summarizes selected parameters of the pre-catalysts after calcination at 823 K. While the specific surface area of the lower loaded samples, which have been precipitated at pH = 4, were similar at about 35 m<sup>2</sup>/g, the higher loaded sample, prepared at pH = 9 as in reference,<sup>11</sup> showed a value of 61 m<sup>2</sup>/g after calcination. All samples contained meso-pores with an average pore volume of 0.18 cm<sup>3</sup>/g and an average pore diameter of 22 nm according to BJH analysis. After calcination, the samples were investigated by SEM-EDX and XRD. EDX at different locations showed that the palladium distribution in case of all investigated samples was homogeneous. A porous structure was observed by microscopy, as shown in figures 2.1 and S2.2b. The iron oxide support phase consisted of crystallites of about 50 nm in diameter and was identified as the hematite polymorph,  $\alpha$ -Fe<sub>2</sub>O<sub>3</sub>, as it can be seen in the XRD (for the 2 wt.-% sample, see figure S2.2 in supporting information). In the 5 wt.-% Pd/Fe<sub>2</sub>O<sub>3</sub> catalyst, broad XRD peaks of PdO can be identified by Rietveld refinement as depicted in figure 2.1. The phase fraction of PdO was determined to 6.7 wt.-% which is in reasonable accordance with the nominal composition of about 6 wt.-% PdO.

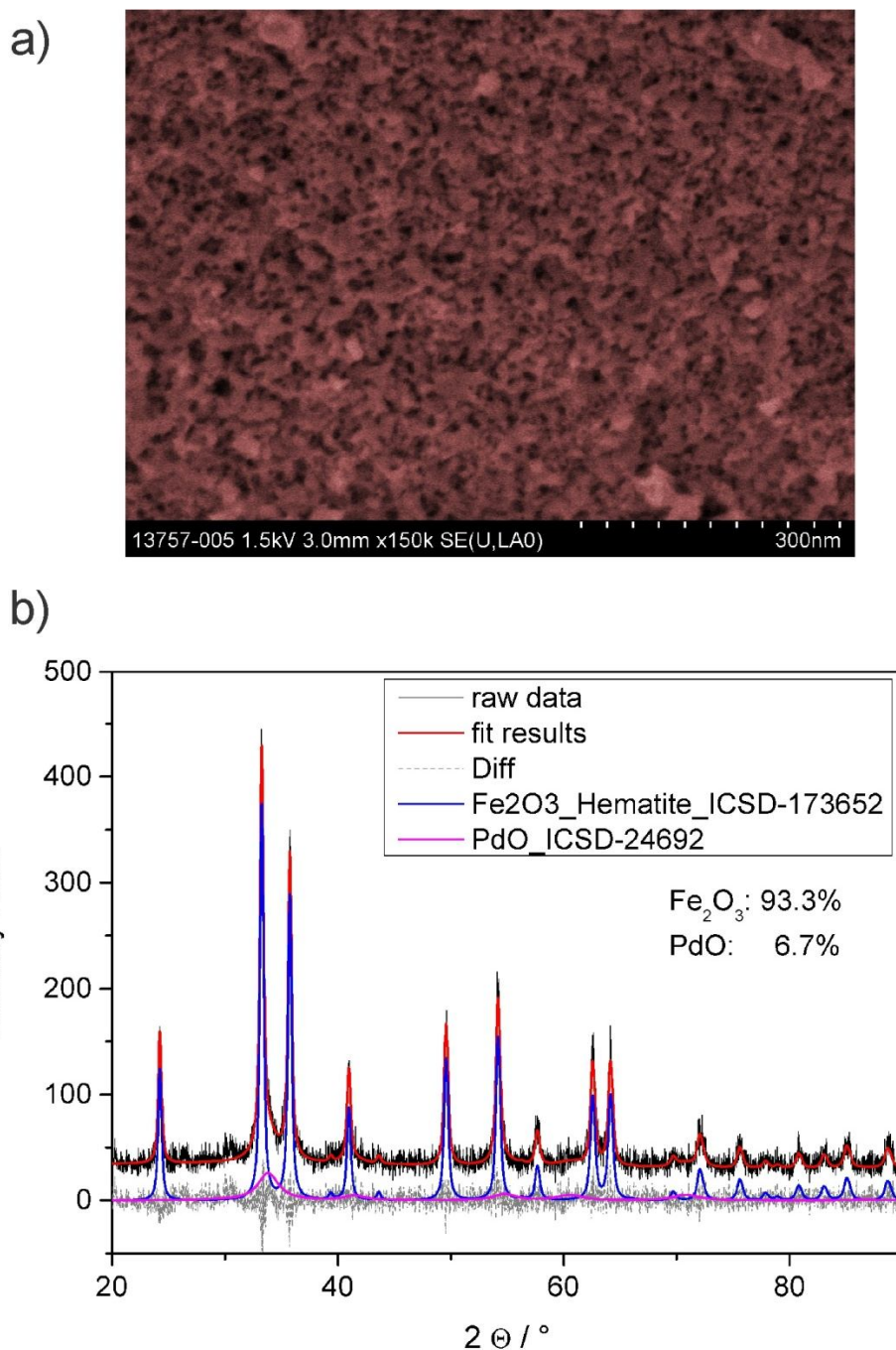


Fig. 2.1: SEM-image (a) and XRD-pattern (b) of the 5% sample after calcination at 823 K.

### 2.3.2. Reduction of the calcined pre-catalysts – bulk effects

The general reduction chemistry of the PdO/Fe<sub>2</sub>O<sub>3</sub> pre-catalysts was studied by TPR and is discussed based on the 5 wt.-% loaded samples in order to detect structural-chemical changes by XRD during reduction in different reducing environments, containing hydrogen or carbon monoxide.

Figure 2.2 shows a comparison of the TPR profile of the calcined sample, performed in 5% H<sub>2</sub>-Ar or in 2% CO-He after pre-drying in He at 573 K. It is notable in figure 2.2a that after a

short activation period of about 0.5 min, the palladium oxide phase formed after calcination is reduced instantaneously at room temperature by hydrogen, which is accompanied by a slight temperature rise indicating the exothermicity of the reaction. With increasing temperature, more water is formed which is an indication for Pd induced hydrogen-spillover that starts to reduce the surface of the iron oxide support, in good agreement to literature.<sup>20</sup> The bulk (hematite) reduction peak appears at about 525 K.

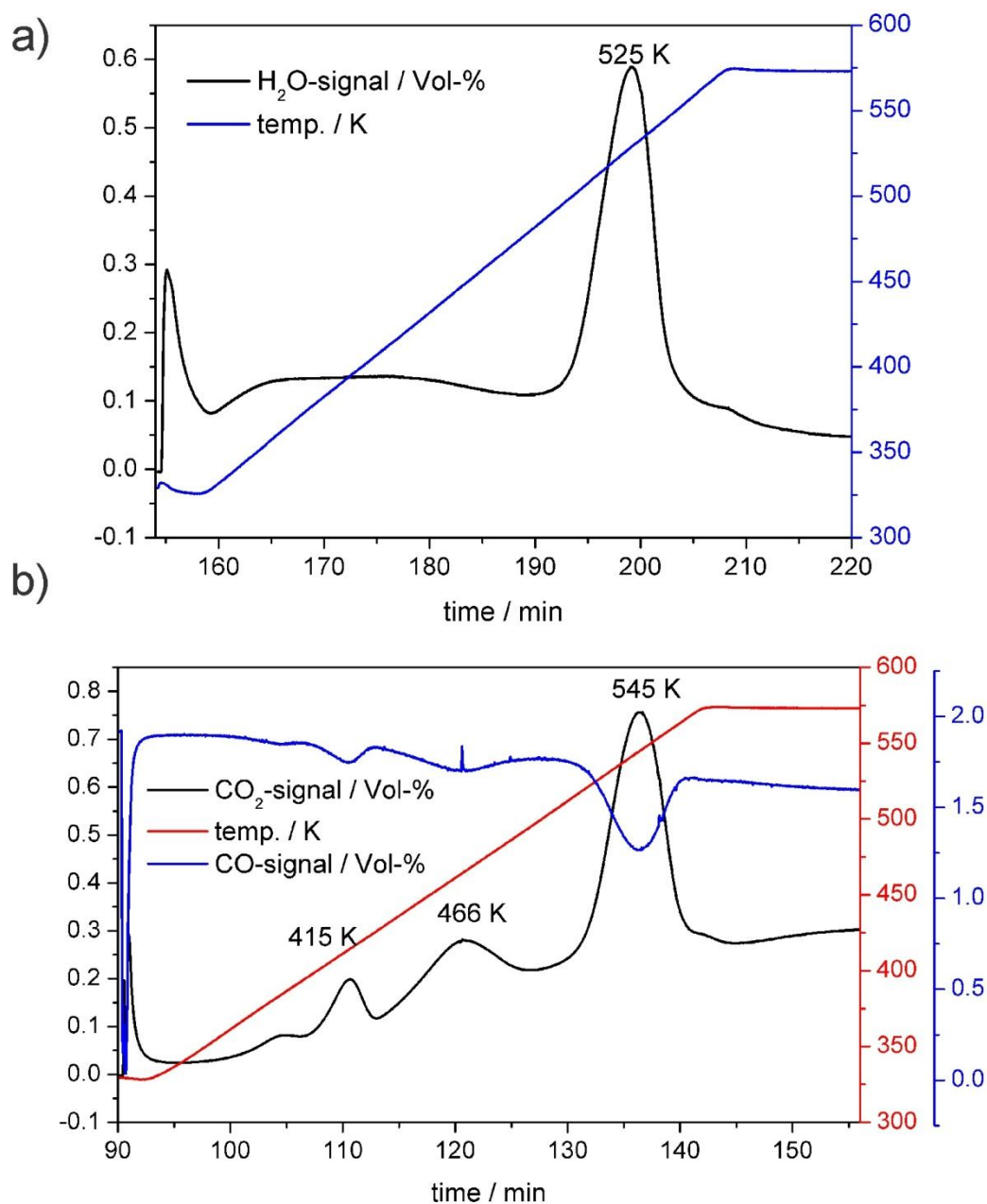


Fig. 2.2: TPR-curves (RT-573 K) of the 5% sample in 5% H<sub>2</sub> (a) and 2% CO (b).

The theoretical calculated ratio between the first reduction signal (PdO-reduction) and the bulk reduction to magnetite is approx. 1:4.3 which is in reasonable agreement to the observed ratio of 1:4.8 if we take into account that the PdO reduction will overlap to certain content with spill-over reduction of the support. The state after the PdO reduction (at around 323 K) is referred to as the room temperature reduction (RTR) state in the following, while the state after hematite reduction at the end of the heating ramp will be called high temperature reduction (HTR). It is noted again that no sharp reduction signal is observed between RTR and HTR, but that a broad water signal is detected indicating surface reduction in that temperature region. We will show later that the formation of an SMSI overlayer occurs already at sub-HTR temperature and assign these broad signals tentatively to formation of an SMSI-state. In case of reduction in H<sub>2</sub> the SMSI formation process seems to occur continuously by spill-over.

Interestingly, this is different from the reduction profile performed in 2% CO (Fig. 2.2b). Besides the RTR and HTR signal, two other signals can be observed, one at 415 K and the other at 466 K. A third, smaller signal appears at around 380 K. Peak integration (not shown) revealed that Pd oxide reduction in that case is only complete after the signal at 415 K, likely due to different Pd species present. In order to better monitor the degree of Pd reduction, TG-DSC experiments were performed that numerically confirmed complete PdO reduction in case of hydrogen atmosphere already at room temperature, compared to 398 K in case of CO (Fig. S2.3), which is in reasonable agreement with the CO-TPR peak found at 415 K. Furthermore, support reduction by spill-over was confirmed.

A first attempt to characterize the sample state at the respective TPR peaks in the different reduction atmospheres was done by XRD of the 5 wt.-% catalyst. Scans performed after RTR in hydrogen atmosphere indicated that the iron oxide phase was still hematite while the palladium oxide was reduced to metallic palladium, supported on  $\alpha$ -Fe<sub>2</sub>O<sub>3</sub>. The size of the particles was very small, indicated by the broad XRD peak. As shown previously for hydrogen reduction, the HTR peak is due to reduction of the support from hematite to magnetite phase, Fe<sub>3</sub>O<sub>4</sub>.<sup>11</sup> After HTR, magnetite formation was also confirmed by XRD in case of reduction with CO.

Reduction in CO atmosphere was performed before and after the central TPR peak at 466 K in order to obtain information about possible structural changes during this reduction step (Fig. S2.4). Both diffractograms were found to look very similar. The bulk iron oxide phase in both cases is still hematite, while the palladium is in its metallic state. No obvious changes in the crystal structure during the formation of SMSI upon reduction could be detected,



indicating that the formed overlayer will be x-ray amorphous or too small to be detected by XRD. The diffractogram of the same sample after 523 K reduction in CO-atmosphere shows reflections for palladium, supported on magnetite, while partial alloy formation cannot be excluded (Fig. S2.5).

The RTR state of the catalysts reduced in hydrogen was investigated by CO-chemisorption, XRD and TEM. The average Pd particle diameter, as determined by CO-chemisorption (Tab. 1), increased with increasing palladium loading, from 1-2 nm (1 wt.-% sample) until about 5-6 nm (5 wt.-% sample). The calculated active metal surface area increased from 2.6 m<sup>2</sup>/g (1 and 2 wt.-%) until 4 m<sup>2</sup>/g (5 wt.-%). The particle sizes determined by chemisorption are not exactly the same as if determined by microscopy, which might be due to the fact that chemisorption is an integral method, different to TEM. On the other hand, in case of CO-chemisorption different assumptions have to be made when calculating the average particle diameter, like particle shape, adsorption stoichiometry (binding geometry of the CO-molecule) and the maximum coverage for a monolayer of CO adsorbed on palladium, that is known not to exceed values of  $\Theta = 0.3-0.5$ , dependent on the surface orientation of ideal Pd surfaces.<sup>21</sup> In fact, after RTR of the 1% sample (see Fig. 2.3a), only sub-nm sized, highly dispersed Pd clusters can be observed in STEM. The TEM image (bright field) and the STEM image (high angle annular dark field - HAADF) of the 2 wt.-% catalyst were recorded after 473 K reduction in order to investigate not only the Pd distribution but also possible surface reduction effects. The images show homogeneously distributed, round shaped palladium particles of about 2 nm in diameter, as dark dots in the first, and white dots in the latter case (Fig. 2.3b+c) confirming the uniform distribution of Pd in the co-precipitated catalysts. Fig. 3b shows a HRTEM image at a state of the catalyst between RTR and HTR, where surface reduction by spill-over hydrogen was proposed.

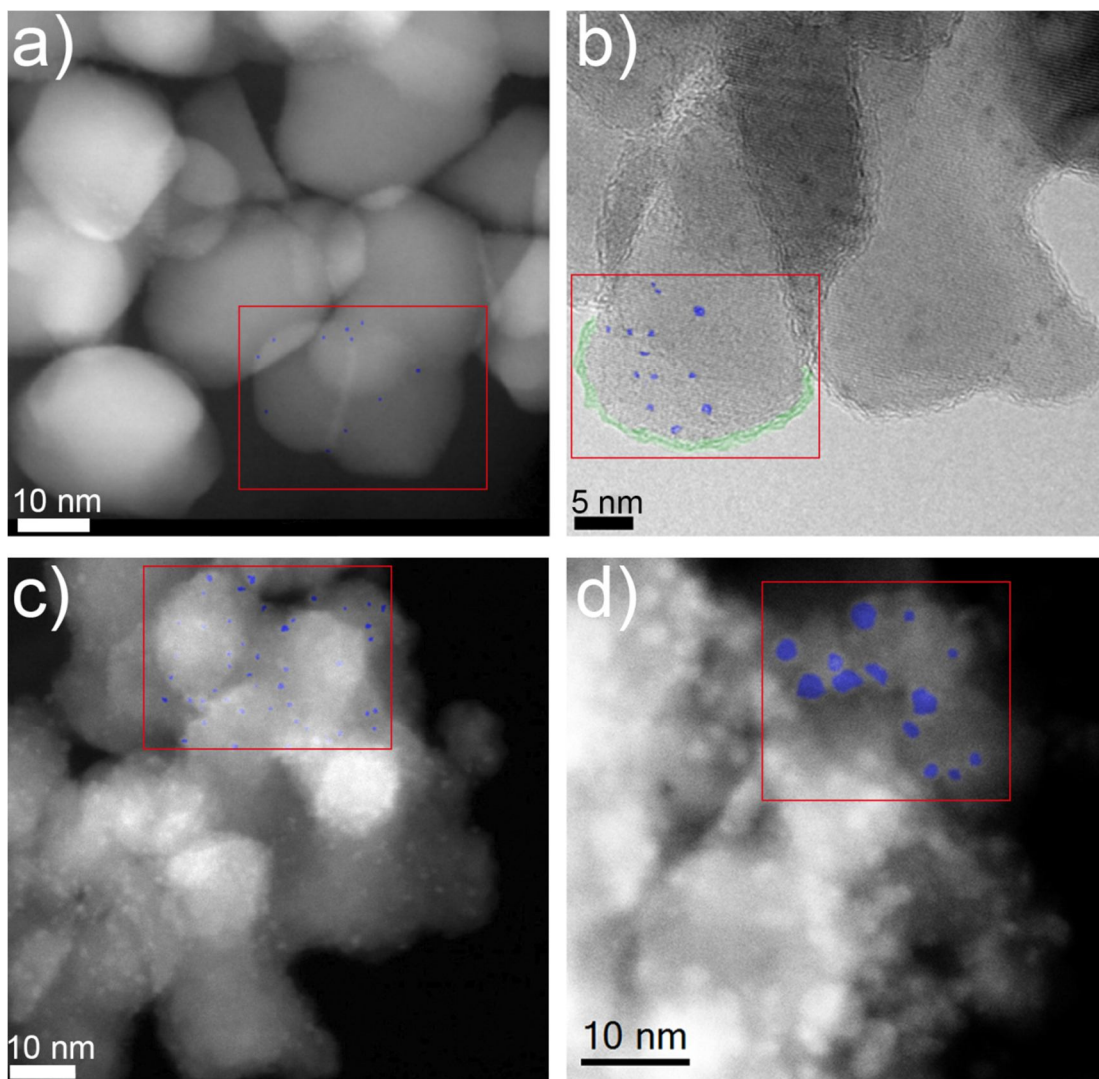


Fig. 2.3: STEM image of the 1% Pd sample after RT-reduction (a), TEM-image (b) and STEM-image (c) of the 2% Pd sample after 473 K reduction and STEM image of the 5% Pd sample after 473 K reduction (d). Pd particles and support overlayer in red frame are marked in blue and green.

Indeed, an amorphous overlayer can be seen at the surface which is interpreted as a hint for a partially reduced surface of the hematite support. Fig. 2.3d presents a STEM image of the 5 wt.-% sample also after 473 K reduction. Homogeneously distributed Pd particles in the size of about 4 nm can be seen, but no overlayer.

One possible state of PdO/Fe<sub>2</sub>O<sub>3</sub> after reduction not considered so far is the formation of Pd-Fe alloys, which can show markedly different catalytic properties compared to non-alloyed Pd.<sup>22,23</sup> Bulk sensitive XRD has been applied on the 5% catalyst to check for alloy formation at HTR. To regulate the formation of an alloyed reference state for these experiments, higher

reduction temperatures than 523 K have been applied. Figure 2.4 shows the Rietveld-fitted results after reduction at 523 K (HTR) and after 723 K. While after HTR, the only bulk phase present is magnetite, the amount of further reduced species, namely alpha iron, is significant after 723 K reduction (about 10 wt.-%). In both cases the palladium phase has been fitted with the ICSD-633135 reference for the cubic intermetallic compound Pd<sub>3</sub>Fe. It has to be noted that there is a close structural relationship with metallic palladium (fcc structure) and that this structural model can be used to satisfactorily fit both phases in the present case due to the poorly crystalline and nano-sized nature of the Pd phase. Thus the lattice parameter has to be carefully evaluated in order to discriminate non-alloyed Pd and the intermetallic. In addition to the lattice parameter change, the increase of the fitted amount of the Pd phase from about 4% at 523 K to about 6% after 723 K reduction is another indication for progressing alloy formation in this temperature regime. It is worth noting that the Pd reflection remains broad, even after 723 K reduction, which is an indication for the prevention of substantial sintering. In order to further study the alloying, the Pd lattice parameter 'a' has been monitored, using the literature parameter of 3.89 Å as a reference for metallic Pd<sup>24</sup> and five phase pure reference alloys with a known composition between Pd<sub>95</sub>Fe<sub>5</sub> and Pd<sub>75</sub>Fe<sub>25</sub> (i.e. Pd<sub>3</sub>Fe), prepared by melting of the elements. From these references, a Vegard plot (Fig. 2.5b) has been created to calibrate the amount of iron in the palladium particles of the 5% catalyst after different reductive treatments. All scans were performed in He atmosphere at RT. The lattice parameter contracts with on-going incorporation of iron: the first scan of the sample, after reduction in 5% H<sub>2</sub> at RT exhibits a lattice parameter of 3.889 similar to the literature value for metallic palladium.<sup>24</sup> Already after HTR (523 K), the parameter has decreased to 3.859 Å, representing a formal composition of Pd<sub>3</sub>Fe, according to the Vegard plot. After further reduction at 623 K only a small decrease of the lattice parameter to 3.848 can be detected, representing still Pd<sub>3</sub>Fe composition. With further increase of the reduction temperature to 723 K the lattice parameter decreases until a value of 3.815 which represents, according to the plot, a formal composition of PdFe. However, according to the XRD pattern, the structure in that state would still be cubic Pd<sub>3</sub>Fe. The differences between the bulk reference materials and the catalysts are likely affected by the nano-structured nature of the Pd phase in the latter and by the poor crystallinity leading to ambiguous diffraction data.

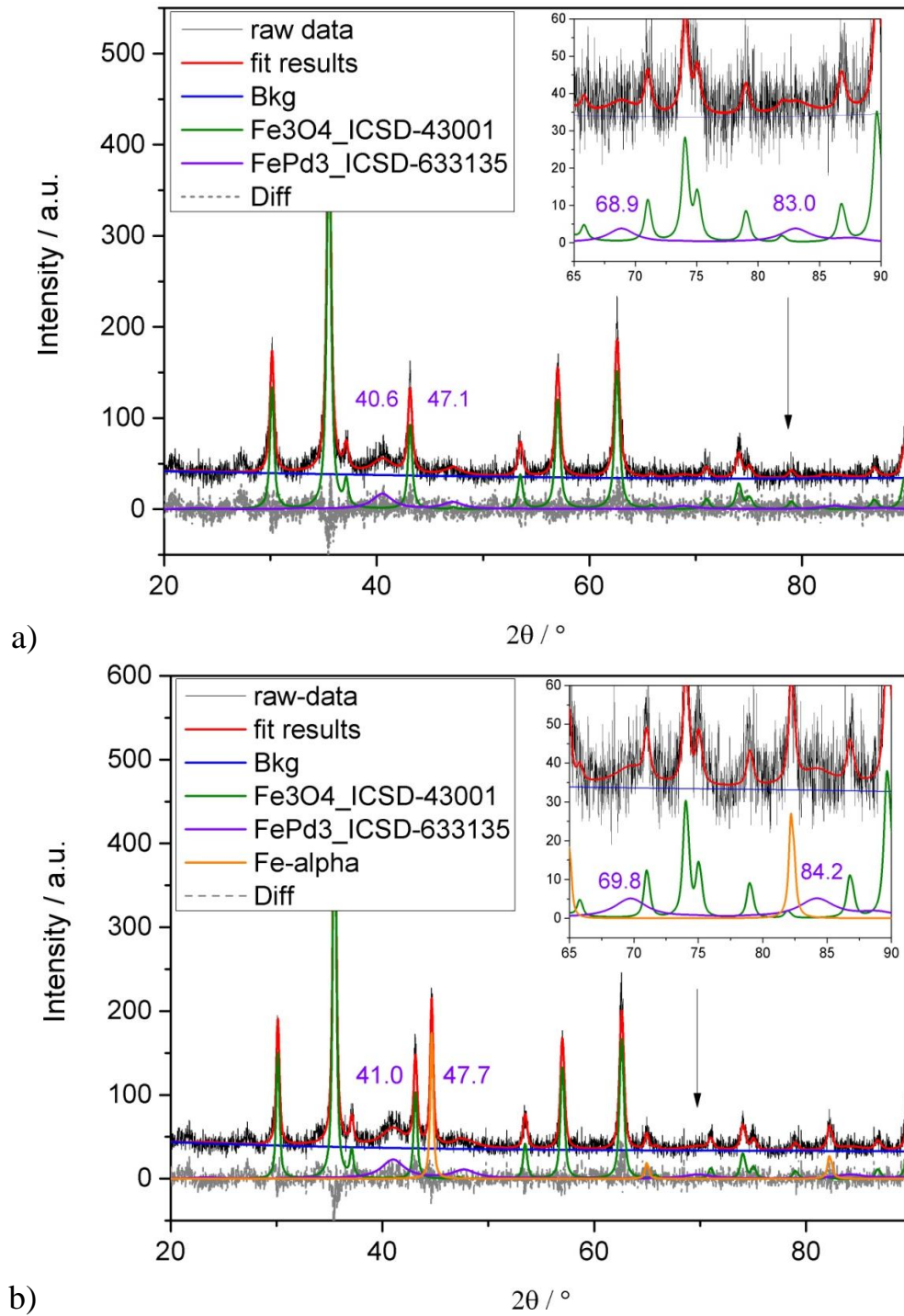


Fig. 2.4: XRD of 5% sample recorded at RT after in-situ reduction at 523 K (a) and 723 K (b) in 5% H<sub>2</sub>. Insets: magnification of region between 65 and 90°.

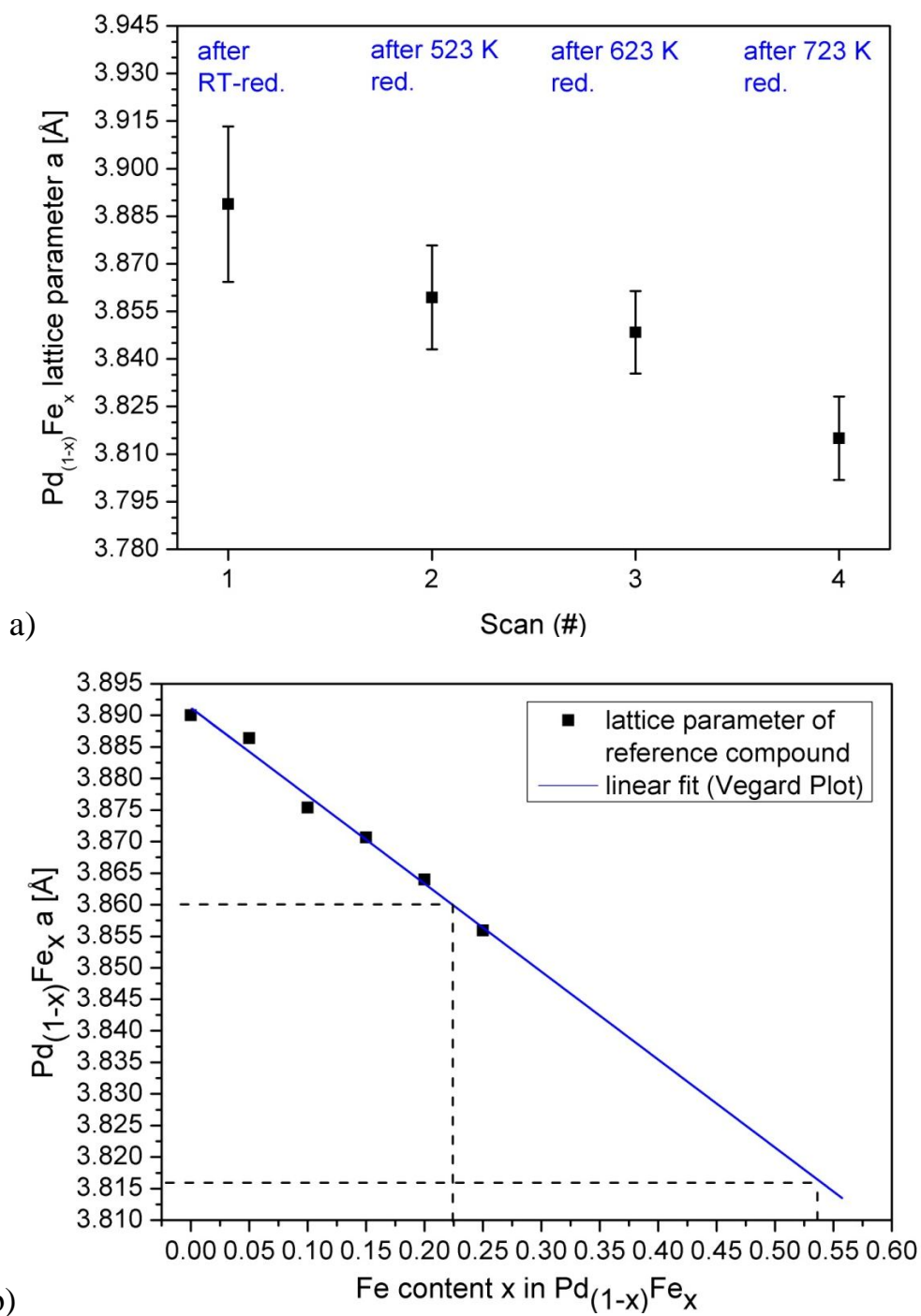


Fig. 2.5: Determined lattice parameter 'a' and error bars (3x standard deviation) of  $\text{Pd}_{(1-x)}\text{Fe}_x$  during reduction series of the 5% Pd catalyst (a) and comparison of the state after 523 K and 723 K reduction to Vegard-Plot of reference alloys (b).

### 2.3.3. DRIFTS surface investigation

IR spectra of CO probe molecules have been measured in different reduction states of the 2 wt.-% (Fig. 2.6-2.7) and the 5 wt.-% (Fig. 2.8) Pd/Fe<sub>2</sub>O<sub>3</sub> catalysts.

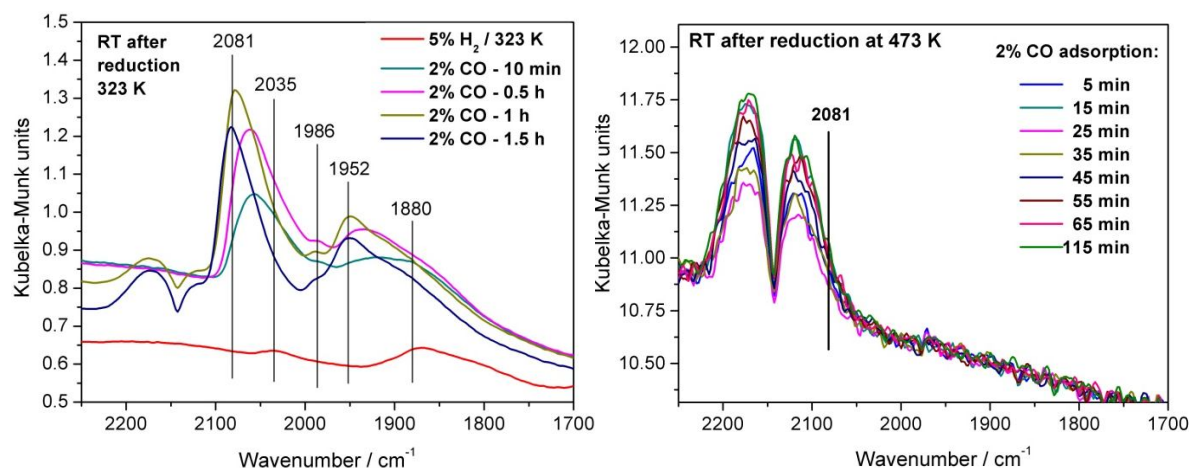


Fig. 2.6: CO-DRIFTS spectra of 2% Pd/Fe<sub>2</sub>O<sub>3</sub> after 323 K-red. (left) and 473 K-red. (right).

For the first part of the IR-measurements, the 2 wt.-% sample has been reduced at 323 K in a 5% H<sub>2</sub>-Ar mixture for 30 min. to simulate RTR conditions. Remaining hydrogen and produced water were purged with argon and a mixture of 2% CO in argon (100 ml/min) was introduced into the chamber to study the CO adsorption on the reduced palladium sites (Fig. 2.6, left side). Spectra have been recorded after 10 min, 30 min, 1h and 1.5 h. Gas phase CO is visible between 2100 and 2200 cm<sup>-1</sup>. The IR band at 2081 cm<sup>-1</sup> can be assigned to linearly adsorbed CO on metallic palladium.<sup>25-27</sup> At the beginning of exposure, a shoulder at 2035 cm<sup>-1</sup> is visible. This is probably due to geometric reasons: a high CO coverage reduces the back-bonding capability and leads to a blue-shift. A second prominent signal is visible at 1952 cm<sup>-1</sup> which represents the carbonyl band for bridged-bonded CO on Pd.<sup>25-27</sup> Due to a broad signal below 1900 cm<sup>-1</sup>, even some abundance of threefold coordinated CO on Pd cannot be excluded.<sup>28,29</sup> These observations confirm that the surface properties of the state after RTR resembles dispersed, but unmodified Pd. The same sample has been reduced afterwards in 5% H<sub>2</sub>-Ar at 473 K (2 Kpm) and flushed again with argon after cool down to room temperature. Then, 2% CO was dosed again to the sample for about 115 min. The recorded spectra are shown in figure 2.6 (right side). Mostly gas phase CO could be detected, with a very small signal of CO species on Pd (2081 cm<sup>-1</sup>) in the shoulder. Purging with argon

eliminated the gas phase signal and no remaining band was observed.

Afterwards CO-oxidation conditions (1% CO, 0.5% O<sub>2</sub>) were simulated in the DRIFTS setup in order to study the influence of the kinetic measurements on the IR properties of the reduced samples. The temperature was increased with 2 Kpm until the maximum reaction temperature of 523 K (hold 30 min.) while CO<sub>2</sub>-formation could be detected in the IR-spectra, indicating the proceeding reaction.

During cooling-down, spectra were recorded. At about 370 K, CO adsorption starts again and the appearance of three dominant signals between 2101 and 2155 cm<sup>-1</sup> that have not been observed in the measurement before CO-oxidation (Fig. 2.6) are observed as soon as the sample temperature falls below 373 K (Fig. 2.7). Besides some gas phase CO present in this measurement design and physisorbed CO on palladium (at around 2150 cm<sup>-1</sup>),<sup>25</sup> the adsorption of CO on Pd<sup>2+</sup> is very likely to contribute to the spectrum.<sup>29-32</sup> Nevertheless, CO on metallic Pd (1979, 1945 cm<sup>-1</sup>) is present as well.

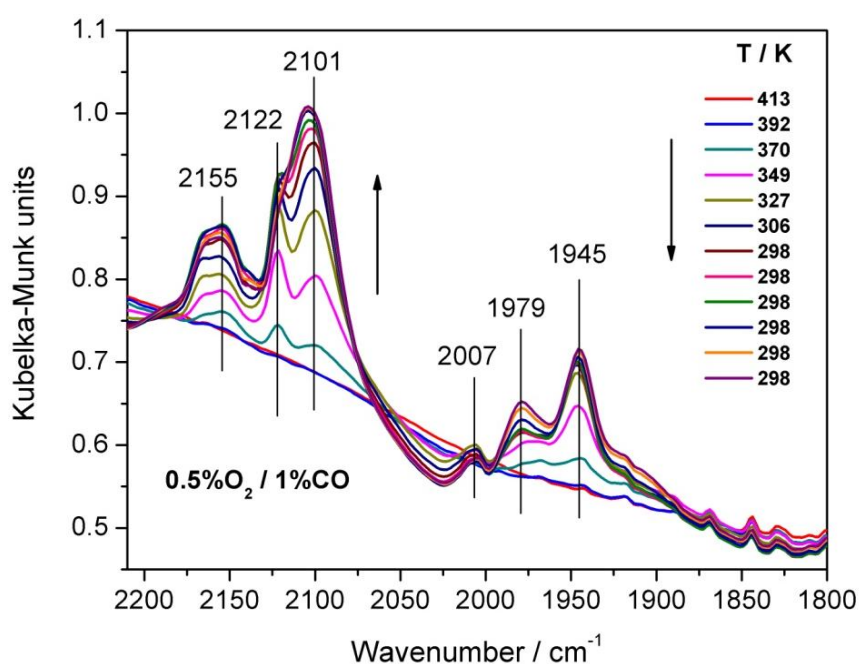


Fig. 2.7: DRIFTS of the 2% sample after re-oxidation in 0.5% O<sub>2</sub> + 1% CO (523 K).

The CO-adsorption properties of the 5 wt.-% sample were investigated at 77 K, after in-situ reduction in 2% CO-Ar atmosphere at 423 and 473 K, to compare the two surface states before and after the TPR-signal at 466 K (see Fig. 2.2). In addition, the support Fe-O-vibration region has been monitored. The results are presented in figure 2.8 (a,b) and in figure S2.6 (Fe-O vibrations, SI).

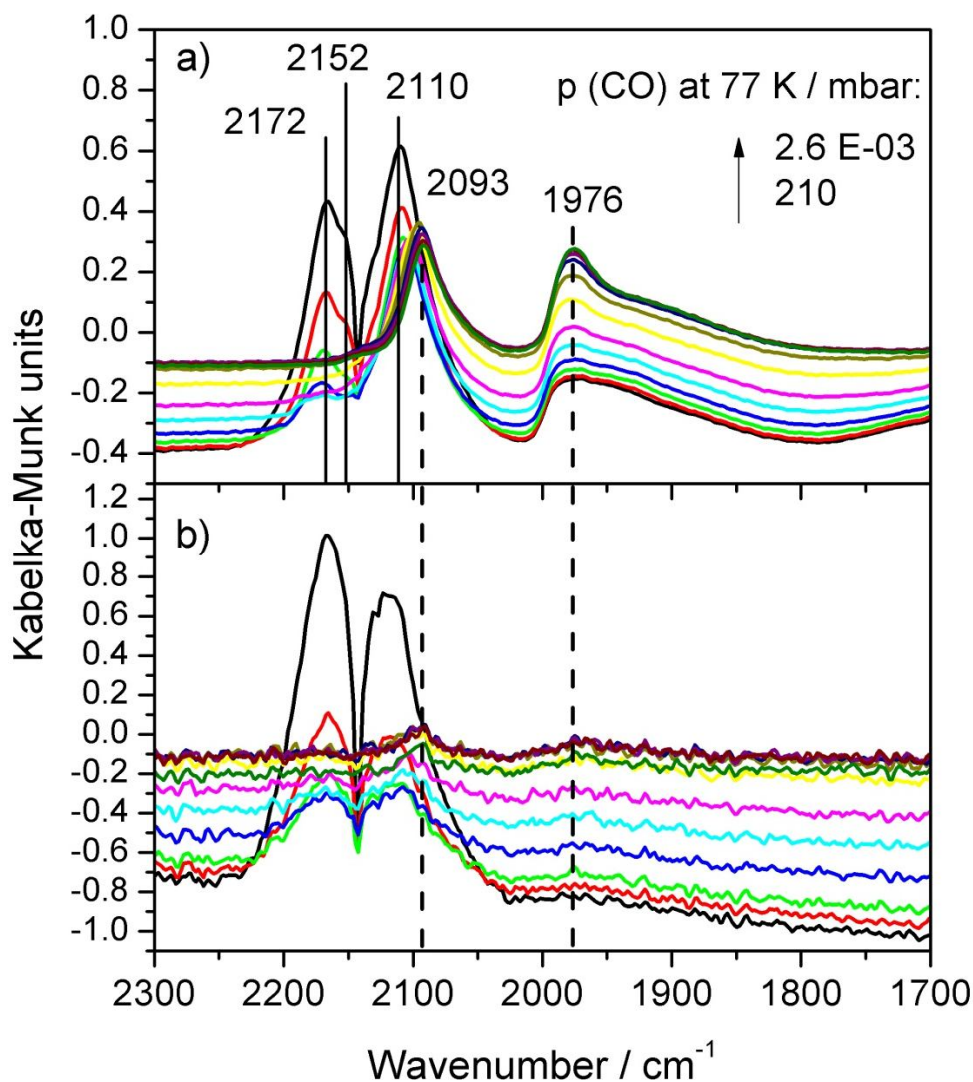


Fig. 2.8: DRIFTS study of 5% Pd sample: CO-desorption spectra measured at 77 K after 30 min reduction in 2% CO/Ar at 423 K (a) and at 473 K (b).

Again, linearly and bridged bonded CO at wave numbers of 2093 and 1976  $\text{cm}^{-1}$  were observed. That is an indication for the presence of metallic palladium after 423 K reduction (Fig. 2.8a). In addition to that a small shoulder at around 2152  $\text{cm}^{-1}$  can be observed after this first reduction step which can be explained by linearly adsorbed CO on some little amounts of residual, not yet reduced PdO that appears at 2150-2160  $\text{cm}^{-1}$  according to literature.<sup>29,31-37</sup> After 473 K reduction, the signal for adsorbed CO decreased to less than 10% (Fig. 2.8b), similar to the study after hydrogen reduction. Compared to 423 K reduction, also the Fe-O-vibration intensity of the support has reduced after 473 K reduction and disappeared completely after further increase of the reduction temperature to 523 K (Fig. S2.6, SI). The fact that even cooling to 77 K did not induce any measurable CO adsorption on the reduced



catalyst suggests that the formation of surface alloys at this temperature (473 K) is rather unlikely because literature reports adsorption signals in the observed region for CO on various Pd alloys.<sup>38,39</sup>

#### 2.3.4. CO chemisorption measurements

To quantify the decrease of active metal surface area the samples containing 1% and 2% Pd were also studied by volumetric CO chemisorption at 313 K after reduction at 323 K (RTR) and 473 K. The active surface area was calculated from the capacity of strongly adsorbed CO, as mentioned before. The adsorption isotherms as there are IC=combined isotherm, IS=strong isotherm (chemisorption) and IW=weak isotherm (physisorption) are plotted in figure S2.7a (2% sample) and S2.7b (1% sample, both SI). The typical behavior for saturation of the surface with strongly bonded CO can be seen after RTR (Fig. S2.7a, panel a). With increasing pressure only the amount of physisorbed CO increased. After reduction at 473 K the CO-chemisorption capacity drastically decreased, but is partly restored with increasing pressure (panel b).

In order to test the reversibility of this effect, the sample was re-calcined and measured for a second time after RTR and successively after 473 K-red. (Fig. S2.7a, panels c+d). For the 1% sample (Fig. S2.7b) the decrease after 473 K reduction in comparison to the RTR is similar.

Re-calcination in both samples partially restored the initial, higher chemisorption capacity, but the total adsorbed volume decreased by 12% for the 2% sample and by 40% for the 1% sample, compared to the original CO uptake: in case of the 2% sample the monolayer capacity was determined to 27  $\mu\text{mol/g}$  and the active surface area was calculated to 2.6  $\text{m}^2/\text{g}$  in the RTR state, with a dispersion of 29% (cubic particles assumed). After 473 K reduction the values decreased to 8  $\mu\text{mol/g}$  and 0.7  $\text{m}^2/\text{g}$ . After the re-calcination procedure the capacity (RTR-state) again reached values of 24  $\mu\text{mol/g}$  and decreased again to 10  $\mu\text{mol/g}$  (after second 473 K red.). Langmuir constants were determined in case of the first RTR state ( $K = 2.3/\text{mbar}$ ) and the first 473 K red. state ( $K = 0.4/\text{mbar}$ ), however these values have limited physical meaning due to the fact that earlier calorimetric measurements on a similar sample in our group (see Fig. S2.7c+d) showed restructuring of the active sites is likely to start at CO pressures of 0.5 mbar already while the first data point of the chemisorption measurements is at 2-3 mbar.

### 2.3.5. CO oxidation experiments

In a first kinetic experiment, the isothermal reaction rate for CO<sub>2</sub>-formation was studied over the 2 wt.-% catalyst at 430 K, after performing 473 K-reduction (5% H<sub>2</sub>-He). Two complete CO-oxidation cycles between RT and 523 K were performed before the measurement, in order to minimize irreversible effects (Fig. 2.9, inset). During the third ramp the temperature of 430 K was kept constant for 300 min (Fig. 2.9, curve 1). Afterwards the sample was re-reduced at 473 K and the isothermal measurements were conducted again at 430 K, but this time during the first CO-oxidation ramp (blue curve, no. 2). After another 300 min the procedure was repeated (curve no. 3).

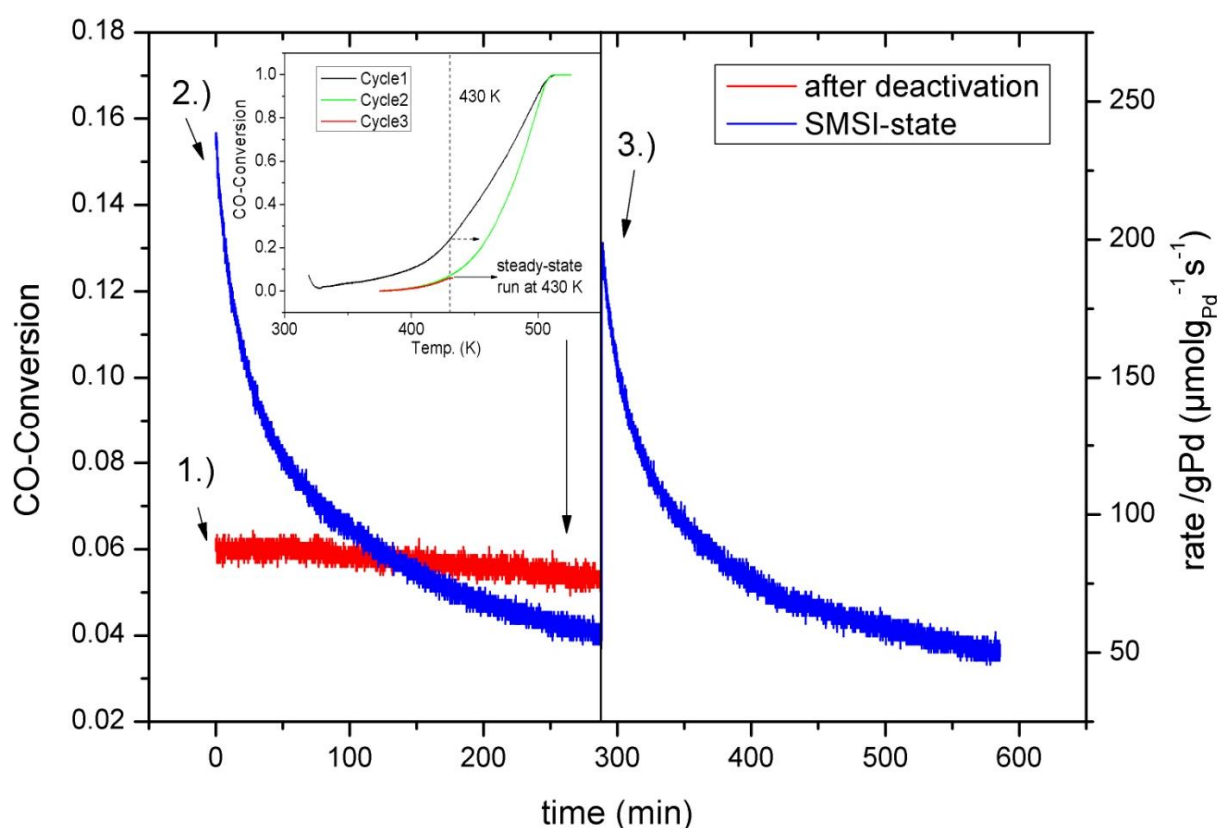


Fig. 2.9: CO-conversion and reaction rate in isothermal CO-oxidation measurements at 430 K over the 2% catalyst after deactivation (1, red curve) and after two times of re-reduction (blue curves, 2+3). Two complete oxidation cycles after 473 K reduction performed before (inset).

As it can be seen, the catalyst is in a kind of deactivated state after the initial CO-oxidation cycles were performed (curve 1) with a CO<sub>2</sub> production rate of about 85 μmol gPd<sup>-1</sup> s<sup>-1</sup> and with little further deactivation upon time. In contrast to that, the isothermal CO<sub>2</sub> formation rate is much higher (almost 250 μmol gPd<sup>-1</sup> s<sup>-1</sup>) directly after the next reduction step (curve 2). However, the activity decreased fast with ongoing reaction until values that were even slightly lower than those of the first deactivated state.

The transient activation effect was found to be reversible as the sample was re-reduced for the second time: the rate increased again until values only slightly lower than after the first re-reduction ( $200 \mu\text{mol g}_{\text{Pd}}^{-1}\text{s}^{-1}$ ) and showed a similar deactivation behavior during the isothermal measurement. Obviously the reduction at sub-HTR temperature of 473 K created a state of the catalyst that is much more active in CO-oxidation but that is also highly instable in the reaction atmosphere on the other hand.

In order to study the activation and deactivation behavior on the differently loaded Pd catalysts and its dependency on the reduction conditions in greater detail, the reactivity in CO-oxidation was determined in form of repeated, temperature-programmed reaction studies, so-called “light-off” curves. The performance of the catalysts in the individual reaction cycles was evaluated and compared based on the temperature of 50% conversion ( $T_{50}$ ) as well as the conversion at 425 K ( $X_{425}$ ). The parameters are summarized in table S2.2. The results for the 1 wt.-% loaded catalyst are presented in figure 2.10:

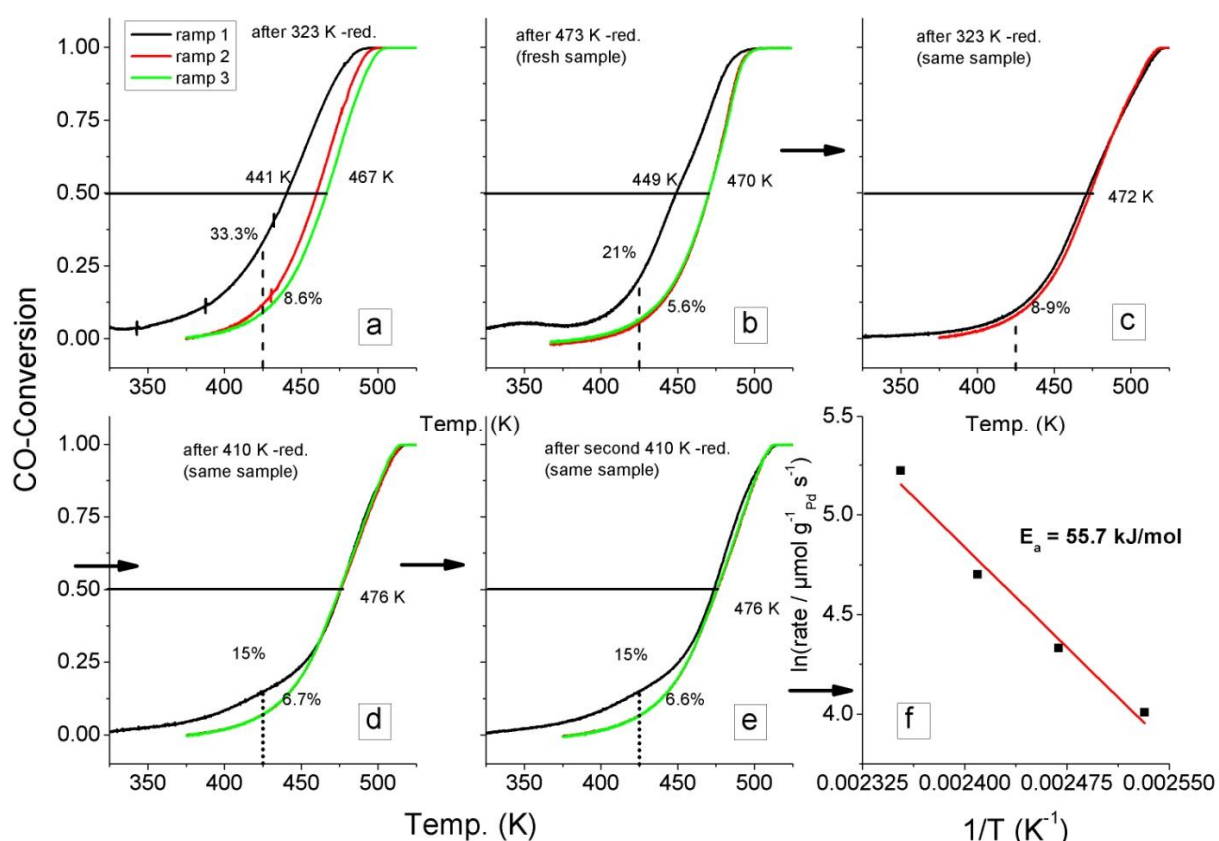


Fig. 2.10: CO-oxidation curves of the 1 wt.-% catalyst after reduction in hydrogen atmosphere at RT (panel a) and at 473 K (panel b, fresh sample), followed by RTR (c), repeated reduction at 410 K (same sample, d,e) and activation energy measurement in deactivated state (f).

In the first panel (a), the measurement after RTR (323 K) in 5% H<sub>2</sub> is presented. The sample has a comparably high initial activity but gradually deactivates with repeated reaction cycles. The second panel (b) shows the performance of a fresh sample, after 473 K – reduction in hydrogen. While the change of the reaction parameters with cycling is similar to RTR, a significant difference can be seen in the shape of the first reaction curve especially at low temperature.

In order to disentangle reversible and irreversible effects, the deactivated state, which is very similar in both experiments, independent of the pre-treatment, has been chosen as a more suitable reference state than the fresh catalyst. Therefore the same sample shown in panel b has been re-reduced (RTR, 323 K) in order to obtain a stable and metallic state of the catalyst. It can be seen in panel c that after this treatment the sample performs relatively stable with very similar T<sub>50</sub> and X<sub>425</sub> values compared to those found for the first measurements, indicating that all irreversible processes have been completed.

This state of the catalyst was further studied with regard to the reversible effects. It was re-reduced according to the TPR (Fig. S2.9) at a sub-HTR temperature of 410 K to set surface decoration of the Pd particles without bulk reduction of the support. Interestingly after this treatment, X<sub>425</sub> increased to 15% in the first oxidation cycle before decreasing again close to the value observed before (Fig. 2.10d). No difference in T<sub>50</sub> can be detected between the cycles. The fast deactivation can be notably seen as the curve after pre-treatment bends and approaches those of the following cycles with increasing temperature and conversion. Only the activity increase seen as the difference between the curves at low temperatures can be safely assigned to the effect of the reducing pre-treatment. The procedure has been repeated (Fig. 2.10e) in order to confirm the reversible promotion. Finally, the activation energy (Fig. 2.10f) of the deactivated state of the catalyst was determined in a temperature range of 395-425 K to about 56 kJ/mol, which is in the range reported for metallic palladium.<sup>21</sup>

A comparative study with a different reducing agent (CO instead of H<sub>2</sub>) and a test of higher reduction temperatures to study possible alloy formation effects was conducted based on the 5 wt.-% catalyst (Fig. 2.11). The catalytic data of the 2 wt.-% loaded sample after reduction in H<sub>2</sub> or CO were in general similar to those of the 1- and 5 wt.-% catalysts and can be found in the SI (Fig. S2.10).

The TPR of the 5 wt.-% Pd/Fe<sub>2</sub>O<sub>3</sub> catalyst was discussed in section 2.3.2 (Fig. 2.2) already. We recall that during reduction in CO additional TPR peaks were detected between RTR and HTR at 415 and 466 K which were not detected using hydrogen.

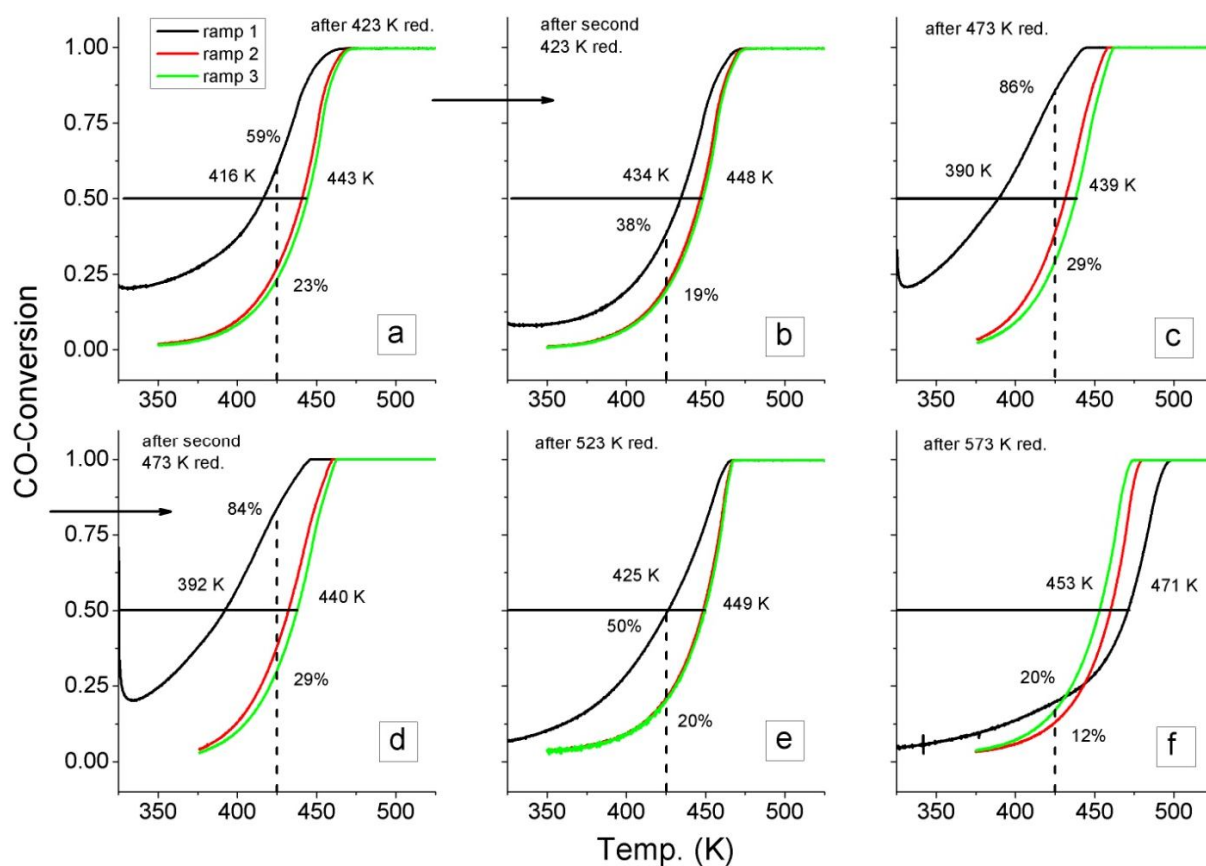


Fig. 2.11: CO-oxidation cycles of 5% catalyst after repeated reduction in 2% CO at 423 K (a,b) and at 473 K (c,d) as well as after HTR (523 K, e) and after 573 K (f).

For the first two measurements (Fig. 2.11a,b) a reduction temperature (2% CO) of 423 K was selected, to achieve a catalytic state present after the first reduction peak. The experiments look qualitatively similar to those of the 1% sample, but the 5% sample is clearly more active. In the first measurement the deactivation after three cycles (Fig. 2.11a) is more pronounced than after repeated reduction (Fig. 2.11b). Here, the initial high activity of the first cycle is only restored to some extent while the second and third cycles are identical which shows that the stable deactivated state was reached.

This is different from the sample that has been measured after reduction at 473 K, in a state after the second reduction peak (panels c+d): the two repeated measurements look almost completely identical with a much more active first reaction cycle. Again, the state was highly instable, though there was little further deactivation recorded between the second and the third cycle. After repeated measurements with the 473 K reduced catalyst, the activation energy in the deactivated state was determined in a range of 395-425 K again which remained in the same range (60 kJ/mol), similar to the 1% sample. Both CO-reduction treatments at 473 K and the  $E_a$  extrapolation can be found in SI (Fig. S2.11).

After HTR (523 K) of a fresh catalyst (Fig. 2.11e) the difference between first and last reaction cycle is less pronounced again. The second and the last cycle are completely overlapping, showing that all kinds of reversible or irreversible processes have finished already after the first cycle. This behavior is more pronounced after reduction of the catalyst at 573 K (panel f): this time, the first cycle is less active at higher temperatures, but still most active at lower temperatures. The second cycle is least active. This can be an indication for counteracting, overlapping processes.

### 2.3.6. XPS investigation before and after CO oxidation

To better connect the structural analysis and the catalytic data, the surface properties of the deactivated reference state and the highly active state formed during reductive pre-treatment of the catalysts were studied by XPS.

The development of the Pd3d core-level signal of the 1% and 2% Pd/Fe<sub>2</sub>O<sub>3</sub> samples was investigated at the HZB synchrotron facility during a temperature programmed reduction procedure. As mentioned, the samples were not in the as-prepared (freshly calcined) state anymore, but had already been reduced at 473 K and successively measured in CO-oxidation (3 cycles, 373-523 K, as described in the kinetic part). Under UHV conditions a first surface sensitive XPS scan at a kinetic energy of 150 eV (about 1 nm of information depth) was recorded. As it can be seen for the 2% sample in figure 2.12 (lower part), most of the Pd3d signal resembles oxidic palladium (337.4 eV, FWHM = 1.99), with a minor content of metallic Pd at 335.7 eV (FWHM = 1.38; Pd3d<sub>5/2</sub>). The binding energy values are slightly higher compared to literature values because of the particle size effect that leads to an up-shift due to the small Pd particles in our case.<sup>18,40-42</sup> Peak fitting showed that the oxidic content was 66 %. After TPR (until 473 K; 0.4 mbar H<sub>2</sub>) and further increase of the hydrogen partial pressure to 10 mbar at 473 K for 1h, the palladium oxide got reduced. As it can be seen in figure 2.12 (upper part), most of the palladium is in its metallic state (335.8 eV, FWHM = 0.95) now (71%). At 336.6 eV (FWHM = 1.50) another palladium species can be fitted that we attributed to SMSI: the palladium at the particle surface will be shifted to higher binding energy when being in contact with an iron oxide overlayer. The integrated amount of the new species of 29% would exactly represent the content of Pd atoms at the surface of the particles in the present Pd particle size, according to the dispersion calculation. Surface alloys like PdFe would also show an energy up-shift, depending on the treatment conditions as described in the literature,<sup>43-47</sup> but our IR data did not confirm alloy-induced shifts in the CO

wave numbers as reported for example by Felicissimo<sup>9</sup> or Wu et al.<sup>23</sup>

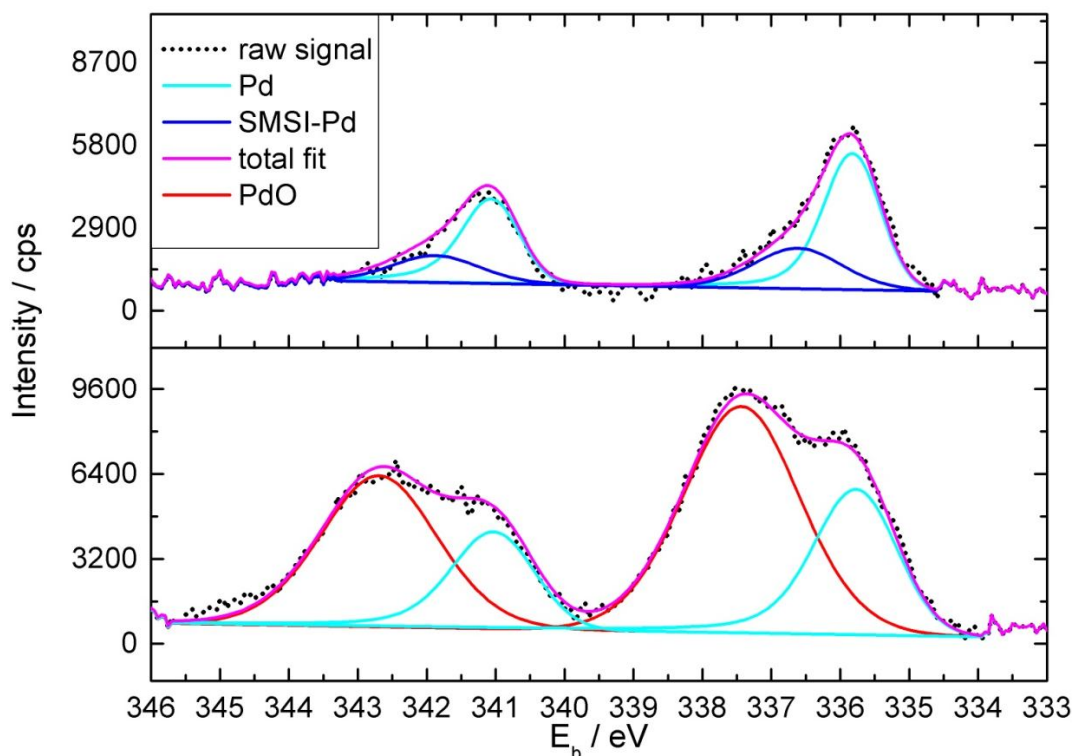


Fig. 2.12: Pd3d signal of 2% Pd/Fe<sub>2</sub>O<sub>3</sub> sample at  $E_{\text{kin}} = 150$  eV in deactivated state (lower panel) and after in-situ reduction (upper panel).

In order to confirm enrichment of iron oxide species on the palladium particles during the reduction process, the intensities of Pd and Fe at the surface ( $E_{\text{kin}} = 150\text{-}200$  eV) and in the bulk (700-800 eV) were integrated at different stages of the reduction, as summarized in table S2.1 (supplemental). The results are depicted in figure 2.13: the atomic ratio of Pd : Fe near the surface before the reduction was 3.1 to 96.9 and decreased until 2.0 to 98.0 after reduction (2% sample). In comparison to the surface, the ratio in the bulk stayed almost constant (2.4 to 97.6 before and 2.5 to 97.5 after reduction). In case of the 1% sample the results were comparable. With ongoing reduction, segregation of iron oxide on the palladium particles was confirmed.

As for the changes in the iron oxide support phase between the deactivated and the freshly reduced state of the 2% sample, we refer to the NEXAFS part (Fe L absorption edge, supporting information, Fig. S2.8). C1s spectra of the same sample before and after in-situ reduction are presented in Fig. S2.12: during reduction, the amount of carbonate species formed during the CO-oxidation decreased.

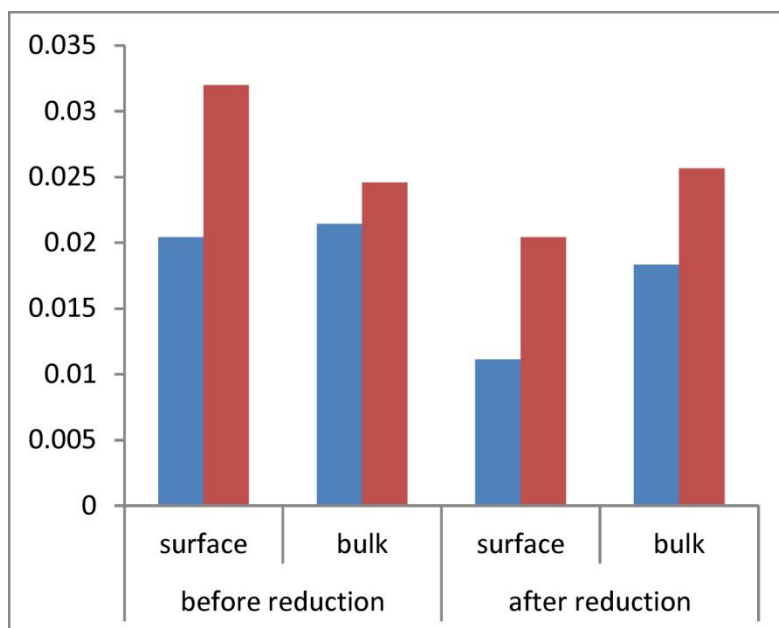


Fig. 2.13: surface and bulk Pd/Fe ratio of the 1% (blue bars) and 2% (red bars) sample, before and after reduction.

## 2.4. Summary and Discussion

In our work we investigated the structural changes in the bulk as well as on the surface of homogeneous, co-precipitated Pd-iron oxide powder catalysts with different palladium loadings during reduction under various conditions and their influence on the catalytic activity in CO-oxidation. All samples were synthesized in a controlled way with a uniform particle size distribution. Therefore size-dependent differences among one investigated sample can be excluded. We were able to find a clear indication for the formation of surface decoration on all differently loaded catalysts depending on the reduction temperature or medium. This SMSI effect was found to be reversible and it was observed independent of bulk phase changes, alloy formation or irreversible processes like sintering or deactivation by possible by-product (e.g. carbonate) formation.

By DRIFTS- and CO-chemisorption measurements, it could be shown that the adsorption capacity for carbon monoxide in the state after reduction at 473 K (both for hydrogen and CO-reduction) got decreased to almost zero, while no additional crystalline phase could be detected in XRD. Re-calcination restored the adsorption capacity by 88% (2% sample) and by 60% (1% sample) compared to the initial capacity. The higher palladium dispersion apparently increases the sensitivity for irreversible deactivation processes like agglomeration. It was shown in the TPR and TG experiments that spill-over plays a significant role in case of



hydrogen atmosphere leading to a continuous reduction of neighboring iron oxide around Pd particles. This increases the mobility and wetting probability of the support and leads to an overgrowth of reduced iron oxides onto the palladium. In contrast to that reduction in CO atmosphere was associated with a separate peak and did not induce SMSI-formation before 423 K. HR-TEM images in the 473 K reduced state confirmed the formation of an amorphous overlayer.

XPS investigation of the 1% and 2% samples by hands of a performed depth profile confirmed an overgrowth of iron oxide support over the palladium particles which was concluded due to a reduced Pd:Fe ratio at the surface with ongoing reduction, in contrast to the unchanged bulk ratio. In case of the 2% sample, detailed fits of the XP-spectra after CO-oxidation measurements compared to those in an in-situ reduced state revealed the presence of metallic and oxidic palladium in the deactivated (reacted) state while the presence of a second palladium species shifted to higher binding energy compared to metallic Pd in case of the freshly reduced state delivered further proof for surface decoration, probably by an Fe-O layer, in analogy to the Pt/FeO<sub>x</sub> model system.<sup>1,4</sup> The amount of the new species was identical with the Pd dispersion determined by CO chemisorption. XPS further confirmed the presence of carbonate species after the CO oxidation measurements as well as their decrease upon reduction.

Palladium oxide formation during the kinetic measurements was also confirmed by DRIFTS (Fig. 2.7) and by the reduction profile after the reaction (Fig. S2.9). However the influence of that process on the activity was limited (Fig. 2.10c). The structural results (XRD) upon increased reduction temperature showed the possible formation of a PdFe alloy, most likely in the structure of Pd<sub>3</sub>Fe but with increased iron content (iso-structural substitution). It started to form only at temperatures higher than 473 K, most likely at the surface. At 473 K, IR experiments however did not confirm alloy formation. NEXAFS spectra of the reduced sample after CO oxidation revealed that most of the support is in the hematite phase, with increasing magnetite content during in-situ reduction.

The surface decorated state led to a transient high activity in CO-oxidation, which is in agreement with earlier studies of the SMSI phenomenon.<sup>1,4,5,11</sup> Furthermore, the high volatility and reversible re-formation of the SMSI state during a second reduction step at sufficiently high temperatures was confirmed. The degree of volatility apparently also depends on the palladium particle size that is in a direct correlation to the palladium loading: electronic conditions at the metal-support interface in case of sub-nm sized palladium particles present on the 1% sample, lead to a faster oxidative destruction of the overgrowth

layer. After several reaction cycles and minimization of irreversible processes, the deactivated state after SMSI destruction was found to be relatively stable, with only moderate further deactivation, probably by carbonate formation. The higher initial activity (first reaction cycle after RTR) is attributed to a higher Pd dispersion and agglomeration during the reaction. The activity of the 5% sample in general was higher compared to the other samples due to a higher BET surface area and a higher Pd surface area.

While the instability of the SMSI state prohibits its industrial application in sustained CO-oxidation, this reaction overall was found to be a suitable test reaction for the convenient study of reactivity and stability of the SMSI phenomenon and decouple it from the other, above-mentioned processes. Though it could be shown that the formation of SMSI is occurring independently of the phase transformation of the bulk hematite phase into the magnetite polymorph or alloying, such processes nevertheless play an important role with regard to activity decrease in the kinetic measurements of CO-oxidation, probably by limiting the metal-support interface. The activation energy of the deactivated samples was comparably low but in the range of literature values for metallic palladium.<sup>11,21</sup>

## **2.5. Conclusion**

The present study revealed that careful CO-oxidation can be applied to detect the specific chemical state of the catalyst. The variations in the present data as well as in the literature are a sign for the chemical dynamics of the system and not of the unsuitability of the CO-oxidation reaction as a chemical spectrometer for the reactivity of a Pd catalyst under ambient conditions. The special case of Pd/Fe will be extended to other catalytic systems in the effort to verify a generic character of the method.

### **Acknowledgement:**

Dr. Marc Armbrüster (MPI Dresden) is acknowledged for the synthesis of the PdFe reference samples for the comparison of the lattice parameters. Maike Hashagen is acknowledged for BET measurements. Wiebke Frandsen and Norbert Pfänder are acknowledged for microscopy measurements. Andrey Tarasov is acknowledged for TG-DSC measurements. The HZB is acknowledged for the allocation of beam time.

## 2.6. References

1. Lewandowski, M. Scanning Tunneling Microscopy Study of Iron Oxide based Model Catalysts. (Technische Universität Berlin, 2011). <<http://opus4.kobv.de/opus4-tuberlin/frontdoor/index/index/docId/3060>>
2. Lewandowski, M., Sun, Y. N., Qin, Z.-H., Shaikhutdinov, S. & Freund, H.-J. Promotional effect of metal encapsulation on reactivity of iron oxide supported Pt catalysts. *Appl. Catal. Gen.* **391**, 407–410 (2011).
3. Willinger, M. G. *et al.* Metall-Substrat-Wechselwirkung: Kombination von hochauflösender Mikroskopie und Modellsystemen, um die atomare Struktur von Grenzflächen aufzuklären. *Angew. Chem.* **126**, 6108–6112 (2014).
4. Schalow, T. Bildung und katalytische Aktivität partiell oxidierter Pd-Nanopartikel. (Technische Universität Berlin, 2006). <<http://opus.kobv.de/ubp/volltexte/2007/1474/>>
5. Schalow, T. *et al.* CO oxidation on partially oxidized Pd nanoparticles. *J. Catal.* **242**, 58–70 (2006).
6. Schalow, T. *et al.* Formation of interface and surface oxides on supported Pd nanoparticles. *Surf. Sci.* **600**, 2528–2542 (2006).
7. Schalow, T. *et al.* Oxygen-induced Restructuring of a Pd/Fe<sub>3</sub>O<sub>4</sub> Model Catalyst. *Catal. Lett.* **107**, 189–196 (2006).
8. Wang, H.-F., Kaden, W. E., Dowler, R., Sterrer, M. & Freund, H.-J. Model oxide-supported metal catalysts – comparison of ultrahigh vacuum and solution based preparation of Pd nanoparticles on a single-crystalline oxide substrate. *Phys. Chem. Chem. Phys.* **14**, 11525-11533 (2012).
9. Felicissimo, M. P., Martyanov, O. N., Risse, T. & Freund, H.-J. Characterization of a Pd–Fe bimetallic model catalyst. *Surf. Sci.* **601**, 2105–2116 (2007).
10. Freund, H.-J., Meijer, G., Scheffler, M., Schlögl, R. & Wolf, M. Die CO-Oxidation als Modellreaktion für heterogene Prozesse. *Angew. Chem.* **123**, 10242–10275 (2011).
11. Naumann d’Alnoncourt, R. *et al.* Strong metal–support interactions between palladium and iron oxide and their effect on CO oxidation. *J. Catal.* **317**, 220–228 (2014).
12. Chen, S., Si, R., Taylor, E., Janzen, J. & Chen, J. Synthesis of Pd/Fe<sub>3</sub>O<sub>4</sub> Hybrid Nanocatalysts with Controllable Interface and Enhanced Catalytic Activities for CO Oxidation. *J. Phys. Chem. C* **116**, 12969–12976 (2012).
13. Jiang, X. C. & Yu, A. B. Synthesis of Pd/ $\alpha$ -Fe<sub>2</sub>O<sub>3</sub> nanocomposites for catalytic CO oxidation. *J. Mater. Process. Technol.* **209**, 4558–4562 (2009).

14. Kalinkin, A. V., Savchenko, V. I. & Pashis, A. V. Mechanism of low-temperature CO oxidation on a model Pd/Fe<sub>2</sub>O<sub>3</sub> catalyst. *Catal. Lett.* **59**, 115–119 (1999).
15. Qiao, B., Liu, L., Zhang, J. & Deng, Y. Preparation of highly effective ferric hydroxide supported noble metal catalysts for CO oxidations: From gold to palladium. *J. Catal.* **261**, 241–244 (2009).
16. Golunski, S., Rajaram, R., Hodge, N., Hutchings, G. J. & Kiely, C. J. Low-temperature redox activity in co-precipitated catalysts: a comparison between gold and platinum-group metals. *Catal. Today* **72**, 107–113 (2002).
17. Liu, L. *et al.* Low-temperature CO oxidation over supported Pt, Pd catalysts: Particular role of FeO<sub>x</sub> support for oxygen supply during reactions. *J. Catal.* **274**, 1–10 (2010).
18. Liu, L. *et al.* Catalytic co-oxidation of CO and H<sub>2</sub> over FeO<sub>x</sub>-supported Pd catalyst at low temperatures. *J. Catal.* **294**, 29–36 (2012).
19. Weiliang, H., Peng, Z., Xia, P., Zhicheng, T. & Gongxuan, L. Highly active Pd/Fe based catalyst prepared with polyol-reduction method for low-temperature CO oxidation. *J. Environ. Chem. Eng.* **1**, 189–193 (2013).
20. Xu, G., Zhu, Y., Ma, J., Yan, H. & Xie, Y. in *Studies in Surface Science and Catalysis* (ed. Can Li and Qin Xin) **112**, 333–338 (Elsevier, 1997).
21. Engel, T. & Ertl, G. A molecular beam investigation of the catalytic oxidation of CO on Pd (111). *J. Chem. Phys.* **69**, 1267–1281 (1978).
22. Zhang, Z. *et al.* Ultrafine nanoporous PdFe/Fe<sub>3</sub>O<sub>4</sub> catalysts with doubly enhanced activities towards electro-oxidation of methanol and ethanol in alkaline media. *J. Mater. Chem. A* **1**, 3620–3628 (2013).
23. Wu, C.-T. *et al.* A non-syn-gas catalytic route to methanol production. *Nat. Commun.* **3**, 1050–1057 (2012).
24. Biehl, G. & Flanagan, T. B. Anomalous lattice parameters and hydrogen solubilities in dilute PdFe alloys. *Solid State Commun.* **28**, 751–755 (1978).
25. Knözinger, H. & Gates, B. C. in *Advances in Catalysis* **47**, xiii–xiv (Academic Press, 2002).
26. Rupprechter, G. *et al.* Sum frequency generation vibrational spectroscopy at solid–gas interfaces: CO adsorption on Pd model catalysts at ambient pressure. *Surf. Sci.* **502–503**, 109–122 (2002).
27. Gabasch, H. *et al.* Comparison of the reactivity of different Pd-O species in CO oxidation. *Phys. Chem. Chem. Phys.* **9**, 533–540 (2007).

28. Choi, K. I. & Vannice, M. A. CO oxidation over Pd and Cu catalysts I. Unreduced PdCl<sub>2</sub> and CuCl<sub>2</sub> dispersed on alumina or carbon. *J. Catal.* **127**, 465–488 (1991).
29. Zhang, Y. *et al.* The effects of the Pd chemical state on the activity of Pd/Al<sub>2</sub>O<sub>3</sub> catalysts in CO oxidation. *Catal. Sci. Technol.* (2014). doi:10.1039/C4CY00552J
30. Dutta, G., Gupta, A., Waghmare, U. V. & Hegde, M. S. CO adsorption on ionic Pt, Pd and Cu sites in Ce<sub>1-x</sub>M<sub>x</sub>O<sub>2-δ</sub> (M = Pt<sup>2+</sup>, Pd<sup>2+</sup>, Cu<sup>2+</sup>). *J. Chem. Sci.* **123**, 509–516 (2011).
31. Baidya, T. *et al.* DRIFTS studies on CO and NO adsorption and NO + CO reaction over Pd<sup>2+</sup>-substituted CeO<sub>2</sub> and Ce<sub>0.75</sub>Sn<sub>0.25</sub>O<sub>2</sub> catalysts. *J. Catal.* **303**, 117–129 (2013).
32. Zhu, H., Qin, Z., Shan, W., Shen, W. & Wang, J. Pd/CeO<sub>2</sub>-TiO<sub>2</sub> catalyst for CO oxidation at low temperature: a TPR study with H<sub>2</sub> and CO as reducing agents. *J. Catal.* **225**, 267–277 (2004).
33. Jusczyk, W. *et al.* Characterization of supported palladium catalysts: III. PdAl<sub>2</sub>O<sub>3</sub>. *J. Catal.* **120**, 68–77 (1989).
34. Martínez-Arias, A. *et al.* New Pd/Ce<sub>x</sub>Zr<sub>1-x</sub>O<sub>2</sub>/Al<sub>2</sub>O<sub>3</sub> three-way catalysts prepared by microemulsion: Part 2. In situ analysis of CO oxidation and NO reduction under stoichiometric CO+NO+O<sub>2</sub>. *Appl. Catal. B Environ.* **31**, 51–60 (2001).
35. Fernandezgarcia, M. Influence of Ceria on Pd Activity for the CO+O<sub>2</sub> Reaction. *J. Catal.* **187**, 474–485 (1999).
36. Bensalem, A., Muller, J.-C., Tessier, D. & Bozon-Verduraz, F. Spectroscopic study of CO adsorption on palladium-ceria catalysts. *J. Chem. Soc. Faraday Trans.* **92**, 3233–3237 (1996).
37. Zhu, H., Qin, Z., Shan, W., Shen, W. & Wang, J. CO oxidation at low temperature over Pd supported on CeO<sub>2</sub>-TiO<sub>2</sub> composite oxide. *Catal. Today* **126**, 382–386 (2007).
38. Rades, T., Borovkov, V. Y., Kazansky, V. B., Polisset-Thfoin, M. & Fraissard, J. Diffuse Reflectance IR Study of CO Adsorption on a Bimetallic Pt–Pd Catalyst Supported on NaY Zeolite. Evidence of Alloy Formation. *J. Phys. Chem.* **100**, 16238–16241 (1996).
39. Han, Y.-F. *et al.* Au Promotional Effects on the Synthesis of H<sub>2</sub>O<sub>2</sub> Directly from H<sub>2</sub> and O<sub>2</sub> on Supported Pd–Au Alloy Catalysts. *J. Phys. Chem. C* **111**, 8410–8413 (2007).
40. Balmes, O. *et al.* Reversible formation of a PdC<sub>x</sub> phase in Pd nanoparticles upon CO and O<sub>2</sub> exposure. *Phys. Chem. Chem. Phys.* **14**, 4796–4801 (2012).

41. Delbecq, F. General trends in the electronic properties of alloys of transition metals: a semi-empirical study of CO adsorption. *Surf. Sci.* **389**, L1131–L1139 (1997).
42. Aiyer, H. N., Vijayakrishnan, V., Subbanna, G. N. & Rao, C. N. R. Investigations of Pd clusters by the combined use of HREM, STM, high-energy spectroscopies and tunneling conductance measurements. *Surf. Sci.* **313**, 392–398 (1994).
43. Tarasevich, M. R. *et al.* Oxygen kinetics and mechanism at electrocatalysts on the base of palladium–iron system. *Electrochimica Acta* **52**, 5108–5118 (2007).
44. Ji, Y. *et al.* Room-temperature synthesis and electrocatalysis of carbon nanotubes supported palladium–iron alloy nanoparticles. *Electrochimica Acta* **111**, 898–902 (2013).
45. Yang, J., Zhou, W., Cheng, C. H., Lee, J. Y. & Liu, Z. Pt-Decorated PdFe Nanoparticles as Methanol-Tolerant Oxygen Reduction Electrocatalyst. *ACS Appl. Mater. Interfaces* **2**, 119–126 (2010).
46. Shao, M.-H., Sasaki, K. & Adzic, R. R. Pd–Fe Nanoparticles as Electrocatalysts for Oxygen Reduction. *J. Am. Chem. Soc.* **128**, 3526–3527 (2006).
47. Zhang, S. L. & Zhang, J. R. Photoemission and Mössbauer Effect Studies of Sputter-Deposited Fe-Pd Alloys. *Phys. Status Solidi B* **182**, 421–427 (1994).

## Supplementary Information

### A. Experimental

#### Catalyst synthesis:

450 ml of a diluted (0.1 M) solution of  $\text{Fe}(\text{NO}_3)_3 \cdot 9\text{H}_2\text{O}$  (Merck) were mixed with appropriate amounts of a  $\text{Pd}(\text{NO}_3)_2$ -solution (8.3 wt.-% Pd-content in 10 wt.-%  $\text{HNO}_3$ ; Alfa Aesar) and precipitated drop-wise with 0.4 M NaOH solution in an automated reactor-system (Labmax, Mettler-Toledo), which contained already about 400 ml of deionized water. During the precipitation (acid solution addition rate of 6 g/min), the pH-value (pH = 4), temperature ( $T = 298 \text{ K}$ ) and stirring rate ( $r = 300 \text{ rpm}$ ) were monitored and kept constant in order to assure the most similar conditions and chemical potential for every forming crystallite and thus the best possible product homogeneity. After precipitation, the product was aged for 1 h (100 rpm, RT), filtered and washed three times (3x 1l of demin. water) until conductivity measurement of the solution detected  $< 0.01 \text{ mS}$ . An example of a co-precipitation protocol is given in figure S2.1. For the highest loaded sample (5%), a metal solution of 0.2 M and a precipitation pH-value of 9 were used.

ICP-OES measurements were performed using an Ultima 2 spectrometer (Horiba Jobin Yvon Inc., 120-800 nm) after sample digestion in HF/aqua regia.

A Hitachi S-4800 SEM was used as well as a FEI Cs-corrected Titan 80-300 microscope for STEM/TEM images. Samples in air-sensitive (SMSI) state (after reduction at about 473 K) were transferred into the microscope without air contact, with the help of a glove box. An energy dispersive X-ray detector (Genesis 4000) was used for elemental mapping and composition analysis.

For the TPR measurements the samples have been pre-dried in pure He (RT - 623 K, 5 Kpm heating rate, hold 30 min.) to minimize the content of residual water. It has to be noted that the exact position of the reduction signals varied between the two 5% samples and also depended on the pre-drying of the sample: smaller crystallite containing and non-dried samples seemed to be reduced slightly earlier compared to the other ones.

DRIFTS measurements were recorded with an MCT detector at a resolution of 4/cm, accumulating 512 scans, using a Praying Mantis<sup>TM</sup> high temperature reaction chamber (ZnSe window) placed in a Bruker IFS 66 spectrometer controlled by OPUS software. Measurements were performed in an in-situ cell capable of heat treatment under gas flow conditions (Bronkhorst mass flow controllers). The samples were activated in flowing hydrogen (5% in Ar, 50 ml/min) at 323 and 473 K (subsequent experiments with one sample, mass: about 85 mg). CO (2% in Ar, 50 ml/min) was purged through the cell at 298 K for 1h, before the gas phase CO was removed by 30 min of Ar purging. The spectra were recorded at room temperature with a background spectrum of pure KBr performed at the same temperature. The used gases were supplied by Westfalen (99.99% purity at least). Ar was further purified by passing through Hydrosorb and Oxysorb cartridges.

The X-ray diffraction (XRD) measurements were performed in Bragg-Brentano geometry on a Bruker AXS D8 Advance theta/theta diffractometer equipped with a secondary graphite monochromator (Cu  $K_{\alpha 1+2}$  radiation) and scintillation detector. The sample powder was filled into the recess of a cup-shaped sample holder, the surface of the powder bed being flush with the sample holder edge. The XRD data were analyzed by full pattern fitting according to the Rietveld method in conjunction with the fundamental parameter approach for the instrumental and double-Voigt approach for the sample contribution to the peak profiles as implemented in the TOPAS software (Bruker, version 4.2). The XRD setup was equipped with an in-situ reactor cell. Reaction gases were mixed by means of mass flow controllers (Bronkhorst).

In case of in-situ reduction in hydrogen atmosphere, measurements were performed before reduction and after reduction of the sample at RT, 523 K, 623 K and 723 K (#13757). All scans were recorded at RT in He atmosphere.

Simultaneous TG-DSC measurements were carried out on a Netzsch STA 449C Jupiter thermoanalyzer equipped with an electromagnetic microbalance with top loading and 0.1  $\mu$ g resolution. The relative error of weight-determination was 0.5%. A highly sensitive sample carrier with a disk-shaped Pt/Pt-Rh thermocouple was used. Measurements were performed in the temperature range of 293-523K under controlled flow conditions (100 ml/min, 21% O<sub>2</sub>,

79% Ar), applying a heating rate of 1 Kpm and using 25 mg of sample, placed in a corundum crucible (45  $\mu$ l) without lids. Gases were monitored by MS.

In-situ XPS was performed at the ISSS beamline at the BESSY II synchrotron at the Helmholtz Zentrum Berlin. The experimental setup has been described in detail in the following references.<sup>1,2</sup> The samples were placed on a sample holder that could be heated by an IR laser (808 nm). The temperature was measured by a Ni-CrNi thermocouple which was fixed onto the sample surface. Gas flow into the analysis chamber was adjusted by mass flow controllers for He and H<sub>2</sub> – up to 10 mbar hydrogen partial pressure were applied for thermal reduction of the catalysts. A QMS was connected to the sample cell by a leak valve in order to control the gas phase composition during the surface characterization. All photoelectron spectra were normalized by the storage ring current and the energy dependent incident photon flux that was measured prior by using gold foil with known quantum efficiency. The binding energy scale was calibrated to the Fermi level of the hemispherical electron analyzer. Surface sensitive detail scans of the Fe2p and the Pd3d binding energy region were performed at a constant kinetic energy of 150 eV and a beam slit of 111  $\mu$ m. The respective binding energy has been calibrated with the help of valence band spectra and the adventitious C1s signal. For one sample, depth profiling has been conducted, measuring electrons with kinetic energy of 700 (Fe2p) resp. 800 (Pd3d) eV. Surface and subsurface concentrations of the respective element have been calculated by normalized, integrated peak intensities, taking into account the photo-energy dependence of the atomic sub-shell photoionization cross-section of the respective orbitals.<sup>3</sup> Additional NEXAFS measurements of the Fe L-edge (700-730 eV photo energy, 15 eV pass energy, 60  $\mu$ m beam slit) have been performed.

The Pd species were fitted with a GL-ratio of 30%, (deshape parameter 0.01, 400) for metallic Pd.

CO-chemisorption measurements were carried out in an Autosorb-1C chemisorption setup (Quantachrome Incorp.), equipped with a reactor for pretreatment of the sample under flow conditions. For reduction the setup was connected to a gas bottle with 5% H<sub>2</sub>-Ar mixture. Usually, the sample was reduced at 323 K for 30 min. to reduce oxidic Pd species before measuring two adsorption isotherms at 313 K and in the pressure range of 3-747 mbar, the first isotherm representing both, reversibly (weakly) and irreversibly (strongly) adsorbed CO and the second isotherm (measured after evacuation) only representing the physisorbed species. By subtracting the second from the first isotherm and extrapolating the volume to a pressure of zero, the volume of chemisorbed CO was determined. By assuming a shape-factor for the Pd-particles of 6 and further assuming that every second Pd surface atom is covered by one CO-molecule, in average, the active surface area, the dispersion and the average diameter of the particles was calculated. Some samples were reduced at higher temperatures to generate and investigate particle decoration by the support (SMSI). After all reduction steps the sample was dried for 2 h (393 K) under He flow, before being evacuated for 2 h at the same temperature.

BET measurements were conducted in an Autosorb-6-B N<sub>2</sub>-physisorption setup (Quantachrome Incorp.) at liquid nitrogen temperature. Samples were degassed in a dynamic vacuum for 2 h at 423 K before starting the measurement. After measuring adsorption and



desorption isotherms, the total surface area of the sample was calculated according the BET method, using 11 points of the linear range of the desorption isotherm.

## B. Figures

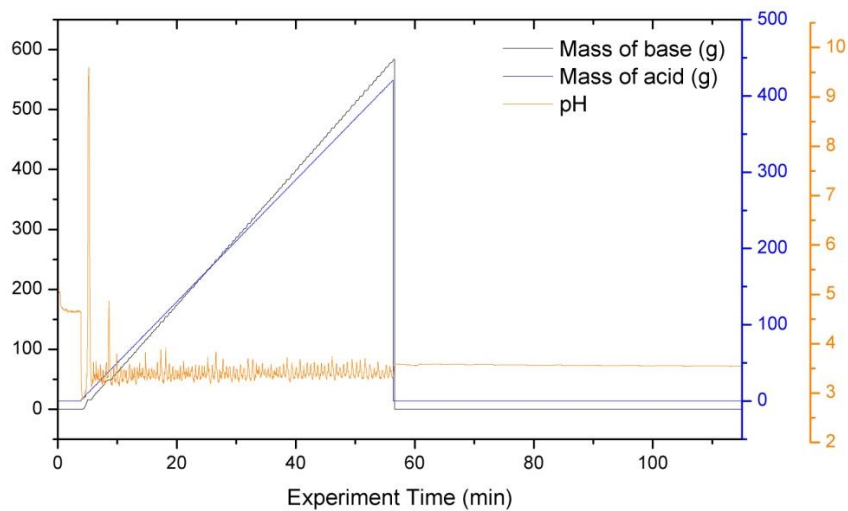


Fig. S2.1: synthesis protocol for 2 wt.-% Pd/FeO<sub>x</sub> (uncalcined precursor of #17233)

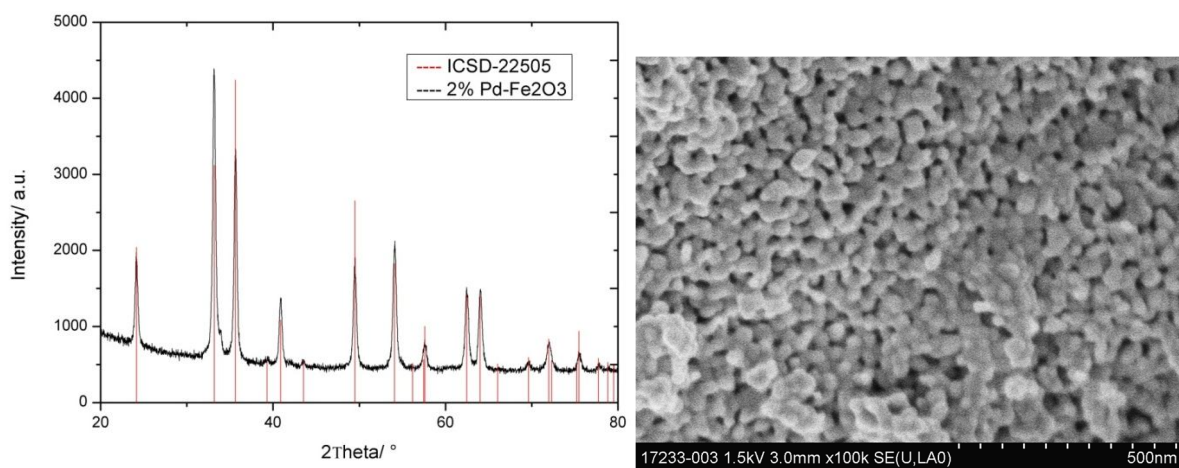


Fig. S2.2a+b: XRD-pattern of #17233 (calcined at 823 K) and corresponding SEM image

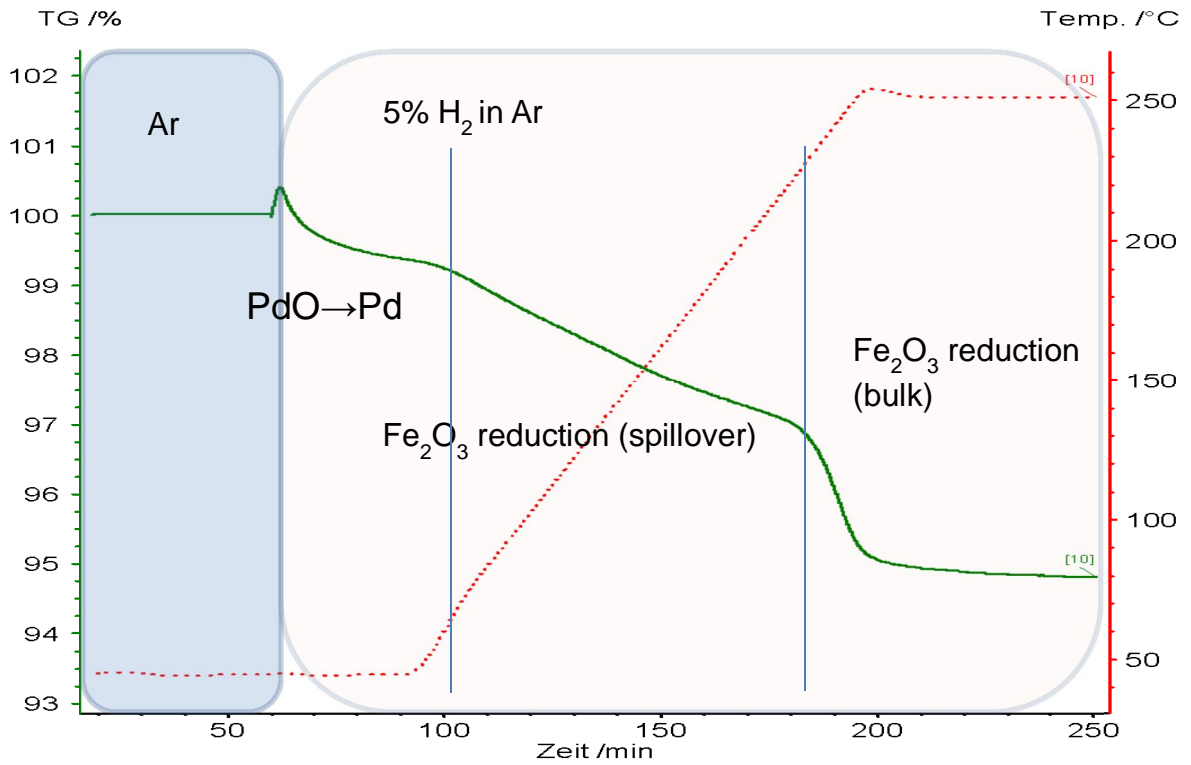


Fig. S2.3a: TG-profile of dried 5% sample 13757 during reduction in 5% H<sub>2</sub>

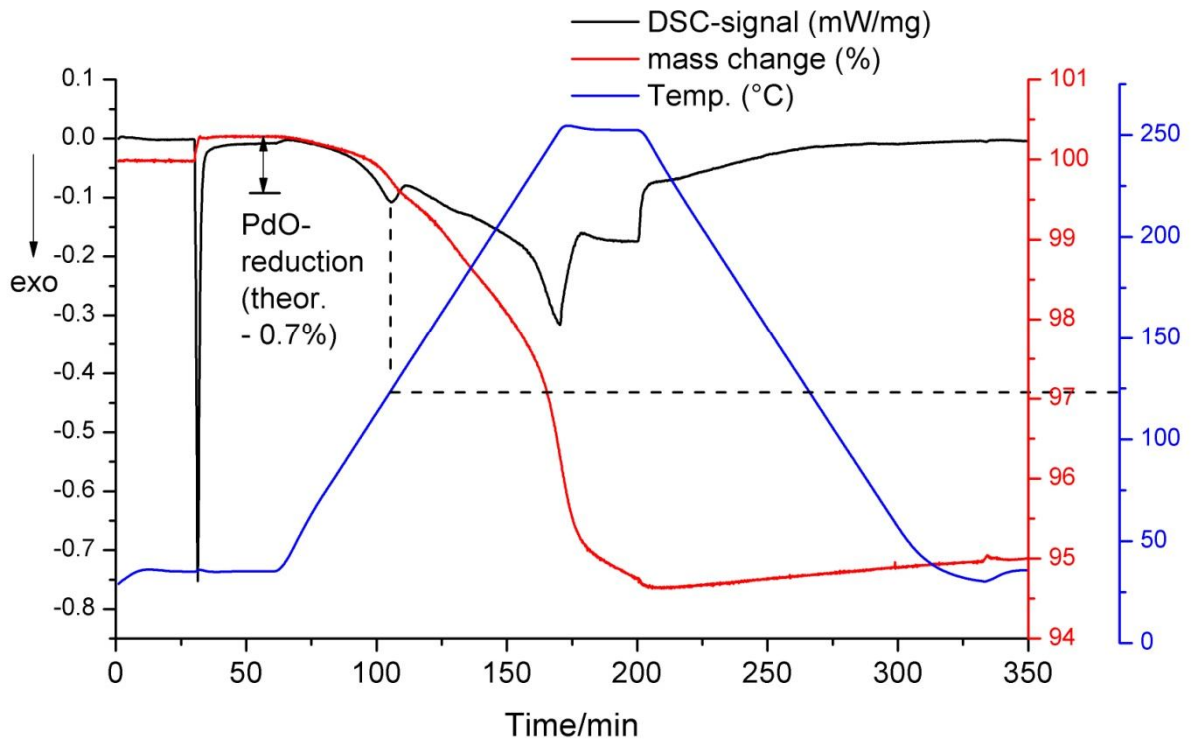


Fig. S2.3b: TG-DSC-profile of dried 5% sample 13757 during reduction in 2% CO.  
(samples dried in 20% O<sub>2</sub>-Ar at 773 K for 30 min.).

As it can be seen in figure S2.3a, the hematite supported PdO is already completely reduced at room temperature, after the feed gas has been switched from pure argon to the H<sub>2</sub>-Ar mixture. The short mass increase corresponds to the Buoyancy effect which is related to the changing density of the flowing gas. Consideration of that change by a blanket measurement does not include the sample volume. The reduction of the mass by about 0.75% corresponds to the calculated mass loss for assumed complete PdO reduction. Upon heating we observe further constant mass loss of about 2% until about 225 °C.

The mass change during TPR corresponds to formation of water by spill-over reduction of the iron oxide support by the hydrogen that is atomically adsorbed on the metallic palladium in the end.

The following step indicates the reduction of bulk hematite to magnetite. The calculated weight loss for that step would be 3.2 %. In our case, the mass loss is only about 2.2% because some content of the bulk hematite has already been reduced by the spill-over that leads to SMSI formation. In case of the TG-DSC measurement in 2% CO-Ar atmosphere (fig. S2.3b), complete Pd oxide reduction is only reached at around 125 °C, with a similar behavior (SMSI-formation, bulk reduction to magnetite) with further increasing temperature as compared to the hydrogen experiment.

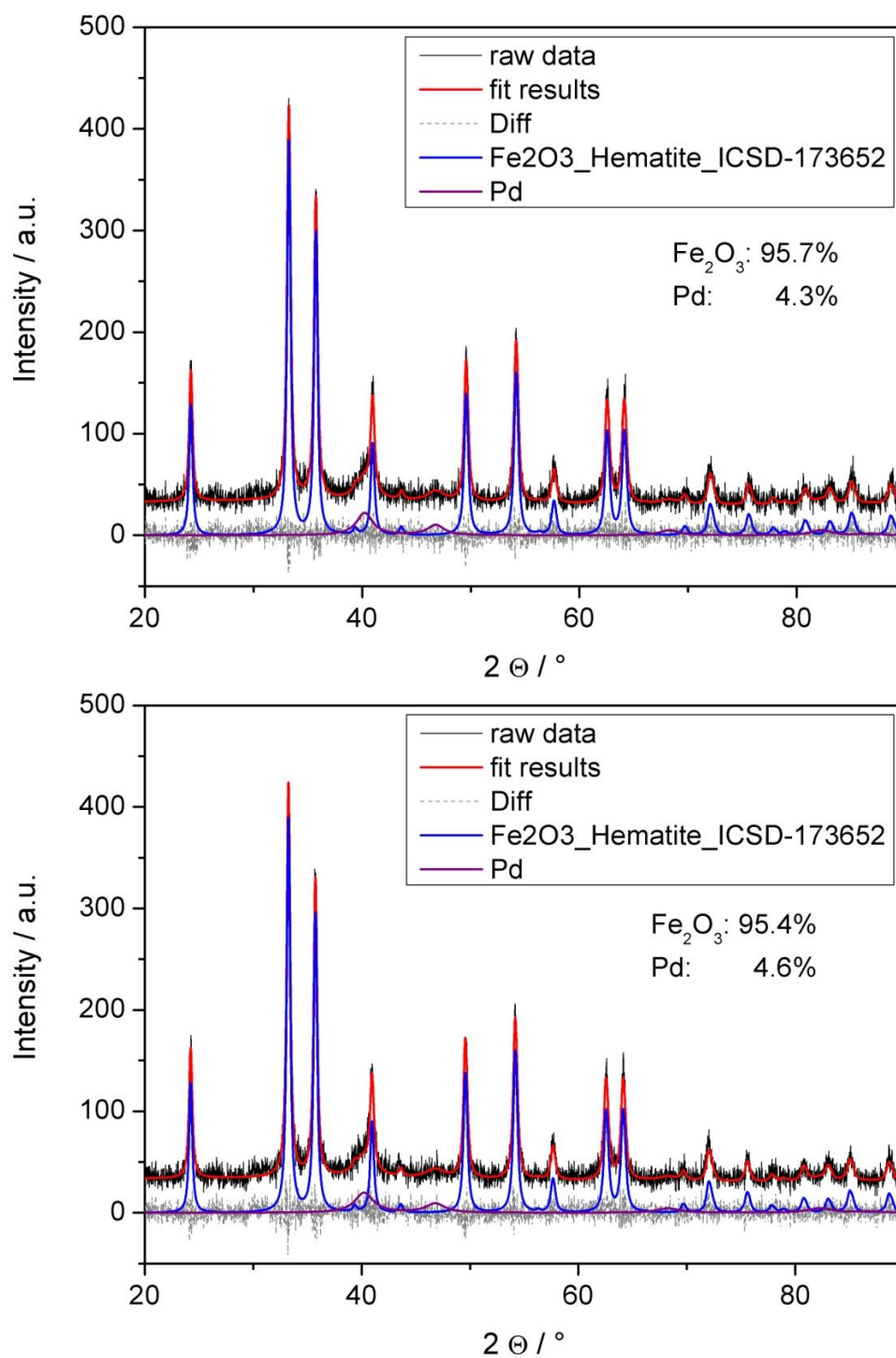


Fig. S2.4: Rietveld refined XRD of 5% sample 13757 after CO-reduction at 423 K (upper part) and at 473 K (lower part)

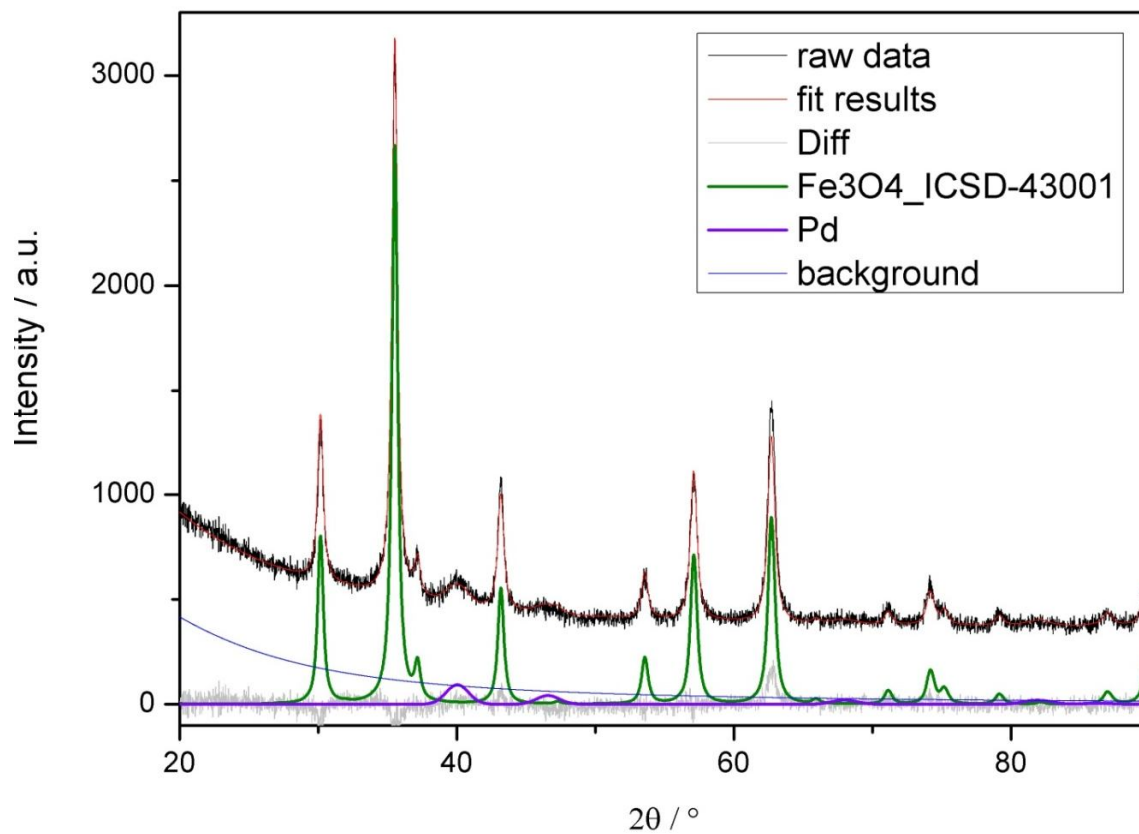


Fig. S2.5: XRD of # 13757 after reduction in 2% CO at 523 K.

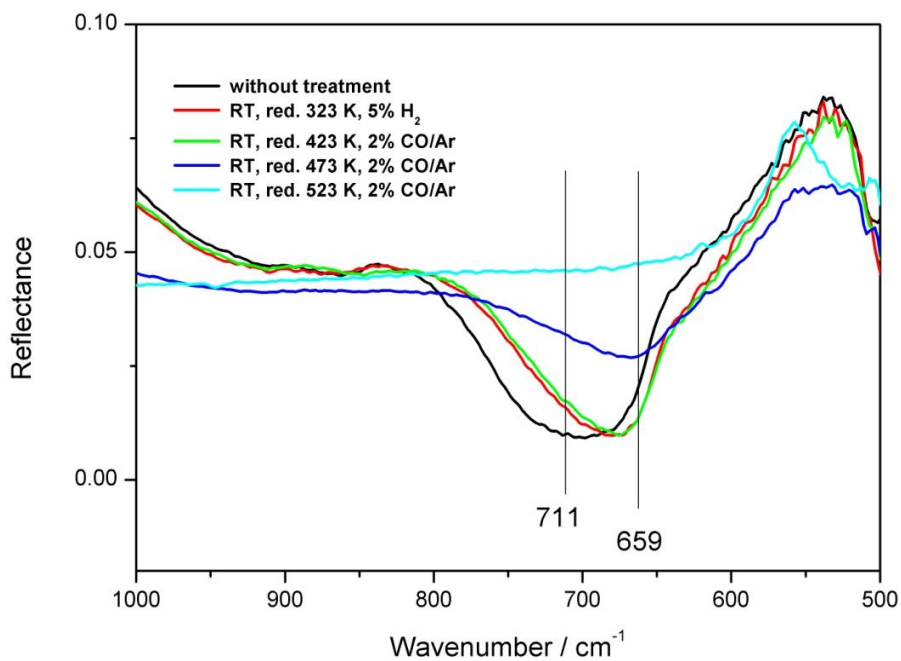


Fig. S2.6: Fe-O-vibrations<sup>4</sup> during reduction of 5% Pd catalyst in 2% CO-Ar.

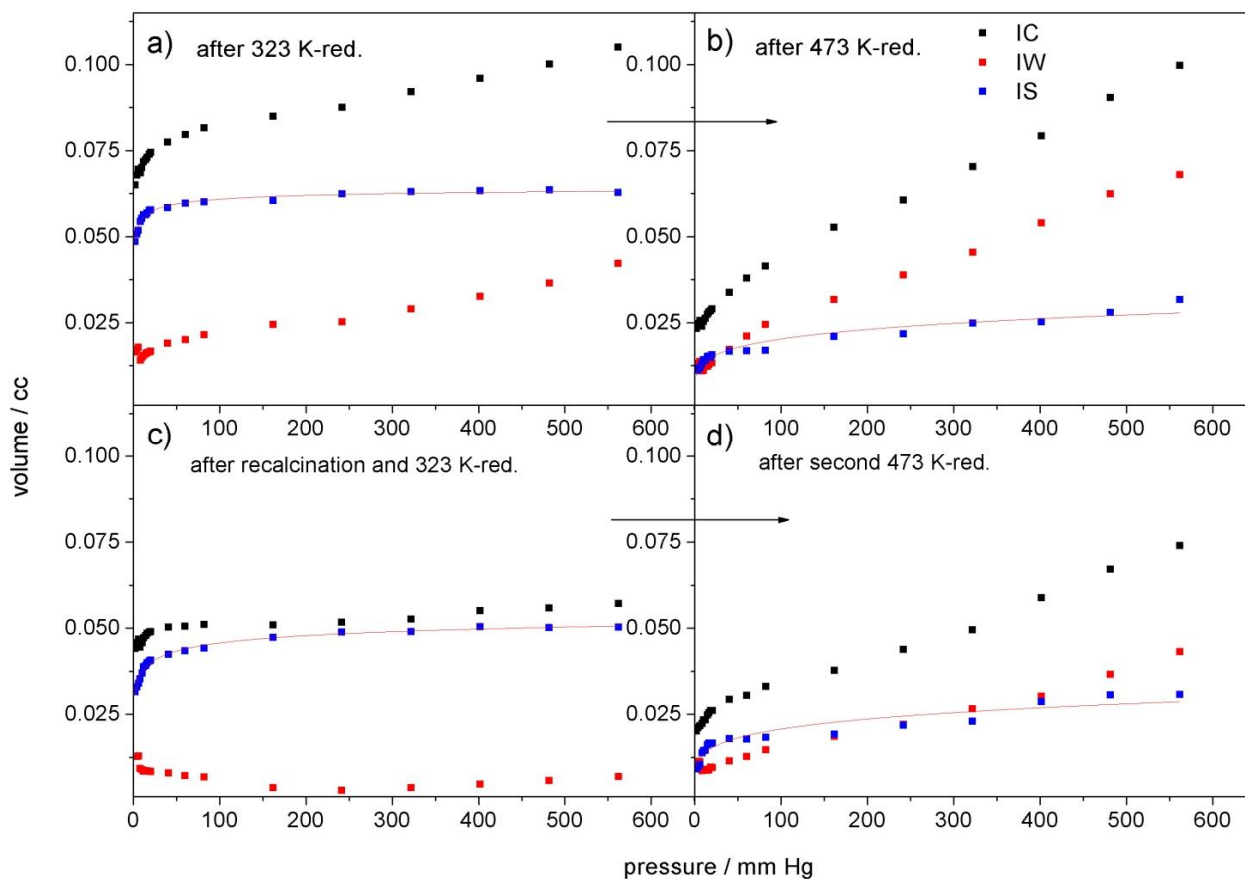


Fig. S2.7a: Volumetric CO-chemisorption at 313 K: 2% Pd catalyst after reduction at 323 K (a) and 473 K (b). Afterwards the sample was re-calcined and re-reduced at 323 K (c) and 473 K (d). IS = strong isotherm (chemisorption content), IW = weak isotherm (physisorption content), IC = combined isotherm (chemisorption+physisorption). IS fitted according to Langmuir model.

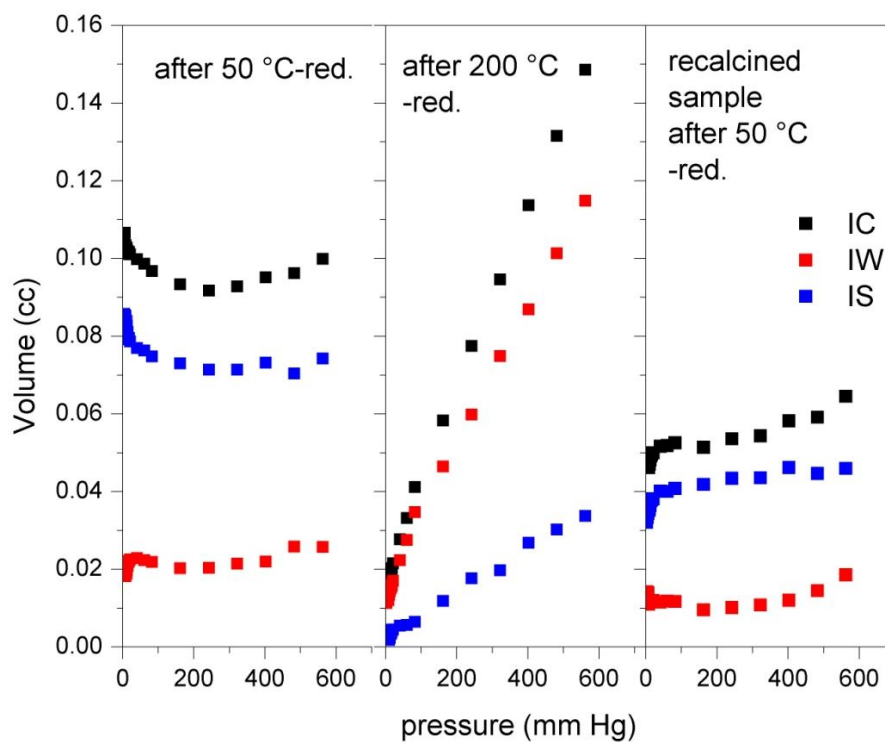


Fig. S2.7b: CO-chemisorption at 313 K: #14889 after 323, 473 and second 323 K-reduction (after re-calcination). IS = strong isotherm (chemisorption content), IW = weak isotherm (physisorption content), IC = combined isotherm (chemisorption+physisorption).

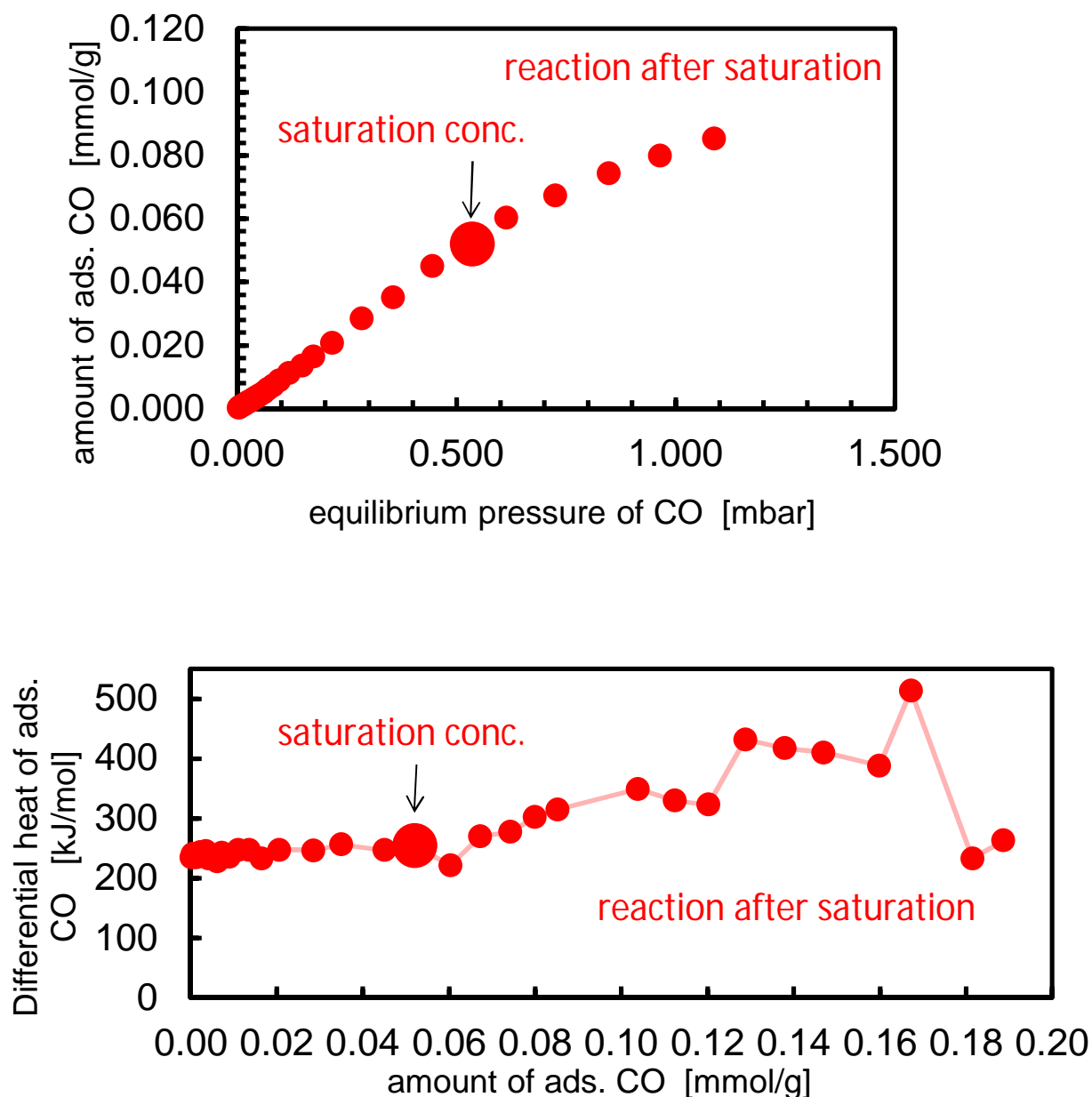


Fig. S7c+d: micro-calorimetric measurement during CO adsorption at 313 K on another 2% Pd/Fe<sub>2</sub>O<sub>3</sub> sample batch (#10524) measured earlier in our department: surface saturation observed at  $p(\text{CO}) = 0.5$  mbar; deviation from Langmuir behavior and large fluctuation of differential adsorption heat at higher pressures (change of active sites).



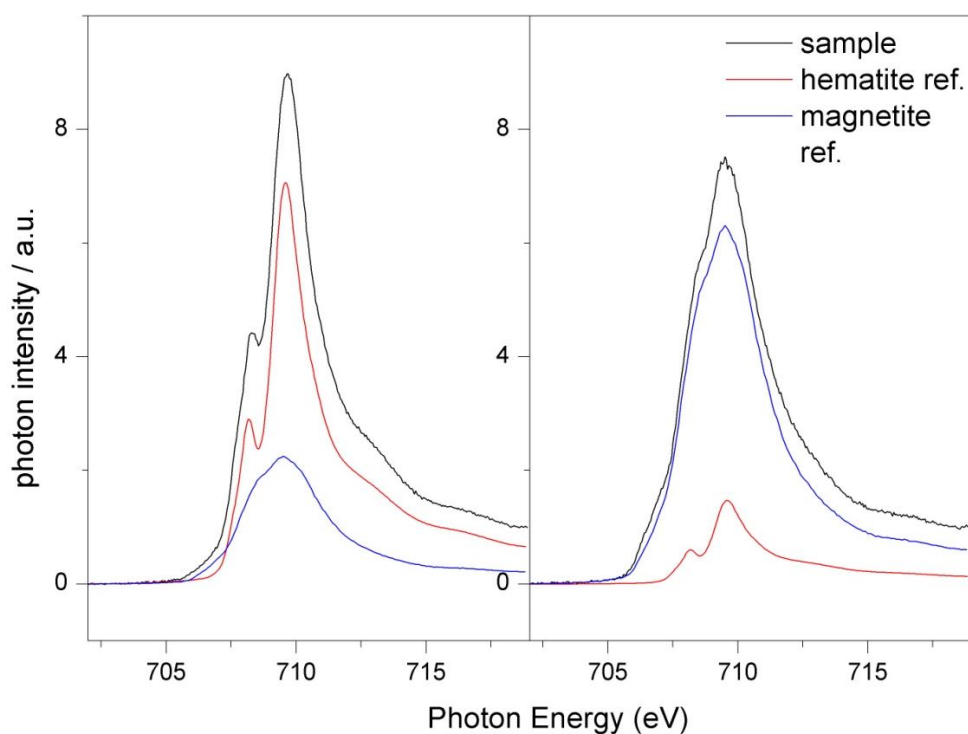


Fig. S2.8: NEXAFS spectra of the Fe-L edge before (left) and after reduction (right)

If we have a look on the NEXAFS spectra of the Fe L edge and compare the two states (deactivated state, Fig. S2.8-left) and the state after the TPR in the XPS chamber (Fig. S2.8-right), we notice that the iron edge can be fitted with two reference spectra, measured at the same setup earlier in our group – one for phase pure hematite, one for pure magnetite. The spectrum of the sample after the CO-oxidation (which had already contact to hydrogen at 473 K) can be fitted with a hematite content of 75% and 25% of magnetite. After the reduction procedure in the XPS chamber, the magnetite content increased to 82% and only 18% of hematite is left. Due to a slightly different background and a bad resonance to edge jump ratio, the magnetite content of the reduced sample might be underestimated. Possibly also some maghemite might have formed upon re-oxidation, as reported by Naumann et al.<sup>5</sup> but that difference has not been fitted. These results fit well to the TPR profile of the 2% sample (Fig. S2.10) that shows that the transformation of the bulk phase is on its way, but not yet finished at the temperature of 473 K. Apparently, the magnetite is being partly re-oxidized again during CO-oxidation, but that process seems not to depend on the surface (SMSI) effects.

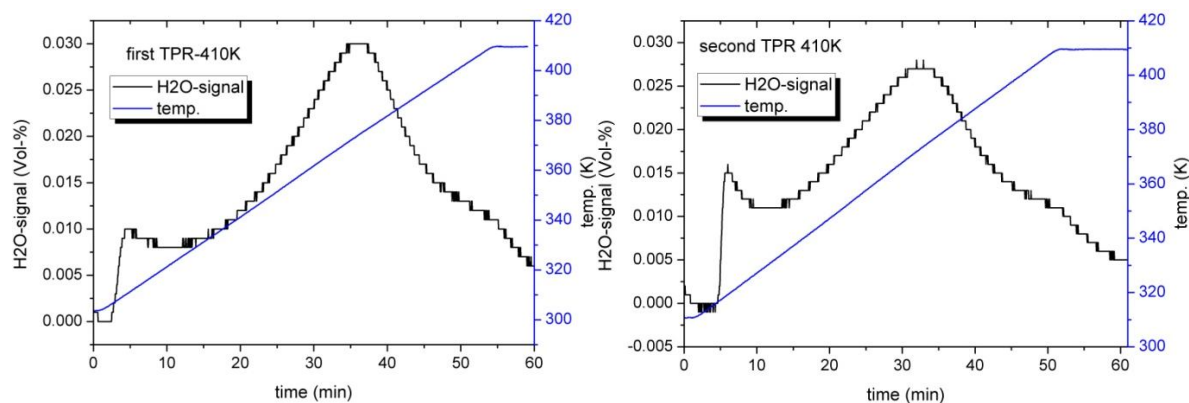


Fig. S2.9: 1% sample (14889): first (left) and second (right) TPR (5% H<sub>2</sub>) until 410 K before CO-ox.

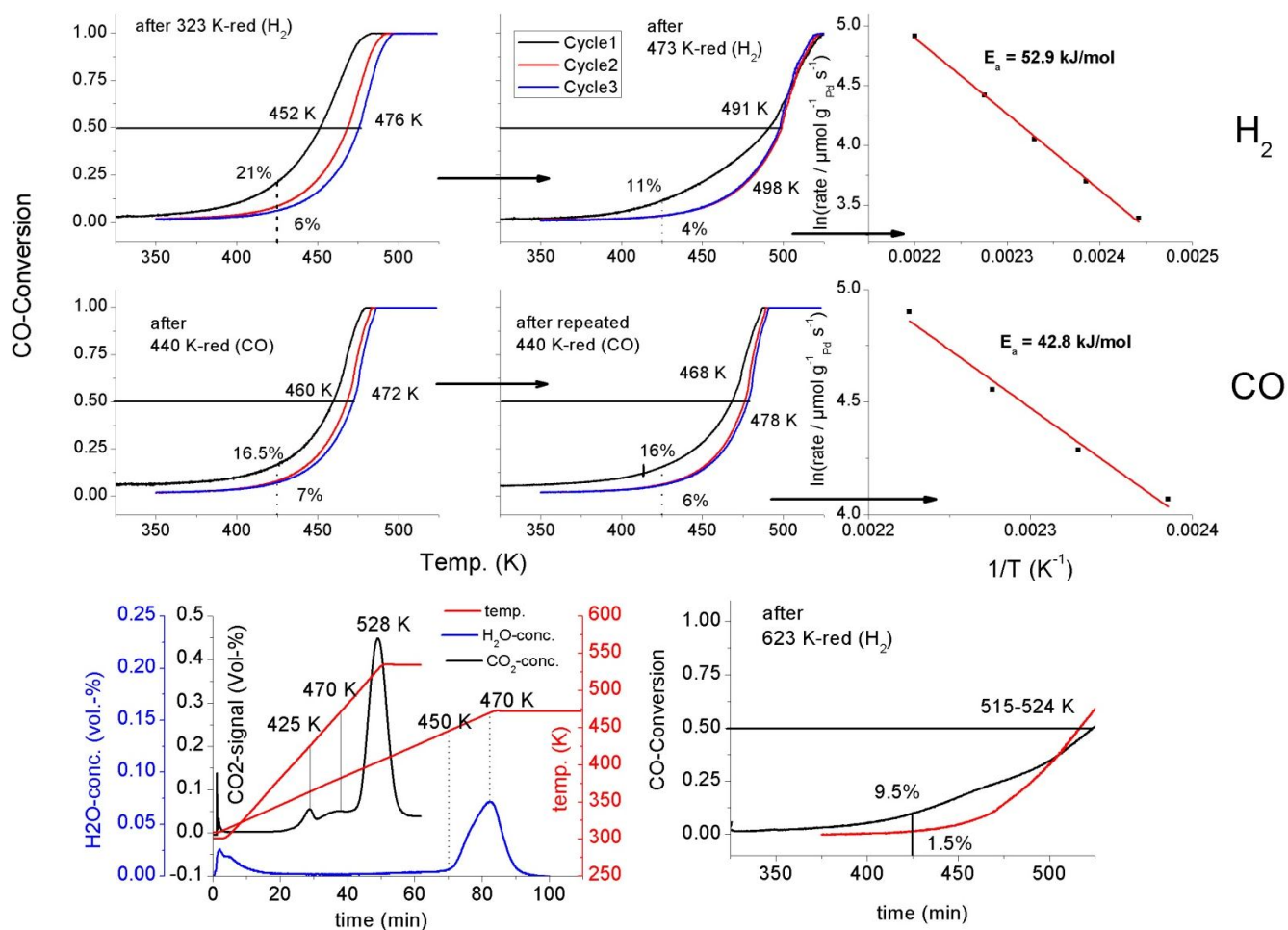


Fig. S2.10: CO-oxidation “light-off-cycles” of 2%-sample (17233) after reduction in hydrogen (first row) and in CO (second row). Activation energy determined afterwards in deactivated state. A comparing TPR graph in both reduction atmospheres and the effect of over-reduction in hydrogen at 623 K are shown in the third row.

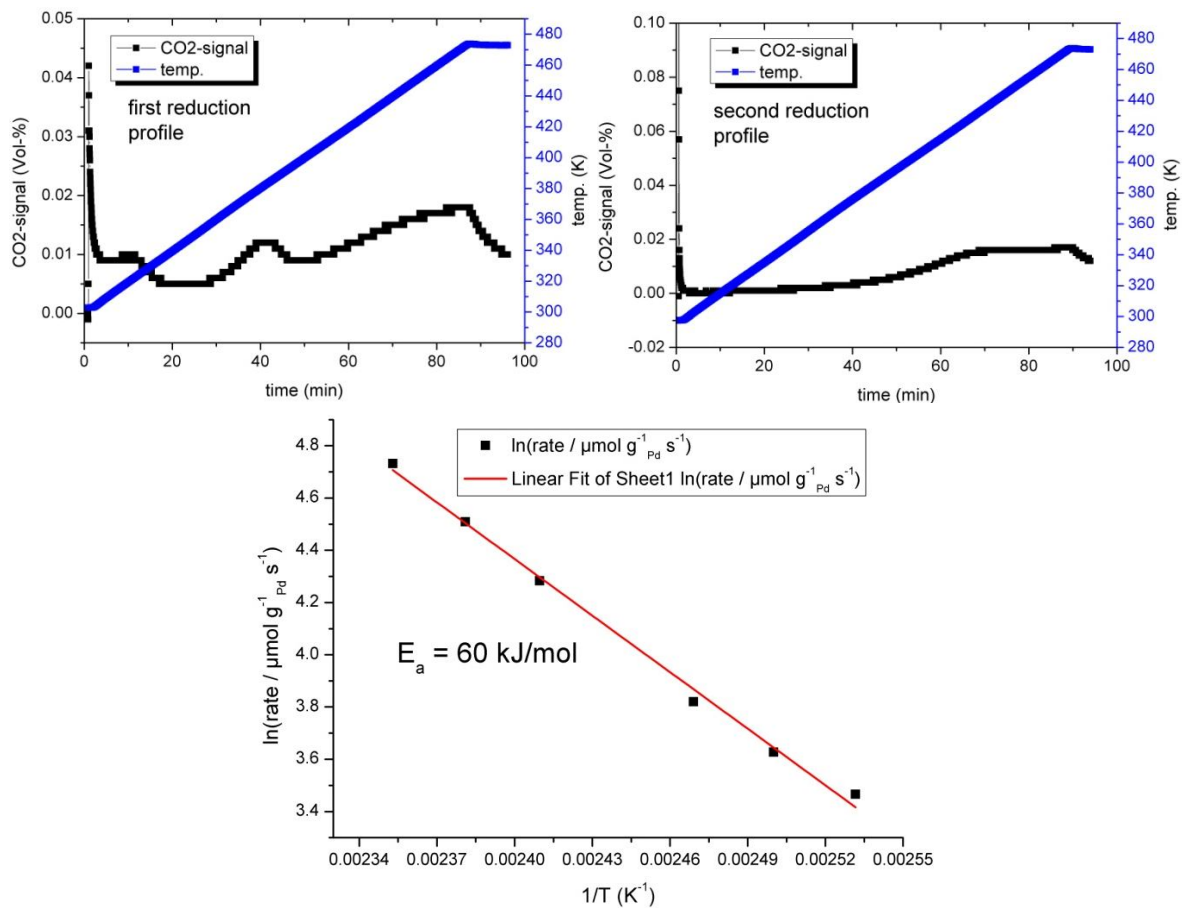


Fig. S2.11: repeated TPR of 5%-sample (13757) in 2% CO until 473 K before CO-oxidation and determination of activation energy afterwards (deactivated state).

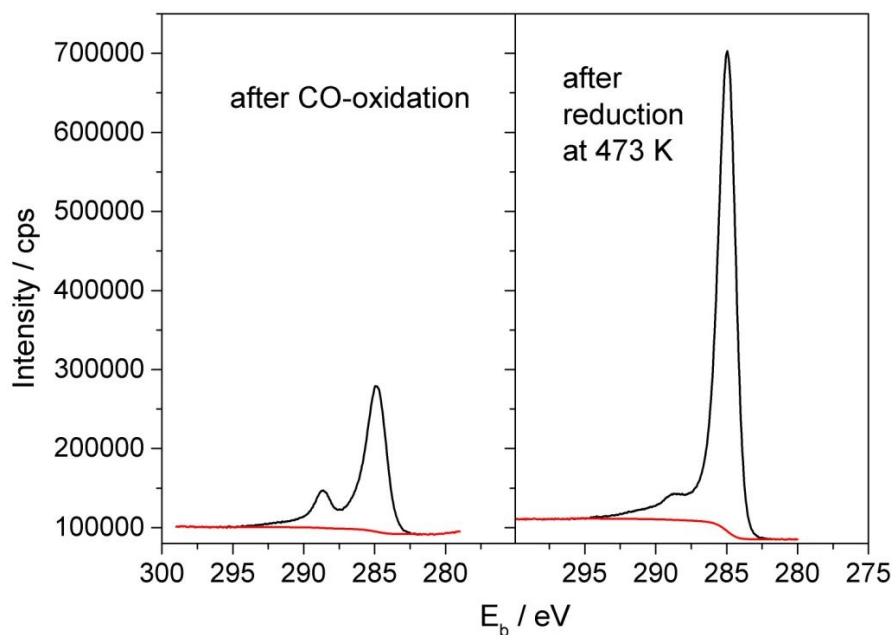


Fig. S2.12: XP-spectra of the C1s region of the 2% sample in deactivated state (left) and after in-situ reduction (right), recorded in surface sensitive mode ( $E_{\text{kin}} = 150$  eV). Amount of carbonate species decreases during reduction; total carbon amount increases.

### C. Tables

Table S2.1: integrated intensities of Pd3d and Fe2p (resp. Fe3p); blue = surface ratio, grey = bulk ratio

Sample no.	conditions	signal	hv /eV	$E_{\text{kin}}$ /eV	cross section <sup>3</sup>	photon flux	at.-%
1% Pd/Fe <sub>2</sub> O <sub>3</sub> after CO-ox. (#16956)	UHV, RT	Pd3d	535	200	2.900	5.63E+10	2.0
		Fe2p	920	200	0.750	1.35E+11	98.0
	0.4 mbar H <sub>2</sub> , 473 K (1h)	Pd3d	1135	800	0.470	1.47E+11	2.1
		Fe2p	1420	700	0.223	1.28E+11	97.9
		Pd3d	535	200	2.900	5.63E+10	1.8
		Fe2p	920	200	0.750	1.35E+11	98.2
	2.5 mbar H <sub>2</sub> , 473 K (2h)	Pd3d	1135	800	0.470	1.47E+11	2.0
		Fe2p	1420	700	0.223	1.28E+11	98.0
		Pd3d	535	200	2.900	5.63E+10	1.5
		Fe2p	920	200	0.750	1.35E+11	98.5
	UHV, RT (after red.)	Pd3d	1135	800	0.470	1.47E+11	2.3
		Fe2p	1420	700	0.223	1.28E+11	97.7
Pd3d		535	200	2.900	5.63E+10	1.1	
Fe2p		920	200	0.750	1.35E+11	98.9	
2% Pd/Fe <sub>2</sub> O <sub>3</sub> after CO-ox. (#17782)	UHV, RT	Pd3d	485	150	3.200	5.49E+10	3.1
		Fe2p	870	150	0.900	1.40E+11	96.9
	0.4 mbar H <sub>2</sub> , 473 K (after TPR)	Pd3d	1035	700	0.610	1.49E+11	2.4
		Fe2p	1420	700	0.223	1.29E+11	97.6
	UHV, RT, after 10 mbar H <sub>2</sub> (1h @473 K)	Pd3d	485	150	3.200	5.49E+10	2.9
		Fe2p	870	150	0.900	1.40E+11	97.1
	UHV, RT, after 10 mbar H <sub>2</sub> (1h @473 K)	Pd3d	485	150	3.200	5.49E+10	2.0
		Fe2p	870	150	0.900	1.40E+11	98.0
	UHV, RT, after 10 mbar H <sub>2</sub> (1h @473 K)	Pd3d	1135	800	0.470	1.51E+11	2.5
		Fe3p	853	800	0.090	1.39E+11	97.5

Table S2.2: reaction parameters ( $T_{50}$ ,  $X_{425}$ ,  $E_a$ ) of the 1% and 5% sample, as determined in CO oxidation light-off measurements after different pre-reduction conditions (Fig. 2.10+2.11).

#14889		reducing agent: H <sub>2</sub>			
(1% Pd)					
sample (T red./K)	ramp no.	T <sub>50</sub> /K	X <sub>425</sub> /%	E <sub>a</sub> /kJmol <sup>-1</sup>	
fresh sample (323)	first	441	33.3		
	last	467	8.6		
fresh sample (473)	first	449	21		
	last	470	5.6		
same sample (323)	first	472	8.5		
	last	472	8.5		
same sample (410)	first	476	15		
	last	476	6.7		
same sample (410)	first	476	15		
	last	476	6.6		
					56

#13757		reducing agent: CO			
(5% Pd)					
sample (T red./K)	ramp no.	T <sub>50</sub> /K	X <sub>425</sub> /%	E <sub>a</sub> /kJmol <sup>-1</sup>	
fresh sample (423)	first	416	59		
	last	443	23		
same sample (423)	first	434	38		
	last	448	19		
fresh sample (473)	first	390	86		
	last	439	29		
same sample (473)	first	392	84		
	last	440	29		
					60
fresh sample (523)	first	425	50		
	last	449	20		
fresh sample (573)	first	471	20		
	last	453	17		

## D. References

- Knop-Gericke, A. *et al.* in *Advances in Catalysis* (ed. Bruce C. Gates and Helmut Knözinger) **52**, 213–272 (Academic Press, 2009).
- Starr, D. E., Liu, Z., Hävecker, M., Knop-Gericke, A. & Bluhm, H. Investigation of solid/vapor interfaces using ambient pressure X-ray photoelectron spectroscopy. *Chem. Soc. Rev.* **42**, 5833 (2013).
- Yeh, J. J. & Lindau, I. Atomic subshell photoionization cross sections and asymmetry parameters:  $1 \leq Z \leq 103$ . *At. Data Nucl. Data Tables* **32**, 1–155 (1985).
- Davydov, A. in *Molecular Spectroscopy of Oxide Catalyst Surfaces* 27–179 (John Wiley & Sons, Ltd, 2003).  
<<http://onlinelibrary.wiley.com/doi/10.1002/0470867981.ch2/summary>>
- Naumann d'Alnoncourt, R. *et al.* Strong metal–support interactions between palladium and iron oxide and their effect on CO oxidation. *J. Catal.* **317**, 220–228 (2014).

## Chapter 3: Strong Metal-Support Interaction and alloying of Pd/ZnO catalysts for CO-oxidation

Patrick Kast, Matthias Friedrich, Frank Girgsdies, Jutta Kröhnert, Detre Teschner, Thomas Lunkenbein, Malte Behrens, Robert Schlögl.

### Abstract:

Pd/ZnO catalysts with different Pd content have been synthesized, thoroughly characterized and investigated with regard to their reduction behavior in hydrogen or carbon monoxide containing atmospheres, by applying CO-chemisorption, photoelectron spectroscopy, X-ray diffraction, electron microscopy, TPR and DRIFTS techniques. As a catalytic test reaction, CO-oxidation has been applied. The interaction of the noble metal with the support has been revealed in a way that could distinguish between alloying and other surface spreading/wetting phenomena, induced by strong metal-support interaction (SMSI).

### 3.1. Introduction

The catalytic system of zinc oxide supported palladium catalysts has attracted broader scientific interest since Iwasa et al.<sup>1</sup> tested a number of Pd catalysts in methanol steam reforming (MSR,  $\text{CH}_3\text{OH} + \text{H}_2\text{O} \rightarrow 3\text{H}_2 + \text{CO}_2$ ) that was discussed with regard to hydrogen production for vehicles.<sup>2-6</sup> They showed high activity and selectivity for the reaction on Pd/ZnO, whereas Pd on irreducible supports only led to the decomposition of methanol to CO and hydrogen. When Iwasa et al.<sup>7</sup> reduced Pd/ZnO up to 773 K, they observed further improved selectivity (>98%) which they attributed to the formation of the intermetallic compound (IMC) PdZn, proven by XRD and XPS. Since then, a lot of studies have been performed to understand the specific electronic properties as well as the geometric structure of these Pd/ZnO based catalysts with regard to their catalytic performance in general, and for methanol steam reforming, which have been summarized in two recent reviews by Föttinger<sup>8</sup> and Armbrüster<sup>9</sup> et al. The most common synthesis method comprises treatment of ZnO-supported Pd systems, which were prepared e.g. by impregnation or co-precipitation in atmospheres that contain hydrogen or other reducing gases at elevated temperatures. When studying the reduction behavior of a 10 wt.-% Pd/ZnO catalyst, Hong et al.<sup>10</sup> reported a H<sub>2</sub> consumption peak maximum at about 673-700 K, representing ZnO support reduction and

PdZn formation, which was confirmed to be complete at 773 K by XRD. Furthermore, hydrogen spill-over was reported already below 360 K which indicates that surface reduction can start much earlier. Iwasa et al.<sup>7</sup> confirmed PdZn formation by observing a broad TPR-peak at 500-750 K as well as XRD reflections when reduced at 623 K. In photoelectron spectroscopy upon reduction, the monitored Zn *LMM* Auger spectra showed a shoulder ascribed to intermetallic zinc at 493 K already, representing further evidence for ZnO surface reduction with hydrogen in the presence of palladium. PdZn reflections in XRD patterns were reported at 523 K already by Tew et al.<sup>11</sup> Chin et al.<sup>12</sup> studied 5-20 wt.-% Pd/ZnO catalysts by TPR and were able to observe a shift of the reduction peak maximum to lower temperatures, by decreasing the loading. With regard to the electronic properties, Pd3d XPS studies have been performed by several groups upon the alloying process.<sup>7,13-18</sup>

Recent studies on metallurgically prepared PdZn with a varied Pd-content (47-59%) by Friedrich et al.<sup>19</sup> were able to show the importance of the Zn-content for MSR selectivity due to the changing electronic properties (Zn-rich samples lead to a higher binding energy for the Pd3d signal in XPS). They could show that bulk Pd also has an influence on the Zn/Pd ratio at the surface, the Pd3d binding energy and the amount of oxidized Zn-species at the surface, that were shown to be important for high activity in MSR. Both, electronic (ligand-) and geometric (ensemble-) effects play a role when talking about the influence of the IMC formation process towards CO-adsorption in IR spectroscopy.<sup>18,20-22</sup> By FTIR and EXAFS, Föttinger et al.<sup>22</sup> confirmed the IMC formation on Pd/ZnO under MSR conditions or upon reduction at 623 K as an ongoing process, proceeding from the outer part of the Pd particle to the inner part, as well as the reversibility of this mechanism by oxygen treatment at 573 K, leading to a formation of metallic Pd and ZnO islands on-top of the pre-formed PdZn-overlayer. Such kind of surface decoration was also studied by Hong et al.<sup>10</sup> who investigated the Pd/ZnO system in terms of SMSI.<sup>23</sup> They proposed a schematic model in which the ongoing reduction (also by spill-over) would lead to ZnOH<sub>x</sub> and ZnO<sub>(1-x)</sub> species around the more and more flattened Pd particles with an increasing metal-support interface, that would, with increasing reduction temperature start to form the PdZn alloy from the bottom to the top of the Pd particle. After reoxidation (e.g. by exposure to air for sample transfer), also ZnO islands as well as PdO on Pd would form and the ZnO<sub>(1-x)</sub> species would be partially reoxidized, as far as accessible.<sup>24</sup> Metal-support interactions were also tested on various supported Pd catalysts for methanol synthesis.<sup>25</sup>

In SMSI state, catalysts have been reported to be more active for certain reactions like CO-oxidation.<sup>26</sup> Due to the simplicity of that reaction it can be used as a test reaction to

characterize also the Pd/Zn/ZnO-system. For example, Iwasa et al.<sup>27</sup> were able to show the highest selectivity for preferential oxidation of CO in the presence of hydrogen (PROX) on the Pd/ZnO, after PdZn formation. Small amounts of H<sub>2</sub> in the feed gas were able to enhance the CO-conversion. The IMC formation was discussed to be responsible for a reduced CO binding energy that made O<sub>2</sub>-adsorption more competitive. The same observations were made by Johnson et al.<sup>28</sup> who investigated CO-oxidation and CO-adsorption on  $\alpha$ - and  $\beta$ -PdZn and observed 5-10 times higher initial rates for the reaction, compared to pure Pd, however observing also deactivation upon time by zinc oxidation. CO-oxidation in general was intensively studied and discussed as a suitable model reaction for various heterogeneous, catalytic processes.<sup>29</sup> In the present work we study the role of SMSI in the Pd/ZnO system, by applying a similar, methodological approach, recently applied on the Pd/Fe<sub>2</sub>O<sub>3</sub> system.<sup>30</sup> The change of activity for CO-oxidation during SMSI/alloy formation as well as the reversibility by reoxidation will be investigated and compared to the changing structural and electronic characteristics.

## 3.2. Experimental

### 3.2.1. Catalyst synthesis

The catalyst precursor was synthesized by co-precipitation, as described earlier.<sup>30</sup> Therefore, 650 ml of a diluted (0.1 M) solution of Zn(NO<sub>3</sub>)<sub>2</sub>\*6H<sub>2</sub>O (Alfa Aesar) were prepared and mixed with a solution of calculated amounts of Pd(NO<sub>3</sub>)<sub>2</sub>\*2H<sub>2</sub>O, that had been dissolved in 3g HNO<sub>3</sub> (65%) in 100 ml H<sub>2</sub>O (sample 16688) or with purchased Pd-nitrate solution (8.3 wt.-% Pd-content in 10 wt.-% HNO<sub>3</sub>, Alfa Aesar) in case of the samples 15657 and 16120.

Precipitation occurred drop-wise with 0.4 M NaOH solution in an automated reactor-system (Labmax, Mettler-Toledo), which contained already about 400 ml of deionized water. During the precipitation (acid solution addition rate of 6 g/min), the pH-value (pH = 7.5), temperature (T = 298 K) and stirring rate (r = 300 rpm) were monitored and kept constant in order to assure the most similar conditions and chemical potential for every forming crystallite and thus the best possible product homogeneity. After precipitation, the product was aged for 1 h (100 rpm, RT), filtered and washed three times (3x 1l of demin. water) until conductivity of the solution was < 0.01 mS. The solid, pale yellow product was dried in air for 24 h (298 K), mortared and calcined under controlled conditions in 20% O<sub>2</sub> – Ar atmosphere (2 h at 623 K, 2 Kpm heating rate). The ochre product consists of PdO supported on hexagonal ZnO. The palladium loading was varied to yield catalysts with 0.75, 2.5 and 5



wt.-% Pd/ZnO. For the 5% sample, a metal solution of 0.2 M and a precipitation pH-value of 9 were used.

### 3.2.2. Catalyst characterization

Elemental composition of the samples was assessed by optical emission spectroscopy (ICP-OES) and energy-dispersive x-ray spectroscopy (EDX, to rule out contaminations). Total surface area was investigated by nitrogen physisorption (BET). Scanning electron microscopy (SEM) was used to check the surface morphology, whereas HR-TEM and STEM was used to investigate the Pd particle distribution and monitor structural changes after treatments or reactions. X-ray diffraction (XRD) was used for analysis of the bulk structure/phase analysis. CO-chemisorption was performed to measure the active surface area and to detect support spreading/wetting (decoration of the Pd-particles). CO-IR measurements (diffuse reflectance infrared fourier-transform spectroscopy, DRIFTS) and photoelectron spectroscopy (XPS) was applied to investigate electronic surface properties during reduction and/or CO-oxidation. ICP-OES measurements were performed using an Ultima 2 spectrometer (Horiba Jobin Yvon Inc., 120-800 nm) after sample digestion in HF/aqua regia. A Hitachi S-4800 SEM was used as well as a FEI Cs-corrected Titan 80-300 microscope for STEM and HR-TEM images. The samples were reduced in a reduction tube, in 5% H<sub>2</sub>-Ar (100 ml/min) at room temperature or at higher temperatures, with a heating rate of 2 Kpm and 30 min of holding time. One sample was reduced in 5% CO/Ar. Samples in air-sensitive (SMSI) state (after reduction at 473-623 K) were transferred into the microscope without air contact, with the help of a glove box. An energy dispersive X-ray detector (Genesis 4000) was used for elemental mapping and composition analysis.

DRIFTS measurements were recorded with an MCT detector at a resolution of 4/cm, accumulating 512 scans, using a Praying Mantis<sup>TM</sup> low temperature reaction chamber (ZnSe window) placed in an Agilent Cary 680 spectrometer controlled by Resolutions Pro software. Measurements were performed in an in-situ cell capable of heat treatment under gas flow conditions (Bronkhorst mass flow controllers). The samples were activated for 30 min in a flowing gas mixture of 2% CO-Ar (50 ml/min), at 323, 523 and 623 K (subsequent experiments with one sample, mass: about 30 mg). For the IR-measurements the gas phase CO was removed by 30 min of Ar purging. The cell was cooling down to liquid nitrogen temperature under flowing vacuum. The CO was flushed in stepwise up to 200 mbar. The desorption of CO was carried out by decreasing the pressure of CO at 77 K. The spectra were recorded at 77 K with a background spectrum of pure KBr. The used gases were supplied by

Westfalen (purity >99.99%). Ar was further purified by passing through Hydrosorb and Oxysorb cartridges.

The X-ray diffraction (XRD) measurements were performed in Bragg-Brentano geometry on a Bruker AXS D8 Advance theta/theta diffractometer equipped with a secondary graphite monochromator (Cu  $K_{\alpha 1+2}$  radiation) and scintillation detector. The sample powder was filled into the recess of a cup-shaped sample holder, the surface of the powder bed being flush with the sample holder edge. The XRD data were analyzed by full pattern fitting according to the Rietveld method in conjunction with the fundamental parameter approach for the instrumental and double-Voigt approach for the sample contribution to the peak profiles as implemented in the TOPAS software (Bruker, version 4.2). The XRD setup was equipped with an in situ reactor cell (Anton Paar XRK 900). Reaction gases were mixed by means of mass flow controllers (Bronkhorst). Some samples were reduced at different temperatures in the cell using 5%  $H_2$ -Ar (100 ml/min) and measured afterwards at room temperature.

In situ XPS was performed at the ISISS beamline of the BESSY II synchrotron, Helmholtz Zentrum Berlin. The experimental setup has been described in literature in detail.<sup>31,32</sup> The samples were placed on a sample holder that could be heated by an IR laser (808 nm). The temperature was measured by a Ni-CrNi thermocouple which was fixed onto the sample surface. Gas flow into the analysis chamber was adjusted by mass flow controllers for He and  $H_2$  – up to 10 mbar hydrogen partial pressure were applied for reduction of the catalysts. A QMS was connected to the sample cell by a leak valve in order to monitor the gas phase composition during the surface characterization. All photoelectron spectra were normalized by the storage ring current and the energy dependent incident photon flux that was measured prior by using gold foil with known quantum efficiency. Surface sensitive detail scans of the Zn3d and the Pd3d core level region were performed at a constant kinetic energy of 200 eV and a beam slit of 111  $\mu$ m. The respective binding energy has been calibrated with the help of valence band spectra and the adventitious C1s signal. In addition to the surface scans, bulk-sensitive scans have been conducted, measuring electrons with kinetic energy of 800 eV. Surface and subsurface concentrations of the respective element have been calculated by normalized, integrated peak intensities, taking into account the photo-energy dependence of the atomic sub-shell photoionization cross-section of the respective orbitals.<sup>33</sup> Metallic palladium has been fitted with a tail exponent factor of -0.07 to match the metallic asymmetry.<sup>34</sup> The Gauss-Lorentz ratio for all species was kept constant (0.3 $\pm$ 0.05).

CO-chemisorption measurements were carried out in an Autosorb-1C chemisorption setup (Quantachrome Incorp.), equipped with a reactor for pretreatment of the sample under flow

conditions. For reduction the setup was connected to a gas bottle with 5% H<sub>2</sub>-Ar mixture. Usually, the sample was reduced at 323 K for 30 min. to reduce oxidic Pd species before measuring two adsorption isotherms at 313 K and in the pressure range of 3-747 mbar, the first isotherm representing both, reversibly (weakly) and irreversibly (strongly) adsorbed CO and the second isotherm (measured after evacuation) only representing the physisorbed species. By subtracting the second from the first isotherm and extrapolating the volume to a pressure of zero, the volume of chemisorbed CO was determined. By assuming a shape-factor for the Pd-particles of 6, a cross-sectional area of Pd of 7.87 Å<sup>2</sup>/atom<sup>35</sup> and further assuming that every second Pd surface atom is covered by one CO-molecule, the active surface area, the dispersion and the average diameter of the particles was calculated. Some samples were reduced at higher temperatures to generate and investigate particle decoration by the support (SMSI). After all reduction steps the sample was dried for 2 h (393 K) under He flow, before being evacuated for 2 h at the same temperature.

BET measurements were conducted in an Autosorb-6-B N<sub>2</sub>-physisorption setup (Quantachrome Incomp.) at liquid nitrogen temperature. Samples were degassed in a dynamic vacuum for 2 h at 423 K before starting the measurement. After measuring adsorption and desorption isotherms, the total surface area of the sample was calculated according to the BET method, using 11 points of the linear range of the desorption isotherm.

### 3.2.3. Catalytic testing

The CO-oxidation as the catalytic test reaction was carried out in a self-constructed catalytic reactor setup, described earlier.<sup>30</sup> Usually, 25 mg of the catalyst, diluted by 250 mg of inert SiC (particle diameter: 250-355 μm) were weighed out, first reduced in 5% H<sub>2</sub>-He (100 ml/min) at 323 K (2 Kpm), holding time 30 min. TPR in 5% H<sub>2</sub>-He or in 2% CO-He were performed usually at higher temperatures and with max. 5 Kpm heating rate. For CO-oxidation, normally three repeated light-off conversion cycles were measured (100 ml/min, 0.5% O<sub>2</sub>, 1% CO, 98.5 % He) from 323 to 523 K (2 Kpm heating rate, 15 min. holding time and 0.5 Kpm for cool down to 373 K (1h holding time).

### 3.3. Results and Discussion

#### 3.3.1. Synthesis and characterization

Table 3.1: physical parameter of the investigated, calcined catalysts

Nr.	Catalyst	Pd-loading (ICP-OES) (wt.-%)	BET surface area (m <sup>2</sup> /g)	Average Pd particle diameter* (CO-chem.; nm)	Active surface area (m <sup>2</sup> /g)*
15657	0.75% Pd/ZnO	1.6	40	2.5	3.1
16688	2.5% Pd/ZnO	3.9	39	6.1	3.2
16120	5% Pd/ZnO	4.6	43	6.7	3.5

\*after 323 K-red.

The precursor synthesis for the Pd/ZnO catalysts was performed via a controlled co-precipitation approach. The pH-value during precipitation with NaOH did not fluctuate much due to buffer effects. No pH-change upon 1h of ageing time could be observed as presented in figure S3.1. After washing and drying the pale yellow precipitate was calcined leading to the formation of PdO on ZnO, hand in hand with a color change to ochre, depending on the loading. Some physical parameters of the differently loaded samples after calcination are shown in table 3.1: the nominal palladium content of the samples was determined by ICP-OES measurements while the content of the two lower loaded samples was found to be higher than expected. The BET area of all samples is in the range of 40 m<sup>2</sup>/g. Meso-pores were found in all samples. Regarding the influence of the palladium content on the average particle size, the chemisorption measurements revealed a particle growth with increased noble metal loading, from about 2 nm for the 0.75 wt.-% samples, to almost 7 nm for 5 wt.-%. Due to some assumptions like shape factor of the particles and the content of CO-molecules that can be adsorbed for example in bridged binding-geometry, small differences between the sizes determined by microscopy might arise. Nevertheless, microscopy measurements (see part 3.4) of the lowest loaded sample confirmed the chemisorption results. The calculated active surface area of the catalysts was very similar with about 3.1 to 3.5 m<sup>2</sup>/g. The reduction behavior of the samples will be discussed in the next section.

#### 3.3.2. Chemical and structural behavior of the system during reduction (2.5 and 5 wt.-% sample)

Since strong metal-support interaction is a phenomenon that depends on the reducibility of the catalyst support,<sup>23</sup> temperature-programmed reductions of the samples have been

performed. For reduction, a 5% hydrogen – helium gas mixture as well as a mixture consisting of 2% CO-He has been applied and the results were compared. Furthermore the structural changes during the reductive heat treatment were monitored by XRD as well as by transmission electron microscopy (part 3.4). The higher loaded samples (2.5 - 5 wt.-%) were selected for the TPR and XRD measurements due to the comparably high detection limit of phases in XRD.

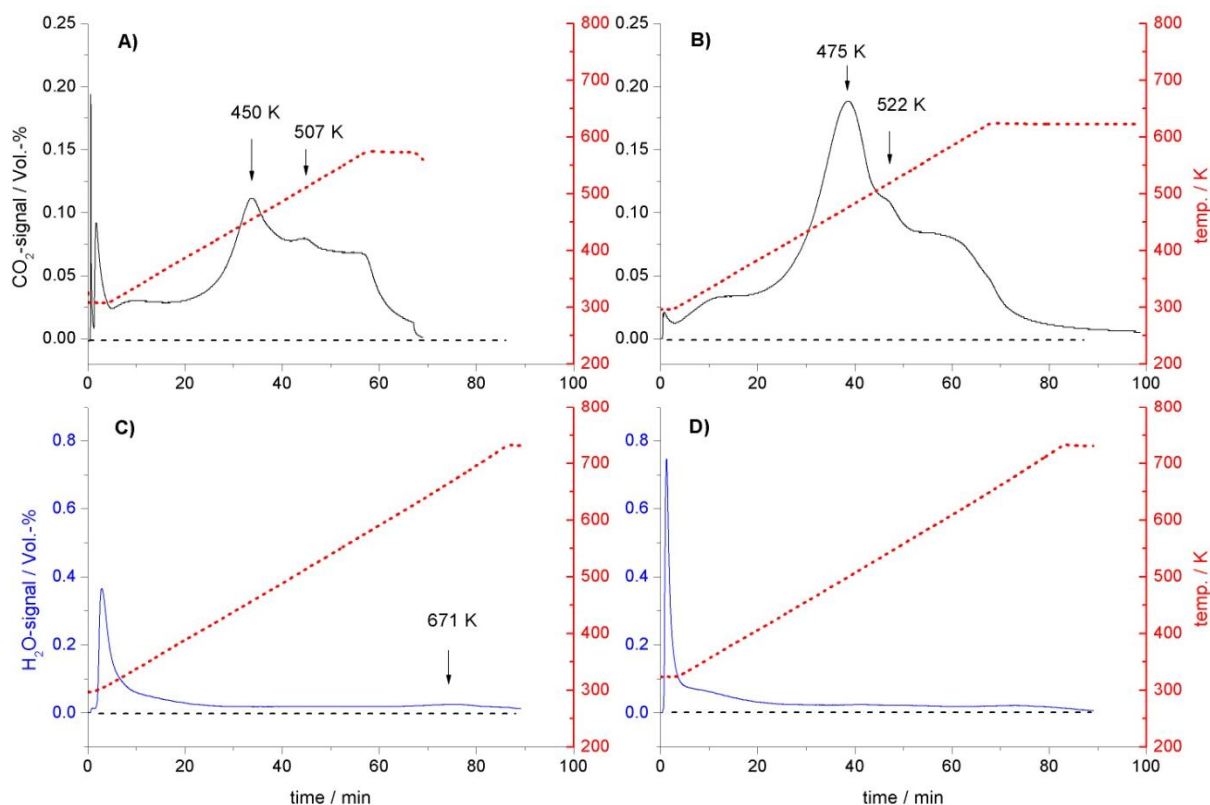


Fig. 3.1: TPR studies of the 2.5 (A,C) and 5 wt.-% (B,D) sample using CO (A,B) or H<sub>2</sub> (C,D) gas mixtures as reducing agent. The dashed black line intersecting the ordinate at zero is a guide to the eye.

The TPR curves are depicted in figure 3.1. In case of the hydrogen gas mixture as reducing agent (C,D), water formation is visible already at room temperature which can be ascribed to reduction of palladium oxide to metallic palladium. With increasing temperature the water peak shows a shoulder due to the drying effect. Until the end of the temperature program (723 K), a continuous amount of water is detected that can be ascribed to spill-over reduction of the zinc oxide support surface,<sup>36</sup> while only a very smooth increase of the water signal could be detected at 671 K (C). In order to better work out the temperature dependence of possible processes like alloy formation or the formation of reduced zinc oxide species

(SMSI), the measurements have been repeated with the milder reducing agent CO (A,B), showing a more nuanced reduction profile. Both samples show an initial increase of the CO<sub>2</sub> formation at the beginning (PdO reduction) while the respective signal in case of the higher loaded sample is less pronounced, which is unexpected and might be explained by an incomplete reduction at this state. With increasing temperature a large CO<sub>2</sub> peak arises at 450 K (A) respectively 475 K (B) with a smaller second peak/shoulder at 507 K (A) respectively 522 K (B). The general appearance of the two differently loaded samples in the TPR experiments is similar, with increased amounts of CO<sub>2</sub> and water formed proportional to the higher palladium loading. In order to assign the observed signals to specific reduction processes further experiments like XRD were performed, applying pre-reduction temperatures observed by the TPR-experiments. After the temperature programmed reduction of the 2.5 wt.-% sample in 2% CO-He, to 473 K in the XRD setup, the Rietveld fitted diffractogram of the sample (figure 3.2A) shows reflections for the hexagonal ZnO phase as well as for metallic palladium, represented among others by a broad signal at 40 ° for the Pd 111 plane. By comparing the results of the XRD measurement after 473 K and the TPR, one can conclude that the formation of probably partially reduced zinc oxide support does not yet lead to detectable alloy formation in the presented case. This is different from the higher loaded sample (5 wt.-%) that has been also investigated by XRD after CO-reduction until 623 K, in the state at the end of the TPR curve (Fig. 3.1B). In that case, the alloy PdZn (ICSD 180143) has been formed as shown in figure 3.2B. Different to the lower loaded sample, the XRD of the higher loaded one has been measured after the reduction processes that are represented by the shoulder at 522 K. Therefore it could be concluded that a most likely amorphous (due to the missing additional phase component information), partially reduced zinc oxide compound forms on the surface during the reduction in the CO-containing atmosphere, and that later, with further increase of temperature, the alloy formation process goes on. Another explanation would be that the alloy formation starts at the surface but cannot be detected as long as it has not yet proceeded sufficiently to the bulk.

Though the different Pd particle sizes present in the two different samples allows us to assume different interaction with the support, integration of the CO-TPRs revealed that the CO<sub>2</sub> amount formed in both cases was larger by a factor of 2.5 compared to the amount that would form by PdO reduction alone. This would fit to the formation of PdZn covered by additional reduced species. However the formation of carbon species in that case cannot be excluded.

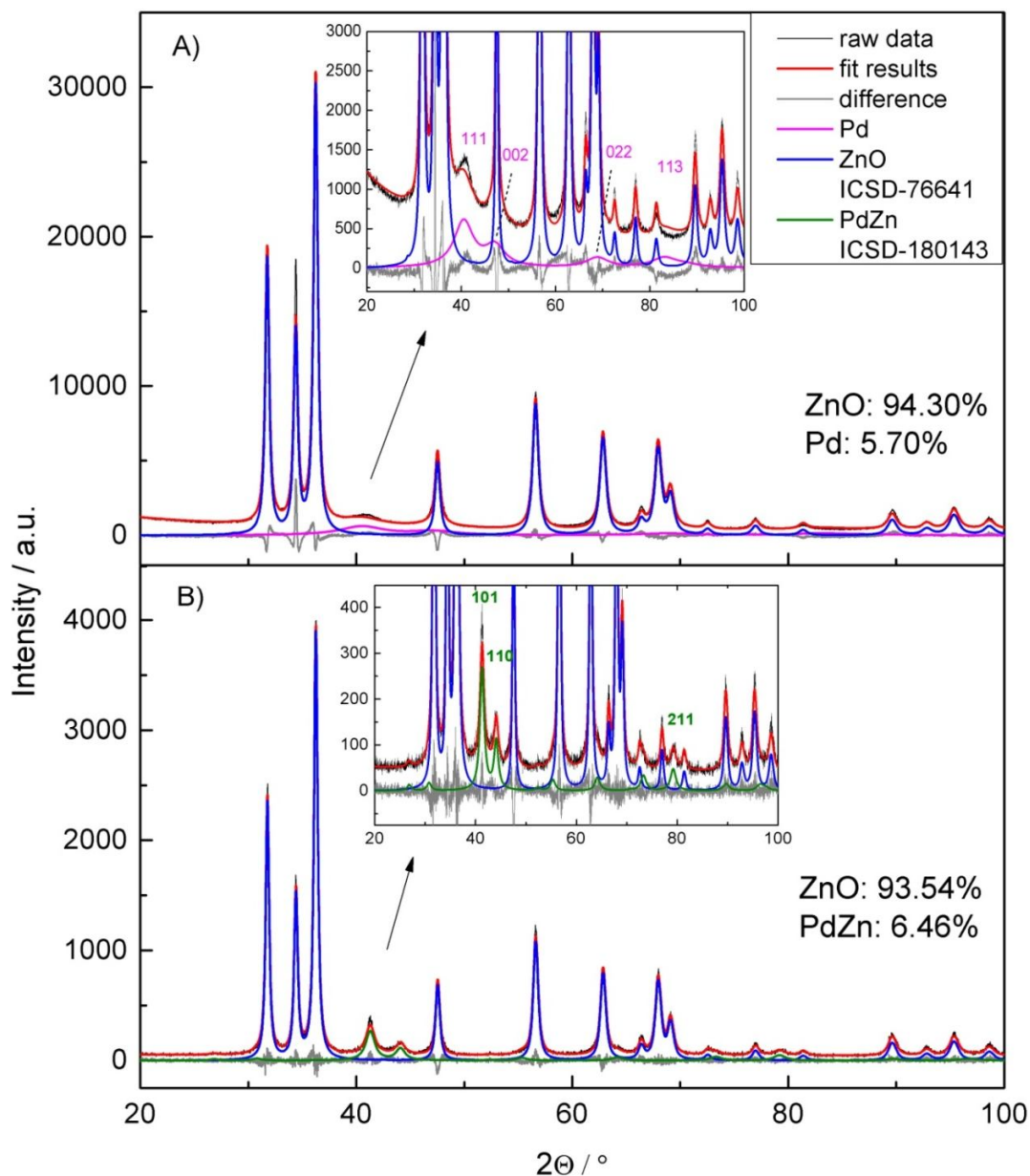


Fig. 3.2: Rietveld refined XRD measurements after reduction in 2% CO of the 2.5 wt.-% sample (reduction temperature 473 K, part A) and of the 5 wt.-% sample (reduction temperature 623 K, part B). Y-axis magnified (inlets).

In addition to the mentioned studies, pseudo in-situ XRD measurements were performed on the 2.5 wt.-% Pd/ZnO sample, reducing the sample in the XRD sample holder in hydrogen containing gas mixture at increasing temperatures and successively measuring the diffraction patterns at room temperature (to exclude thermal effects), in order to further study the behavior of the system with regard to (bulk)- alloy formation.

As it can be seen in figure S3.2 (supporting information), the formation of a PdZn alloy compound upon reduction in a 5% hydrogen containing atmosphere starts between 573 K and

623 K, indicated by the magnified region that shows the prominent 101 and 110 reflections of the compound at angles of about 41 and 44 °. With further increase of the reduction temperature the signals get sharper due to PdZn crystallite growth.

### 3.3.3. Influence of reductive treatments on the activity in CO-oxidation

In order to investigate the influence of the described reduction procedures of the catalysts on the catalytic performance in CO-oxidation and to be able to compare the structure function relationship, two differently loaded catalysts, the 0.75% and the 2.5 wt.-% samples have been selected. The temperature at 50% conversion ( $T_{0.5}$ ) and the conversion at 425 K ( $X_{425}$ ) are compared as reaction parameters (Table S3.2). Figure 3.3 shows the kinetic measurements for the lower loaded sample (three repeated TPO-cycles for each measurement) after reduction in CO-containing atmosphere and according to the previously determined TPR (Fig. 3.3, first panel). It can be seen that when being reduced at a temperature below the first peak in the TPR (423 K, state at position 1), the catalyst is less active in the first CO-conversion cycle, compared to the others.

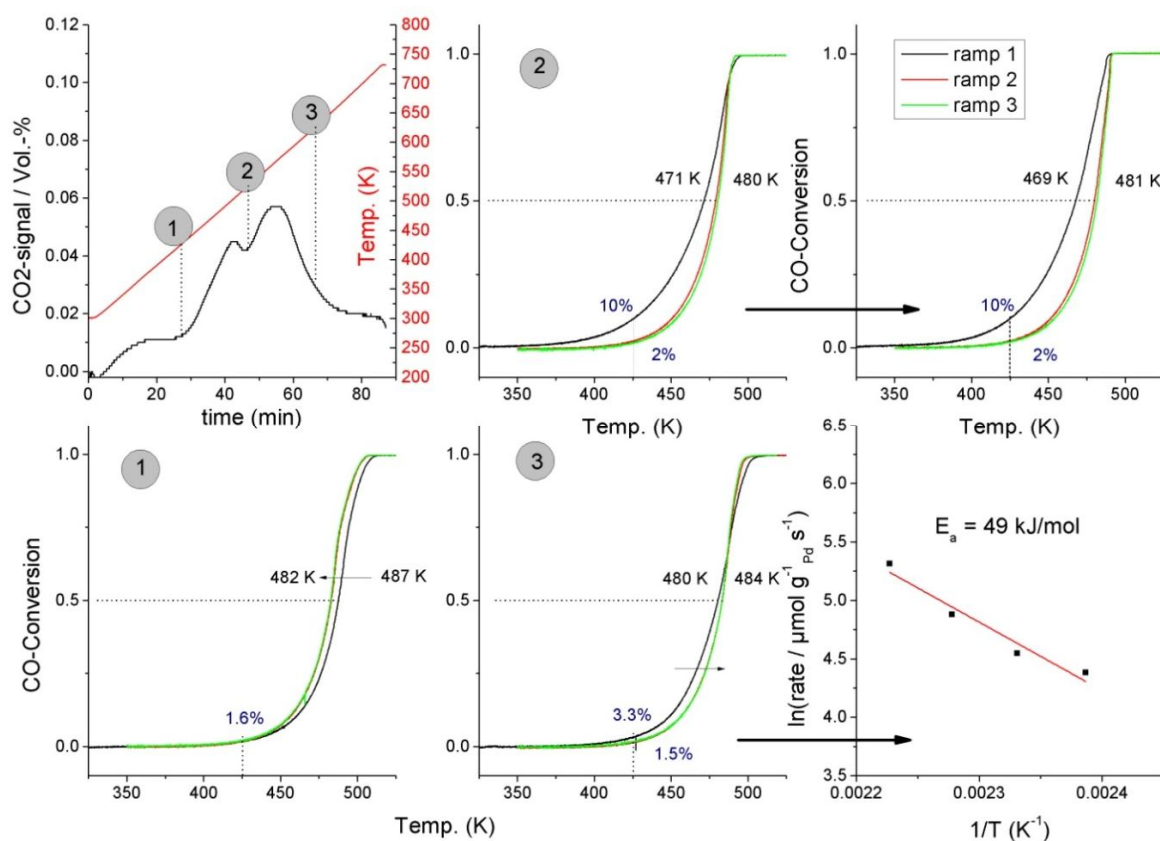


Fig. 3.3: CO-oxidation (conversion cycles) of 0.75% Pd/ZnO sample after reduction in 2% CO-He at 423 K (1), 523 K (2, repeated measurement) and 623 K (3) and activation energy determined after the last measurement. According TPR-experiment presented in first row (left).



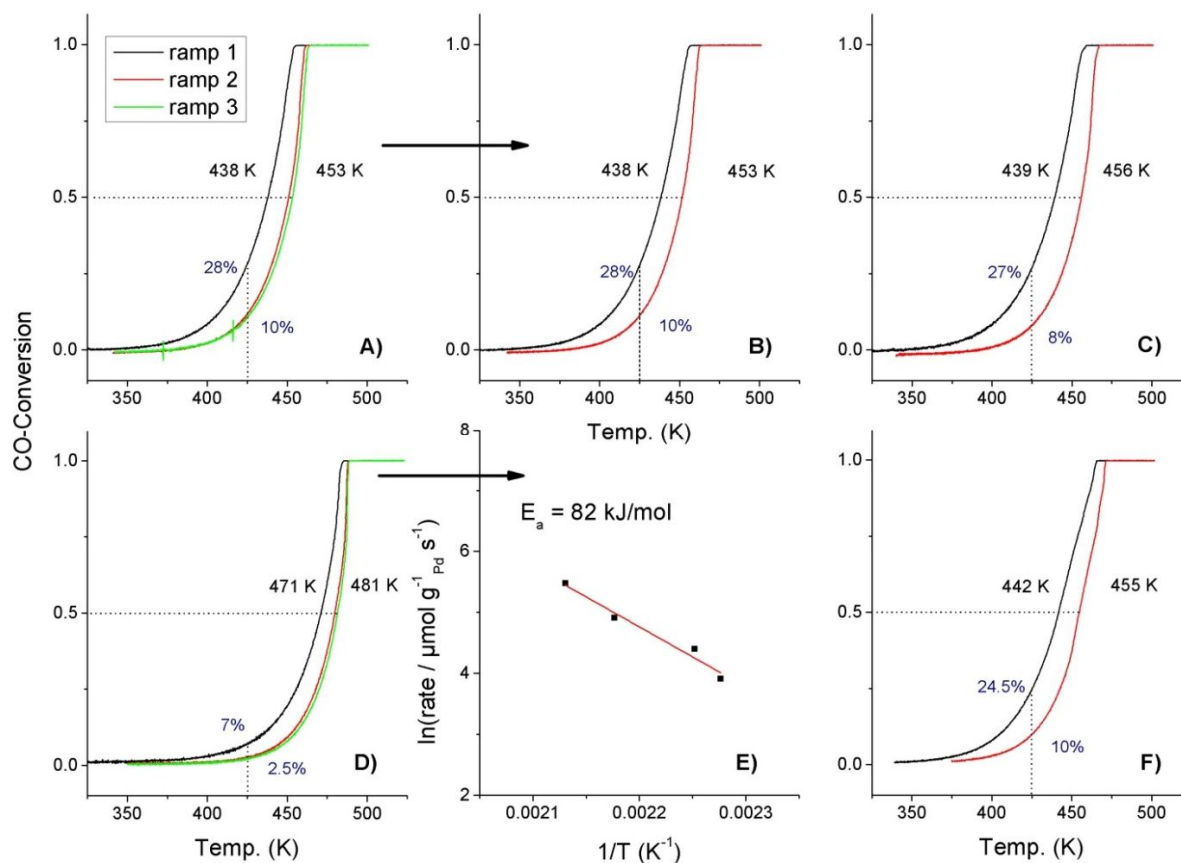


Fig. 3.4: CO-oxidation cycles of the 2.5% Pd/ZnO sample after repeated reduction in 5% H<sub>2</sub> at 473 K (A,B), at 573 K (new sample, C) and at 723 K (new sample, D, with determination of activation energy in the deactivated state afterwards, E) and comparison to measurement after reduction in 2% CO at 473 K (F).

From the activation behavior it can be suspected that the palladium species might not have been completely metallic after reduction in CO at 423 K or that some carbon species, formed upon reduction might become decomposed during the oxidation which might lead to a kind of re-dispersion. After reduction in CO containing atmosphere at 523 K (in the valley between the two TPR peaks), the first conversion cycle shows a lower slope and a more active catalytic system compared to the following cycles. When being repeated (reduction at 523 K and CO-oxidation cycles with the same sample), the catalytic behavior is exactly reproduced, only experiencing a negligible deactivation due to irreversible processes. When measured in state 3, after the reduction at the highest temperature, 673 K, the first conversion cycle still shows a slightly higher CO-oxidation activity, though the difference between the first and the following cycles is not so pronounced anymore as in case of the repeated measurements after 523 K reduction. Obviously the activating processes upon reduction must have been counteracted by some kind of other process, probably delimiting the active surface area. The activation energy which was determined in the deactivated state of the catalyst after 623 K

reduction (after the three conversion cycles), was 49 kJ/mol however, similar to earlier determined values of 42-60 kJ/mol.<sup>30</sup>

In case of the higher loaded sample (Fig. 3.4), hydrogen containing reducing atmosphere has been applied and CO-oxidation runs were repeated twice, each time after reduction at 473 K (panels A+B). A similar reversible process of activation in the first cycle and deactivation upon CO-oxidation, compared to the lower loaded sample, reduced in CO atmosphere, was observed with exactly the same values for  $T_{0.5}$  and  $X_{425}$  for runs A+B. When a fresh batch of the sample was reduced until 573 K, the behavior was very similar again, the sample only experiencing slight deactivation (Fig. 3.4C). Another measurement with a fresh catalyst was performed after reduction at 723 K, where according to the TPR-profile of the sample (see Fig. 3.1C) further changes should occur (Fig. 3.4D). At this high reduction temperature all palladium should be in the PdZn state already, according to the XRD-measurements. Nevertheless the TPO profile still shows the first cycle being more active than the other cycles, though with a pronounced overall deactivation, probably due to sintering or other irreversible effects like carbonate formation. The activation energy determined after the cycles (Fig. 3.4E) was higher than the one in case of the lower loaded sample, namely 82 kJ/mol. For further comparison of the influence of the reducing atmosphere, one measurement with a fresh amount of sample after reduction in 2% CO-He, also at 473 K, has been conducted, presented in the last panel (Fig. 3.4F): the influence on position and shape of the first and the second curve was negligible, but the sample is slightly less active than in case of the hydrogen which might be explained also by the difference, CO and hydrogen show with regard to reactivity towards the palladium (dissolving probability, re-dispersion and hydride/carbon formation effects). Catalytic measurements for the 5 wt.-% sample showed similar trends.

### 3.3.4. Electron microscopy study of the 0.75 wt.-% Pd/ZnO sample in different states

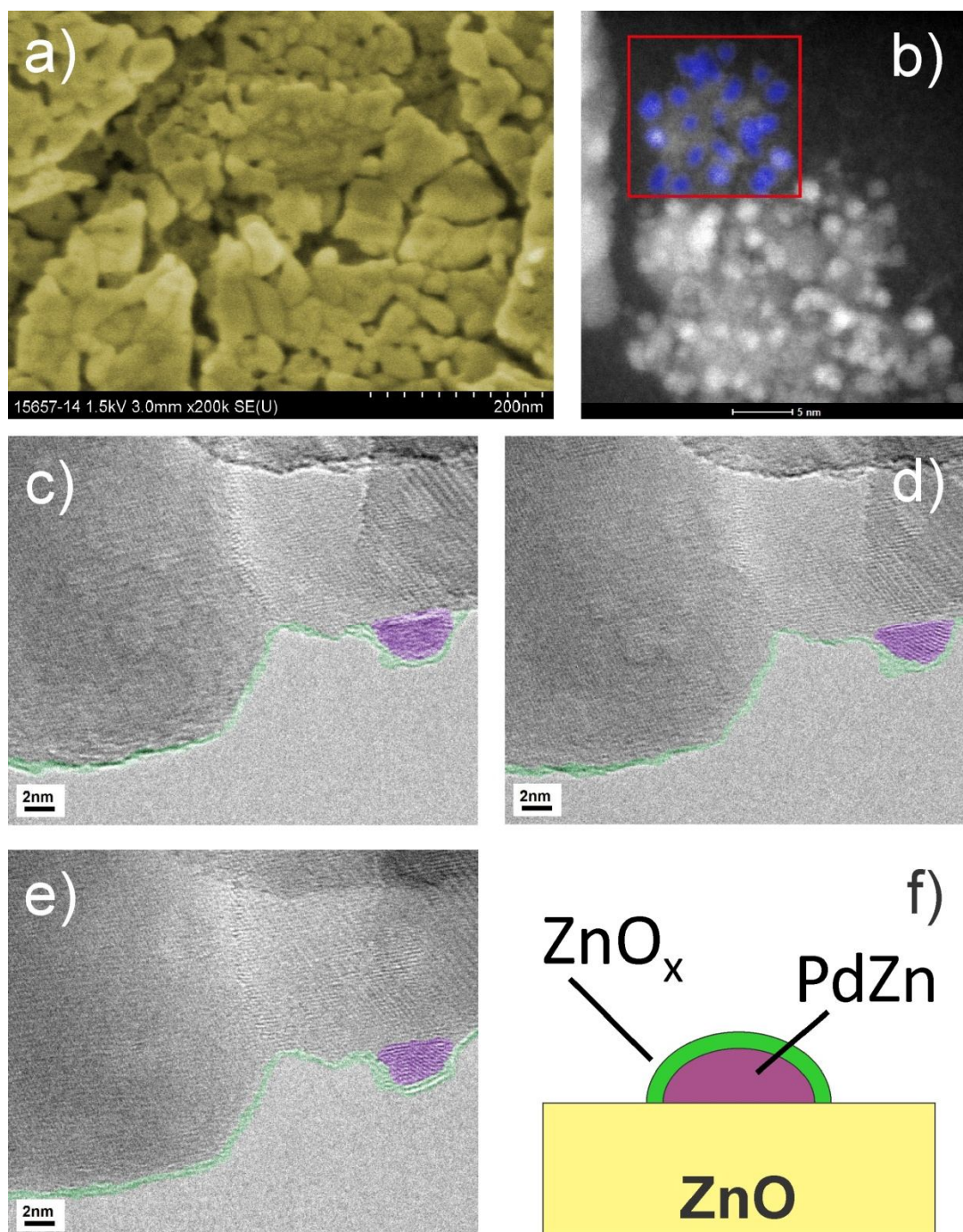


Fig. 3.5: 0.75 wt.-% Pd/ZnO sample: SEM-image in calcined state (colored yellow, a), HAADF-STEM image after reduction in hydrogen at 323 K (Pd in red frame colored blue, b), HR-TEM images after reduction in 5% CO/Ar at 623 K at different focus (c-e) and proposed schematics for the catalyst state after 623 K-reduction (PdZn colored purple,  $\text{ZnO}_x$  overlayer colored green, f). Original image presented in SI (Fig. S3.5).

A plate-like, porous structure of the calcined 0.75% Pd/ZnO sample with crystallite diameters of about 40 nm can be observed in the SEM micrograph presented in figure 3.5a. The HAADF-STEM image of the same sample after reduction in hydrogen atmosphere at 323 K is presented in figure 3.5b. In that mode, it is possible to distinguish the metallic palladium from the oxide support due to its much higher atomic number. The particles are depicted as bright grey spheres with almost uniform size in the image and are homogeneously distributed. The size of about 2-3 nm for the lowest loading confirms the CO-chemisorption results, presented in table 3.1. Since the size and distribution of the palladium particles in that sample was found to be appropriate to study the processes previously discovered by the TPR and catalytic measurements in greater detail, some amount of the sample has been reduced at 623 K in 5% CO/Ar gas mixture, similar to the kinetic experiment (Fig. 3.3) and transferred to the TEM without air-contact. Figure 3.5 c-e presents a series of images taken from one specific region of the sample, where a palladium particle in exposed position at the support surface could be found. By variation of the focus of the microscope, we were able to identify a zinc oxide over-layer covering the palladium particle as well as parts of the support. That would be an explanation for the further decrease in activity found in the kinetic studies in that state. A slight astigmatism might also be present in panels c-e. Though it was not possible to directly study the PdZn lattice parameter by microscopy, according to our XRD-experiments and supported by the kinetic studies, such small Pd particles should be alloyed already almost completely. Based on that observation we propose a model scheme in figure 3.5f, where the palladium after 623 K reduction is present as PdZn, covered by a partially reduced ZnO<sub>x</sub> over-layer (SMSI). To further proof the over-growth, surface sensitive investigations (IR, XPS, chemisorption) were performed.

### **3.3.5. Electronic and structural surface investigations: reversible formation of SMSI overlayer versus alloying**

#### a) DRIFTS:

Due to the benefit of a low palladium loading on reflectivity in general, the highly dispersed 0.75 wt.-% Pd/ZnO sample studied by electron microscopy has also been selected for the diffuse reflectance infrared measurements. The sample has been reduced in-situ by a mixture of 2% CO in Argon (30 min.) at increasing temperatures, according to the TPR-profile, presented in figure 3.3, first panel, and infrared spectra after adsorption of CO at liquid nitrogen temperatures (77 K) were recorded during desorption by pressure decrease. The first reduction took place at 323 K, where most of the palladium present is expected to be in its

elemental state, and successively the sample got reduced and was measured at 523 K and afterwards at 623 K, in the state of the HR-TEM images. The respective Kubelka-Munk spectra are presented in the following figure 3.6 (A-C):

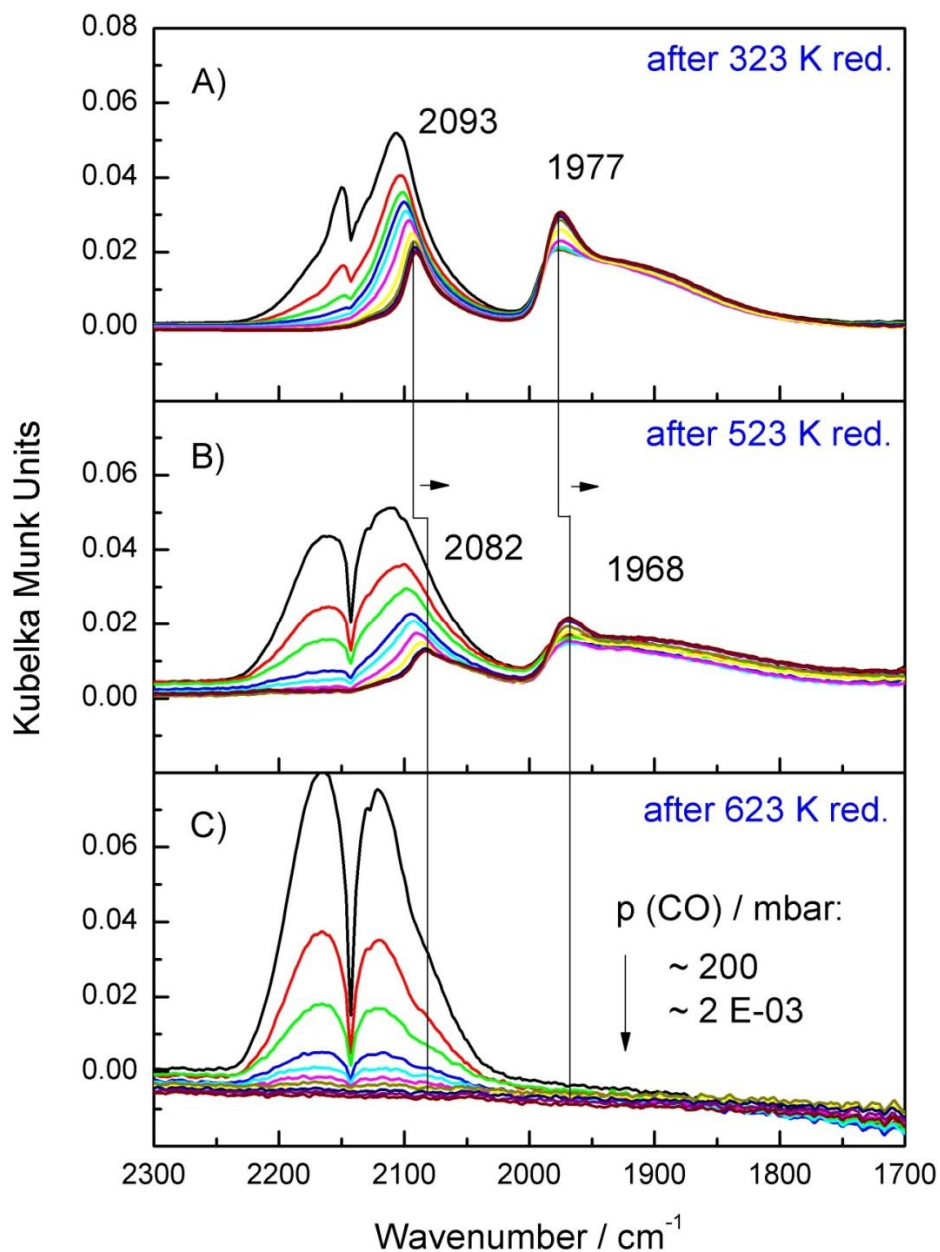


Fig. 3.6: DRIFTS measurement of 0.75% Pd/ZnO sample during decreasing CO-partial pressure at 77 K, after reduction for 30 min in 2% CO-Ar at 323 K (A), 523 K (B) and 623 K (C).

After reduction of the sample at 323 K in the CO-Ar gas mixture, pure CO is flushed in at liquid nitrogen temperature and gets adsorbed on the noble metal. Besides the typical vibrational features for CO linearly bonded to metallic Pd (2093 cm<sup>-1</sup>) and bridged bonded to metallic palladium (1977 cm<sup>-1</sup>), a palladium species at 2150 cm<sup>-1</sup> is present on which CO weakly bonds and desorbs again with decreasing partial pressure. The vibrational frequencies observed in our study are in agreement with literature values for CO linearly and bridged bond on metallic palladium,<sup>18,20–22,36,37</sup> supported on zinc oxide as well as for linearly bond CO on oxidic palladium (PdO, 2150 cm<sup>-1</sup>).

After 323 K reduction, most of the Pd is in its metallic state with a minor content of palladium oxide. After reduction of the sample at 523 K (cf. after the first reduction peak in the TPR-profile of figure 3.3) and CO-adsorption again at 77 K, the wave numbers for the linearly and bridged bond CO on the palladium species got shifted towards lower numbers, namely 2085 cm<sup>-1</sup> and 1970 cm<sup>-1</sup>. This red-shift has been reported earlier<sup>8,37</sup> and is typical for the electronic modifications that take place during alloy formation. Compared to metallic palladium, a negative partial charge of Pd in PdZn is present and therefore the capability to electron back-donation into anti-bonding states of the CO-molecule that weakens the C-O-bond, increases.

The total intensity of the adsorbed CO got slightly decreased during the higher temperature reduction, without significant changes in the intensity ratio between linearly and bridged bond species. Literature reports a decrease of bridged bond species with increasing formation of intermetallic PdZn<sup>37</sup> due to the increasing distance between two palladium atoms which would get too large for the CO-molecule. Therefore, Pd segregation seems possible. Another measurement after reduction at 573 K was performed revealing complete reproducibility of the results. After the third reduction step at 623 K (after the second reduction peak in the TPR-profile) however, the signals for CO on palladium or palladium-zinc alloy have completely disappeared – only gas phase CO is detected. This is a clear indication for the formation of a ZnO<sub>x</sub> over-layer which has been formed on the metal through the influence of strong metal-support interaction and inhibits CO to get adsorbed onto palladium. The measurements therefore confirm our observations of the covering of the palladium particles by hexagonal zinc oxide (Fig. 3.5) as well as the slight decrease of activity in the CO-oxidation measurements compared to a lower reduction temperature (Fig. 3.3) and support the hypothesis that alloy formation - at least in case of the lowest loaded sample – starts before complete decoration of the sample with a reduced support over-layer. Similar

processes were reported by Föttinger et al.<sup>22</sup> who confirmed the IMC formation on Pd/ZnO during MSR conditions or upon reduction at 623 K as an ongoing process, proceeding from the outer part of the Pd particle to the inner part, as well as the reversibility of this mechanism by oxygen treatment at 573 K, leading to a formation of metallic Pd and ZnO islands on-top of the pre-formed PdZn-overlayer.

b) XPS:

In order to study the surface decoration effects as well as electronic surface modifications XPS measurements after reductive and oxidative in-situ treatment have been performed using two different kinetic energies of the photo-electrons for accessing different information depth. Furthermore, the shift in the binding energy during the treatments was monitored in order to detect electronic modifications due to possible alloy formation. For the photoelectronic studies the 2.5 wt.-% Pd/ZnO sample was investigated to understand the differences between the cycles observed in kinetic measurements (Fig. 3.4). A part of the probe was pre-reduced in the kinetic measurements setup (473 K in 5% H<sub>2</sub>-He gas mixture, sample 16949) and transferred to the XPS setup with the help of a vacuum transfer box to avoid air contact. Another batch was deactivated by 3 CO-oxidation cycles (373-523 K, common reaction conditions) after the pre-reduction at 473 K (16957). Table S3.1 and Fig. 3.7 summarize the results of the integrated peak areas of the Pd3d and the Zn3d core levels and at two different information depths ( $E_{kin} = 200$  and 800 eV). It can be noted that the Pd/Zn ratio stays more or less the same if the photoelectrons are being emitted from deeper regions, namely 4.5 to 5.7 percent of palladium independent of the treatment. The situation is different at surface near regions ( $E_{kin} = 200$  eV): The batch that has been pre-reduced and transferred to the XPS chamber shows a Pd:Zn ratio of 7.6 to 92.4 (UHV-measurement at RT). The sample that was in its deactivated state, showed a much higher Pd-content at the surface with 12.7%. When being reduced in-situ inside the XPS chamber (0.4-2.5 mbar H<sub>2</sub> partial pressure, maximum 2h at 473 K), the palladium content at the surface got reduced more and more until similar values that were discovered in the pre-reduced sample. That could be an indication for surface decoration and for the reversibility of the decoration process, since both measurements show very similar results, or an indication for reversible surface alloying, as described earlier<sup>8</sup> which would also lead to a decrease in the Pd/Zn intensity ratio.

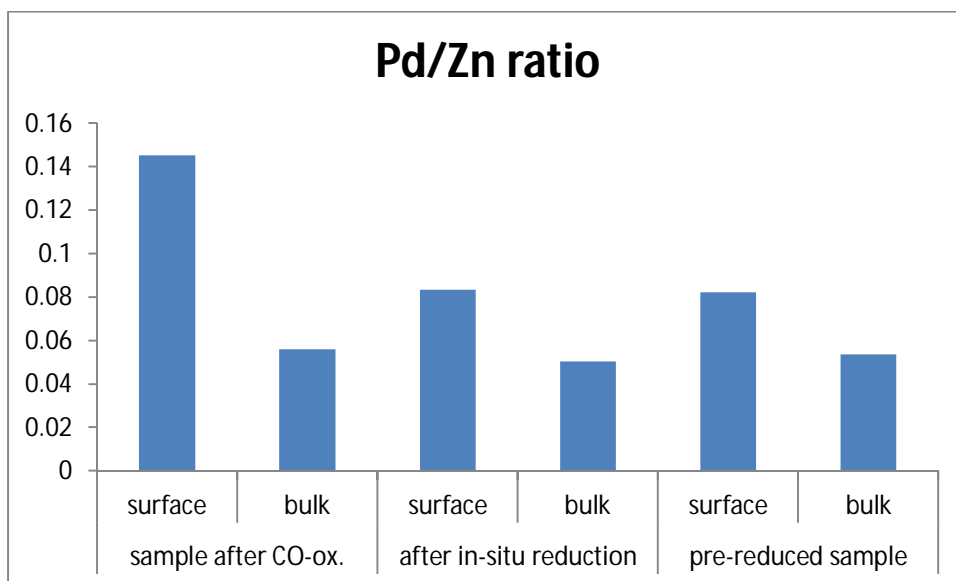


Fig. 3.7: Zn segregation at the surface relative to the bulk composition during reduction of sample # 16688.

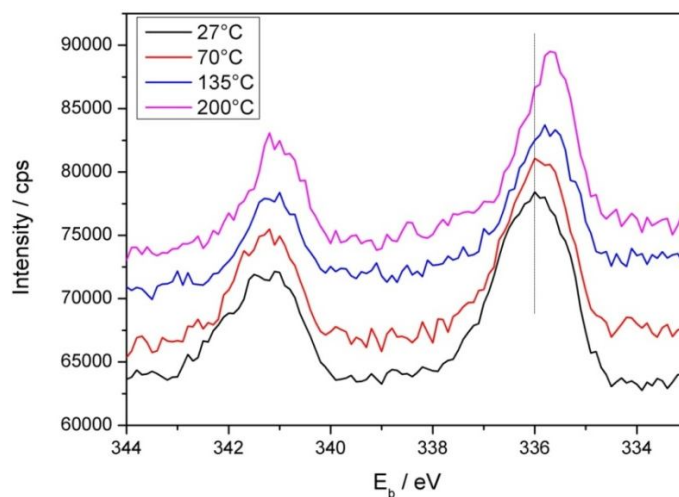


Fig. 3.8: Pd-3d signal ( $E_{kin} = 200$  eV) of pre-reduced 2.5 % Pd/ZnO sample (16949) during in-situ CO-oxidation (RT - 473 K, 5 Kpm, 0.3 mbar, 1 ml/min  $O_2$ , 2 ml/min CO).



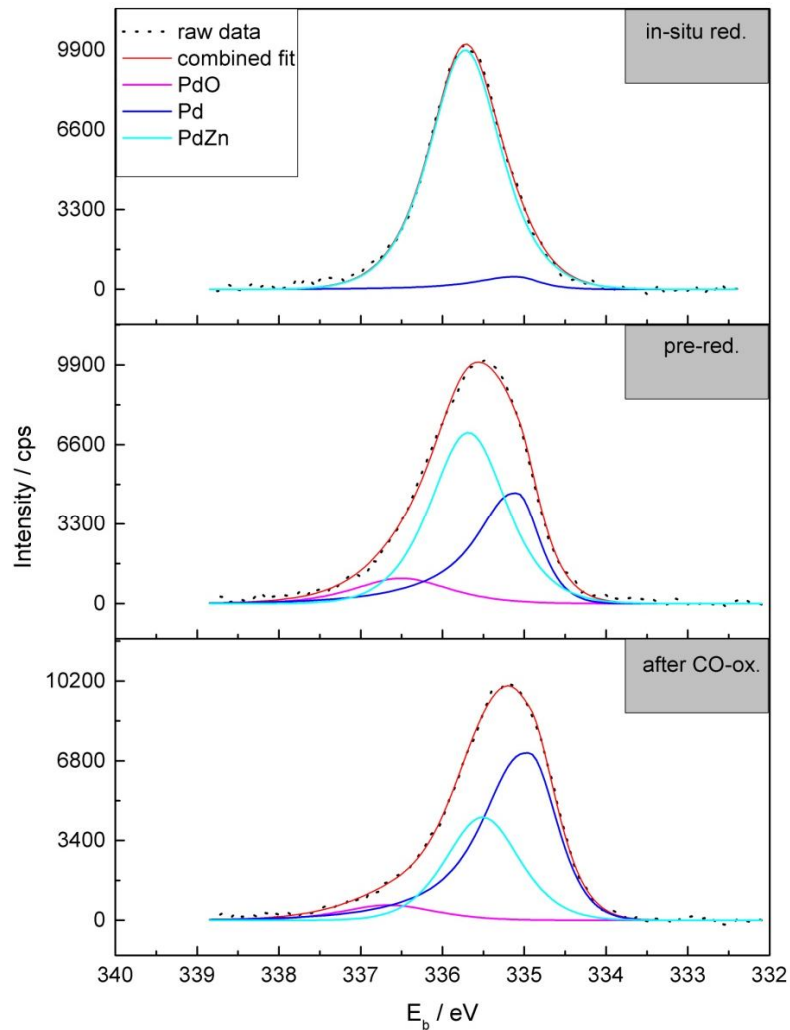


Fig. 3.9: Comparison of Pd3d<sub>5/2</sub> composition at different conditions ( $E_{\text{kin}} = 200$  eV). Pre-reduced 2.5% sample (16949, center) and deactivated sample (16957) after CO-oxidation (lower layer) and after successive in-situ reduction process in XPS-setup (top layer).

After the UHV measurement of the pre-reduced sample at room temperature, a temperature programmed CO-oxidation procedure was conducted in the XPS-chamber (RT-473 K, 5 Kpm heating ramp) with a total gas pressure of 0.3 mbar and a flow of 1 ml/min of oxygen and 2 ml/min of CO in order to simulate the conditions of the light-off experiments. Figure 3.8 shows the Pd3d signal ( $E_{\text{kin}} = 200$  eV) during the experiment, with in-situ scans at 300, 343, 408 and 473 K. Increasing CO<sub>2</sub> formation was detected by mass spectrometry with increasing temperature, as expected. A continuous shift of the palladium signal to lower binding energies is visible with ongoing oxidation and increasing temperature which is a hint for the instability of the (alloyed) surface state formed during the reduction towards oxidative conditions.

Due to the monitored changes in the electronic behavior, alloy formation is expected to play a role at least at the surface, when the system is being reduced under the executed conditions. Regarding figure 3.9, we can discuss the energy shift as well as the composition of the palladium species in more detail: in the freshly (in-situ) reduced state (1h at 473 K), the energy shift is most pronounced with a peak maximum ( $3d_{5/2}$ ) at 335.7 eV. The shape of the peak is symmetric, both being an indication for PdZn alloy formation.<sup>19</sup> The fit suggests that about 5% of Pd remained in its metallic state. The spectrum of the pre-reduced sample (16949) shows that the alloy must already partially decomposed during the transport (PdZn: 56%, Pd: 34%, PdO: 10%). The binding energy shifted to lower values (about 335.5 eV). Decomposition could lead to formation of ZnO islands covering the Pd and leading to a similar Pd/Zn surface ratio as compared to the in-situ reduced state.<sup>24</sup>

After CO-oxidation (deactivated sample 16957 measured under UHV-conditions at RT) the signal got shifted to even lower binding energies and closer to those expected for metallic palladium (335.2 eV).<sup>38</sup> Also the shape of the signal indicates the presence of a single metallic species.<sup>39</sup> The composition was estimated to be 34% PdZn, 57% Pd and 9% PdO.

The binding energies are in good agreement to literature.<sup>19,36,40,41</sup> While Iwasa et al.<sup>7,13</sup> reported a shift in the Pd  $3d_{5/2}$  signal of 0.1 eV by reduction of a 10 wt.-% Pd/ZnO catalyst from RT to 493 K, attributed to metal-support interaction, and of further 0.6 eV to 335.9 eV between 573 and 673 K reduction, Zsoldos et al.<sup>14</sup> reported an increase of the binding energy by 1 eV to 335.85 eV in between 420 and 880 K reduction of a 8.5 wt.-% catalyst. Earlier, Wehner et al.<sup>15</sup> noticed a reversible shift of the binding energy of a 2 wt.-% Pd/ZnO catalyst after 523 K reduction in hydrogen (336 eV), exposure to air at RT (335.5 eV) and repeating the 523 K reduction. This reversibility was confirmed by their Zn *LMM* Auger measurements by a shoulder at higher  $E_{kin}$  in the reduced state, representing the intermetallic compound. More recent measurements confirmed the alloying process in aerosol-derived PdZn particles<sup>16</sup> (335 eV  $\rightarrow$  335.7 eV) and by monitoring the Zn3d peak.<sup>17</sup> A difference from metallic palladium (335 eV) to monolayer PdZn (335.3 eV) and multilayer PdZn (335.8 eV) has been reported by Rameshan et al.<sup>18</sup>

Details to the fit components presented in figure 3.9 are listed in the following table 3.2. The higher FWHM of Pd after CO oxidation might indicate the presence of small amounts of zinc and/or carbon species incorporated into Pd or particle restructuring.

Table 3.2: parameters of the fitted Pd3d species

	component	binding energy / eV	content / %	FWHM / eV
in-situ red.	Pd	335.1	4.8	0.9
	PdZn	335.7	95.2	1.1
pre-red.	Pd	335.1	34.0	1
	PdZn	335.7	55.8	1.2
	PdO	336.5	10.2	1.5
after CO- ox.	Pd	335.0	57.3	1.4
	PdZn	335.5	33.9	1.2
	PdO	336.7	8.8	1.5

## c) CO-chemisorption:

As a third surface sensitive technique and following to earlier studies of the SMSI phenomenon<sup>26,30</sup> the chemisorption of carbon monoxide has been applied to investigate the total uptake of CO on the noble metal surface, calculate its dispersion and study the dependence of the chemisorption capacity on the reduction of the system. Similar to these studies, the CO-chemisorption capacity of the Pd/ZnO system markedly reduced when the catalyst had been treated in reducing atmosphere at elevated temperatures. In this case the 2.5 % sample has been measured after reduction at 323 K (in hydrogen gas mixture), measured again after reduction at 623 K, re-calcined at 573 K (30 min.) in 20% O<sub>2</sub>-Ar and measured for the second time after reduction at 323 K. As shown in figure 3.10, the initial CO-chemisorption capacity and the active metal surface area get reduced to about 30% of the values of the room temperature reduced sample, after being further reduced at 573 K. After re-calcination and subsequent reduction at 323 K the initial chemisorption capacity of the sample gets restored completely. A fresh batch of the sample has furthermore been reduced at 723 K in order to study the surface properties after the reduction peak in the TPR profile, shown in figure 3.1. Further reduction of the chemisorption capacity, compared to the measurement after 573 K treatment could be detected. Whereas the reduced uptake after reduction until 573 K could be ascribed to alloy formation, the decrease after 723 K reduction should be a result of the additional formation of a ZnO<sub>x</sub> over-layer respectively Zn enrichment at the surface of the alloy, induced by SMSI.

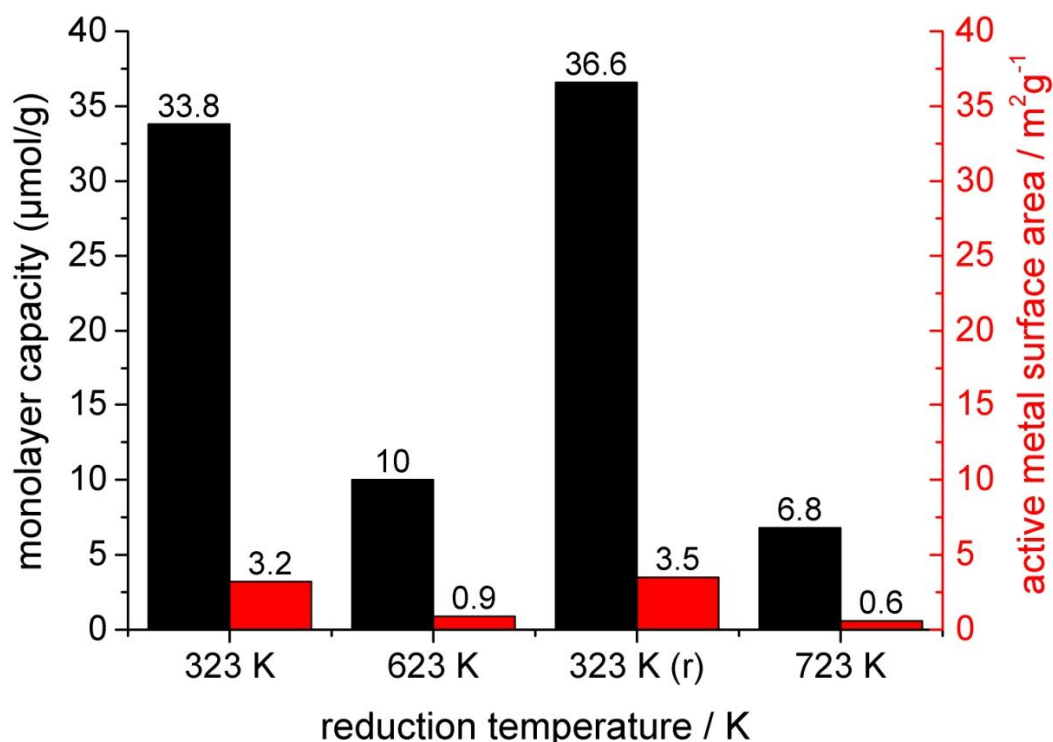


Fig. 3.10: monolayer capacities (black bars) in CO chemisorption and determined active metal surface area (red bars) of the 2.5 % Pd/ZnO sample after reduction at 323 K, 623, re-calcination and repeated 323 K-reduction and after 723 K-reduction (fresh sample).

The 5wt.-% sample has also been studied by CO-chemisorption after different reductive pre-treatments, according to the TPR-profile shown in figure 3.1D. In supplemental part (Fig. S3.3), the dependence of the strong (chemisorption) adsorption isotherms of the reduction temperature 323, 573 and 723 K is presented. The adsorbed CO volume until saturation of the noble metal surface got reduced by 50% after the 573 K-reduction, which could be again explained by alloy formation. After 723 K-reduction, the CO-uptake has been further reduced, now by 75% compared to the original uptake after 323 K reduction.

### 3.4. Summary and Conclusion

In the present study the structure-function relationship during reductive treatment of various loaded Pd/ZnO catalysts in different reducing atmospheres was investigated. We hereby studied the electronic and structural constitution at the metal-support interface and at the surface on the CO-oxidation activity. Homogeneously distributed Pd particles on zinc oxide support with very narrow variation of BET surface area were obtained by controlled co-precipitation. We found that TPR in CO-atmosphere was a more specific method to distinguish between different reduction steps, compared to hydrogen atmosphere. XRD measurements of the 2.5 and the 5 wt.-% sample showed that the phase transformation in the bulk into intermetallic PdZn happens to a major extent above 473 K, while beginning alloying at the surface starting already at this temperature in hydrogen atmosphere cannot be excluded. Further measurements confirmed that major PdZn formation takes place in case of reduction at 623 K in CO-atmosphere. All CO-TPR profiles showed two pronounced reduction signals above the palladium oxide reduction temperature, while the intensity ratio was different in case of the lower loaded 0.75% sample. Catalytic measurements were able to confirm a reversible process happening at the surface and being beneficial for CO-oxidation activity. This was basically independent of the reduction atmosphere, reduction temperature and catalyst loading. Though the nature of the chemical species might differ, the density of states at the Fermi edge can be similar.

However as for the 0.75% sample reduced in CO below the temperature of the first TPR signal (423 K), the sample became more active during the reaction cycles which might be an indication for not completely reduced palladium species in that case or beginning surface changes. When being reduced after the first TPR signal (523 K) the activity during the first reaction cycle is remarkably higher than in the following cycles, when the catalyst returns to a deactivated state. When reduced above the temperature of the last TPR signal (623 K) the sample got deactivated in general, with the first cycle still being more active, but also with a less pronounced difference between the cycles. The shape and slope of the curves are an indicator for the chemical dynamics and the distribution of active sites. A sharp increase of the slope would indicate a more uniform distribution of these sites. Activation energy determined in deactivated state was found to vary between 49 (0.75% sample, CO-reduction at 623 K) and 82 kJ/mol (2.5% sample, H<sub>2</sub>-reduction at 723 K). HR-TEM and DRIFTS studies in case of the lowest loaded sample both confirmed the formation of an SMSI induced

ZnO<sub>x</sub> over-layer after reduction at 623 K in CO, leading to a suppressed CO-adsorption capacity. This is an explanation for the loss of activity in CO-oxidation measurement, compared to the experiment after 523 K reduction. IR measurements furthermore confirmed the presence of surface alloy already after 523 K reduction. On the other hand the XPS investigation of the 2.5 wt.-% sample confirmed the electronic modification at the surface, induced by surface alloying in case of reduction in hydrogen at 473 K already as well as the reversibility of that process and the oxidative decomposition of the surface alloy after air contact as reported previously by Föttinger et al.<sup>22</sup> This reversible process was also confirmed by CO-chemisorption measurements, by a reduced CO adsorption capacity after reduction and a restoration during re-calcination and RT-reduction. Furthermore these measurements confirmed the trend of loss of active surface area with increasing reduction temperature.

All these observations lead to the final conclusion that electronic and structural surface modifications like alloying and ZnO<sub>x</sub> over-layer formation both take place during the performed treatments and cannot be clearly separated. Though both processes can be explained by the presence of strong metal-support interaction, the original idea of SMSI just described the over-growth of the noble metal by a reduced oxidic support without discussing alloying before or afterwards. The order of the described processes during TPR might also be dependent on the palladium loading, but according to our results there is a tendency of the occurrence of electronic surface modifications (alloying), increasing the CO-oxidation activity before additional SMSI-induced over-growth by a ZnO<sub>x</sub> layer decreasing the CO-oxidation activity due to a loss of accessible active sites.

#### **Acknowledgement:**

Maik Hashagen is acknowledged for BET measurements. Margit Lang of the department of analytical chemistry at the University of Ulm is acknowledged for the ICP-OES measurements. Wiebke Frandsen and Norbert Pfänder are acknowledged for electron microscopy measurements. The HZB is acknowledged for the allocation of beam time.

### 3.5. References

1. Iwasa, N., Kudo, S., Takahashi, H., Masuda, S. & Takezawa, N. Highly selective supported Pd catalysts for steam reforming of methanol. *Catal. Lett.* **19**, 211–216 (1993).
2. Trimm, D. L. & Önsan, Z. I. Onboard Fuel Conversion for Hydrogen-Fuel-Cell-Driven Vehicles. *Catal. Rev.* **43**, 31–84 (2001).
3. Takezawa, N. & Kobayashi, H. N. Takezawa and H. Kobayashi, Hyomen (Surface) 11 (1981) 456. **11**, 456 (1981).
4. Agarás, H., Cerrella, G. & Laborde, M. A. Copper catalysts for the steam reforming of methanol. *Appl. Catal.* **45**, 53–60 (1988).
5. Karim, A., Conant, T. & Datye, A. The role of PdZn alloy formation and particle size on the selectivity for steam reforming of methanol. *J. Catal.* **243**, 420–427 (2006).
6. F. Brown, L. A comparative study of fuels for on-board hydrogen production for fuel-cell-powered automobiles. *Int. J. Hydrog. Energy* **26**, 381–397 (2001).
7. Iwasa, N., Masuda, S., Ogawa, N. & Takezawa, N. Steam reforming of methanol over Pd/ZnO: effect of the formation of PdZn alloys upon the reaction. *Appl. Catal. Gen.* **125**, 145–157 (1995).
8. Föttinger, K. in *Catalysis* (2013).  
<<http://pubs.rsc.org/en/content/chapter/bk9781849735780-00077/978-1-84973-578-0>>
9. Armbrüster, M. *et al.* The Intermetallic Compound ZnPd and Its Role in Methanol Steam Reforming. *Catal. Rev.* **55**, 289–367 (2013).
10. Hong, C.-T. & Yu, F.-H. Effect of reduction and oxidation treatments on Pd/ZnO catalysts. *Appl. Catal.* **48**, 385–396 (1989).
11. Tew, M. W., Emerich, H. & van Bokhoven, J. A. Formation and Characterization of PdZn Alloy: A Very Selective Catalyst for Alkyne Semihydrogenation. *J. Phys. Chem. C* **115**, 8457–8465 (2011).
12. Chin, Y.-H., Dagle, R., Hu, J., Dohnalkova, A. C. & Wang, Y. Steam reforming of methanol over highly active Pd/ZnO catalyst. *Catal. Today* **77**, 79–88 (2002).
13. Iwasa, N. & Takezawa, N. New supported Pd and Pt alloy catalysts for steam reforming and dehydrogenation of methanol. *Top. Catal.* **22**, 215–224 (2003).
14. Zsaldos, Z., Sarkany, A. & Guzzi, L. XPS Evidence of Alloying in Pd/ZnO Catalysts. *J. Catal.* **145**, 235–238 (1994).

15. Wehner, P. S., Tustin, G. C. & Gustafson, B. L. XPS Study of the Reduction and Reoxidation of ZnO-Supported Palladium. *J. Catal.* **88**, 246–248 (1984).
16. Halevi, B. *et al.* Aerosol-Derived Bimetallic Alloy Powders: Bridging the Gap†. *J. Phys. Chem. C* **114**, 17181–17190 (2010).
17. Halevi, B. *et al.* Catalytic reactivity of face centered cubic PdZn<sub>n</sub> for the steam reforming of methanol. *J. Catal.* **291**, 44–54 (2012).
18. Rameshan, C. *et al.* Subsurface-Controlled CO<sub>2</sub> Selectivity of PdZn Near-Surface Alloys in H<sub>2</sub> Generation by Methanol Steam Reforming. *Angew. Chem. Int. Ed.* **49**, 3224–3227 (2010).
19. Friedrich, M., Teschner, D., Knop-Gericke, A. & Armbrüster, M. Influence of bulk composition of the intermetallic compound ZnPd on surface composition and methanol steam reforming properties. *J. Catal.* **285**, 41–47 (2012).
20. Conant, T. *et al.* Stability of bimetallic Pd–Zn catalysts for the steam reforming of methanol. *J. Catal.* **257**, 64–70 (2008).
21. Lebarbier, V. *et al.* CO/FTIR Spectroscopic Characterization of Pd/ZnO/Al<sub>2</sub>O<sub>3</sub> Catalysts for Methanol Steam Reforming. *Catal. Lett.* **122**, 223–227 (2008).
22. Föttinger, K., van Bokhoven, J. A., Nachttegaal, M. & Rupprechter, G. Dynamic Structure of a Working Methanol Steam Reforming Catalyst: In Situ Quick-EXAFS on Pd/ZnO Nanoparticles. *J. Phys. Chem. Lett.* **2**, 428–433 (2011).
23. Tauster, S. J., Fung, S. C. & Garten, R. L. Strong metal-support interactions. Group 8 noble metals supported on titanium dioxide. *J. Am. Chem. Soc.* **100**, 170–175 (1978).
24. Friedrich, M., Penner, S., Heggen, M. & Armbrüster, M. High CO<sub>2</sub> Selectivity in Methanol Steam Reforming through ZnPd/ZnO Teamwork. *Angew. Chem. Int. Ed.* **52**, 4389–4392 (2013).
25. Ryndin, Y. A., Hicks, R. F., Bell, A. T. & Yermakov, Y. I. Effects of metal-support interactions on the synthesis of methanol over palladium. *J. Catal.* **70**, 287–297 (1981).
26. Naumann d’Alnoncourt, R. *et al.* Strong metal–support interactions between palladium and iron oxide and their effect on CO oxidation. *J. Catal.* **317**, 220–228 (2014).
27. Iwasa, N., Arai, S. & Arai, M. Selective oxidation of CO with modified Pd/ZnO catalysts in the presence of H<sub>2</sub>: Effects of additives and preparation variables. *Appl. Catal. B Environ.* **79**, 132–141 (2008).
28. Johnson, R. S. *et al.* The CO oxidation mechanism and reactivity on PdZn alloys. *Phys. Chem. Chem. Phys.* **15**, 7768–7776 (2013).



29. Freund, H.-J., Meijer, G., Scheffler, M., Schlögl, R. & Wolf, M. Die CO-Oxidation als Modellreaktion für heterogene Prozesse. *Angew. Chem.* **123**, 10242–10275 (2011).
30. Kast, P. *et al.* CO oxidation as a test reaction for strong metal-support interaction (SMSI) in nanostructured Pd/FeO<sub>x</sub> powder catalysts, *Appl. Catal. A.* (2015) submitted.
31. Knop-Gericke, A. *et al.* in *Advances in Catalysis* (ed. Bruce C. Gates and Helmut Knözinger) **52**, 213–272 (Academic Press, 2009).
32. Starr, D. E., Liu, Z., Hävecker, M., Knop-Gericke, A. & Bluhm, H. Investigation of solid/vapor interfaces using ambient pressure X-ray photoelectron spectroscopy. *Chem. Soc. Rev.* **42**, 5833–5857 (2013).
33. Yeh, J. J. & Lindau, I. Atomic subshell photoionization cross sections and asymmetry parameters:  $1 \leq Z \leq 103$ . *At. Data Nucl. Data Tables* **32**, 1–155 (1985).
34. Briggs, D. & Seah, M. P. *Practical Surface Analysis, Auger and X-ray Photoelectron Spectroscopy.* (Wiley, 1990).
35. Anderson, J. R. & Pratt, K. C. *Introduction to Characterization and Testing of Catalysts.* (Academic Press London, 1985).
36. Eblagon, K. M., Concepción, P. H., Silva, H. & Mendes, A. Ultraselective low temperature steam reforming of methanol over PdZn/ZnO catalysts—Influence of induced support defects on catalytic performance. *Appl. Catal. B Environ.* **154–155**, 316–328 (2014).
37. Föttinger, K. The effect of CO on intermetallic PdZn/ZnO and Pd<sub>2</sub>Ga/Ga<sub>2</sub>O<sub>3</sub> methanol steam reforming catalysts: A comparative study. *Catal. Today* **208**, 106–112 (2013).
38. Teschner, D. *et al.* Alkyne hydrogenation over Pd catalysts: A new paradigm. *J. Catal.* **242**, 26–37 (2006).
39. Doniach, S. & Sunjic, M. Many-electron singularity in X-ray photoemission and X-ray line spectra from metals. *J. Phys. C Solid State Phys.* **3**, 285–291 (1970).
40. Rodriguez, J. A. & Kuhn, M. Interaction of Zinc with Transition-Metal Surfaces: Electronic and Chemical Perturbations Induced by Bimetallic Bonding. *J. Phys. Chem.* **100**, 381–389 (1996).
41. Engels, V. *et al.* Nanoparticulate PdZn—pathways towards the synthetic control of nanosurface properties. *Nanotechnology* **22**, 205701–205710 (2011).

## Supplementary Information

### A. Figures

1. Synthesis protocol for the 2.5% Pd/ZnO sample („Labmax“-co-precipitation)

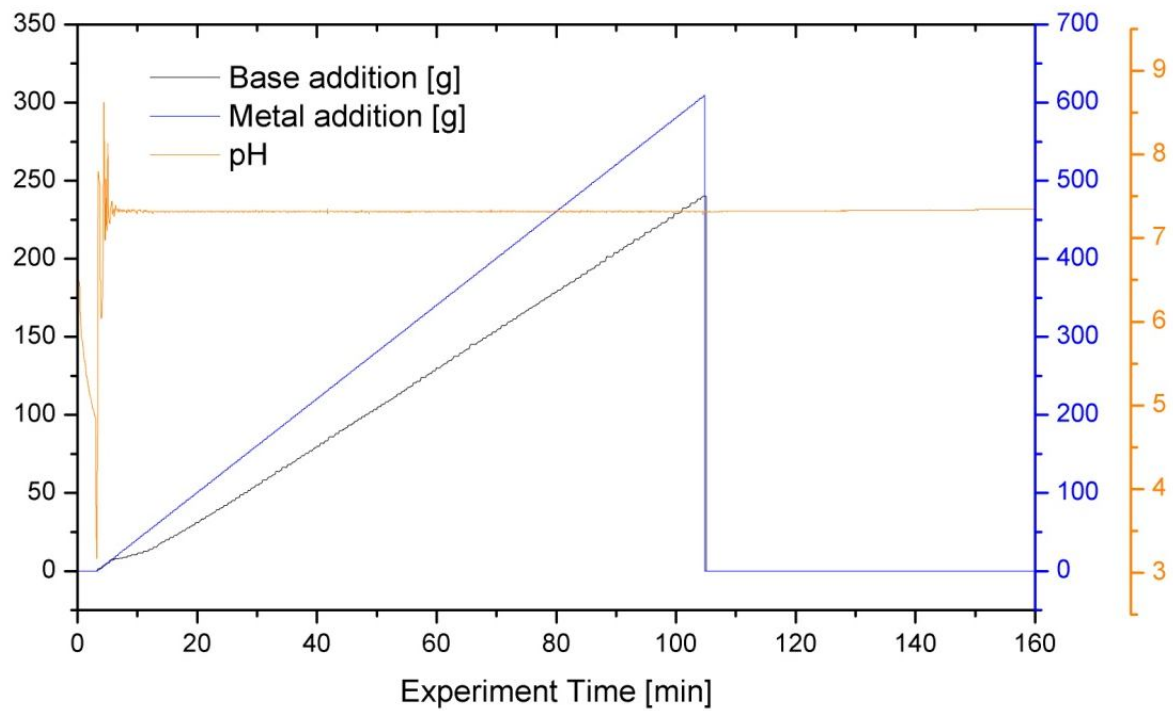


Fig. S3.1: Synthesis protocol for the 2.5% Pd/ZnO sample („Labmax“- co-precipitation)

2. Pseudo in-situ XRD measurements after reduction of the 2.5% Pd/ZnO sample at different temperatures in 5% H<sub>2</sub>-He

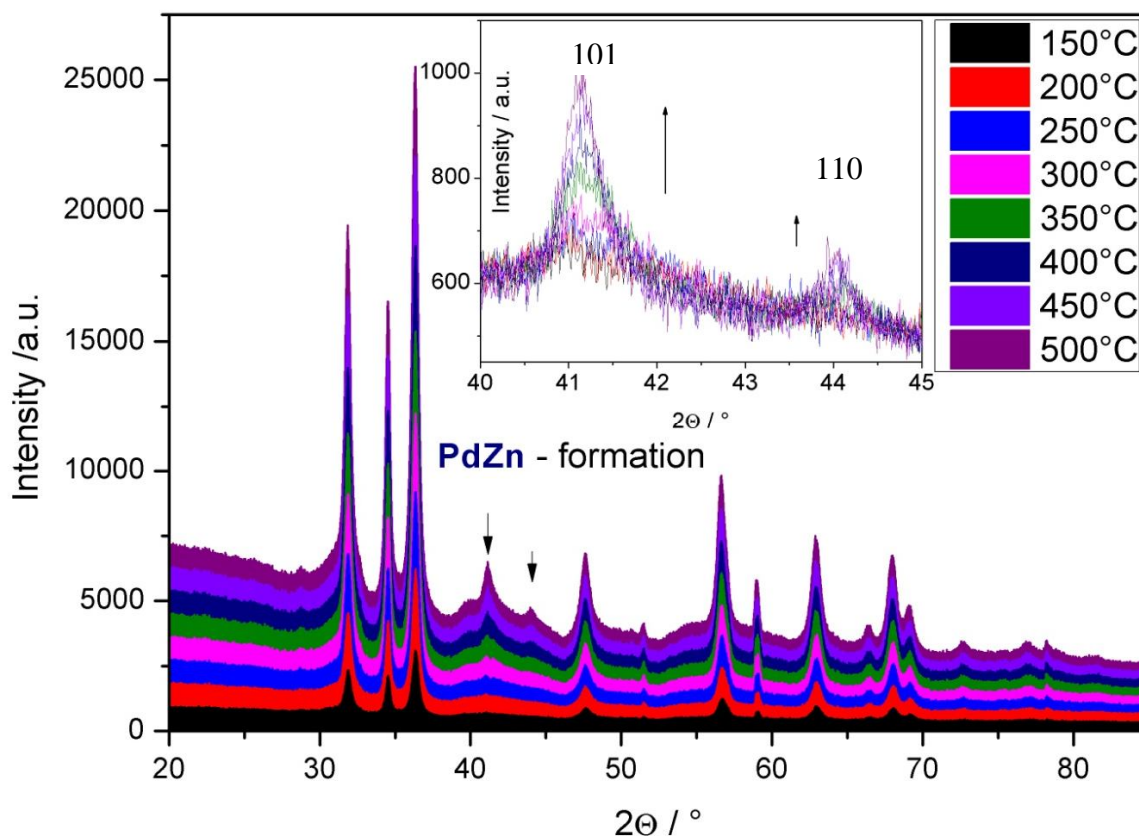


Figure S3.2: 2.5% Pd/ZnO sample during pseudo in-situ reduction in hydrogen gas mixture in the XRD setup. Note: shoulder at 40 ° at higher temperatures due to background effects in the stack-plot depiction; no metallic Pd detected.

3. Comparison of the CO-chemisorption of the 5% Pd/ZnO sample dependent on the temperature of pre-reduction

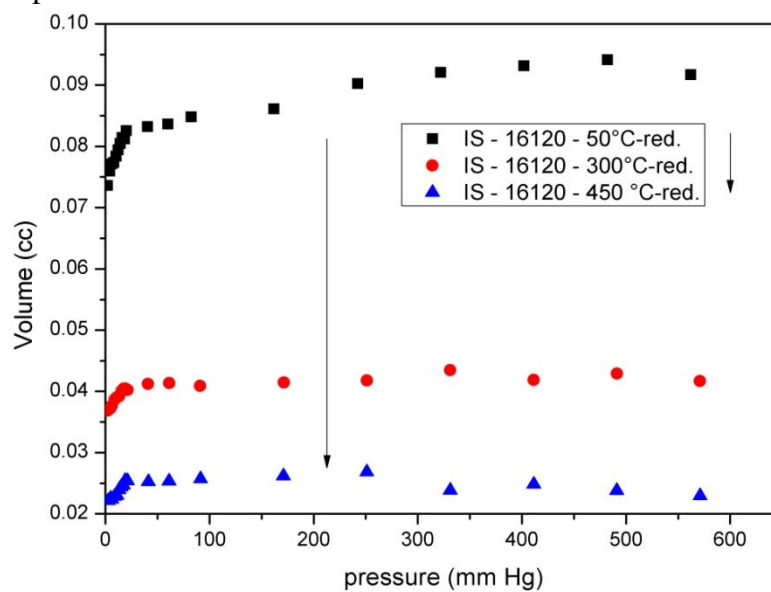


Fig. S3.3: CO-chemisorption isotherms of sample the 5 wt.-% sample after reduction at 323 K (black squares), 573 K (red circles) and 723 K (blue triangles).

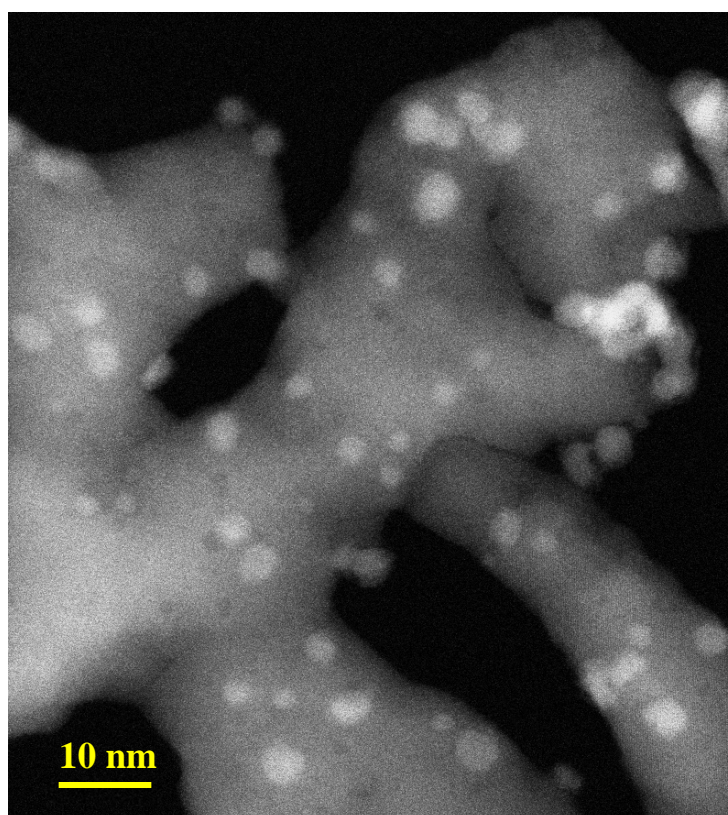


Fig. S3.4: HAADF-STEM image of 2.5% Pd/ZnO (16688) after reduction in 2% CO-He at 473 K.

4. Original version of figure 3.5, presenting the SEM (a), STEM (b) and HR-TEM (c-e) images of the 0.75% Pd/ZnO sample:

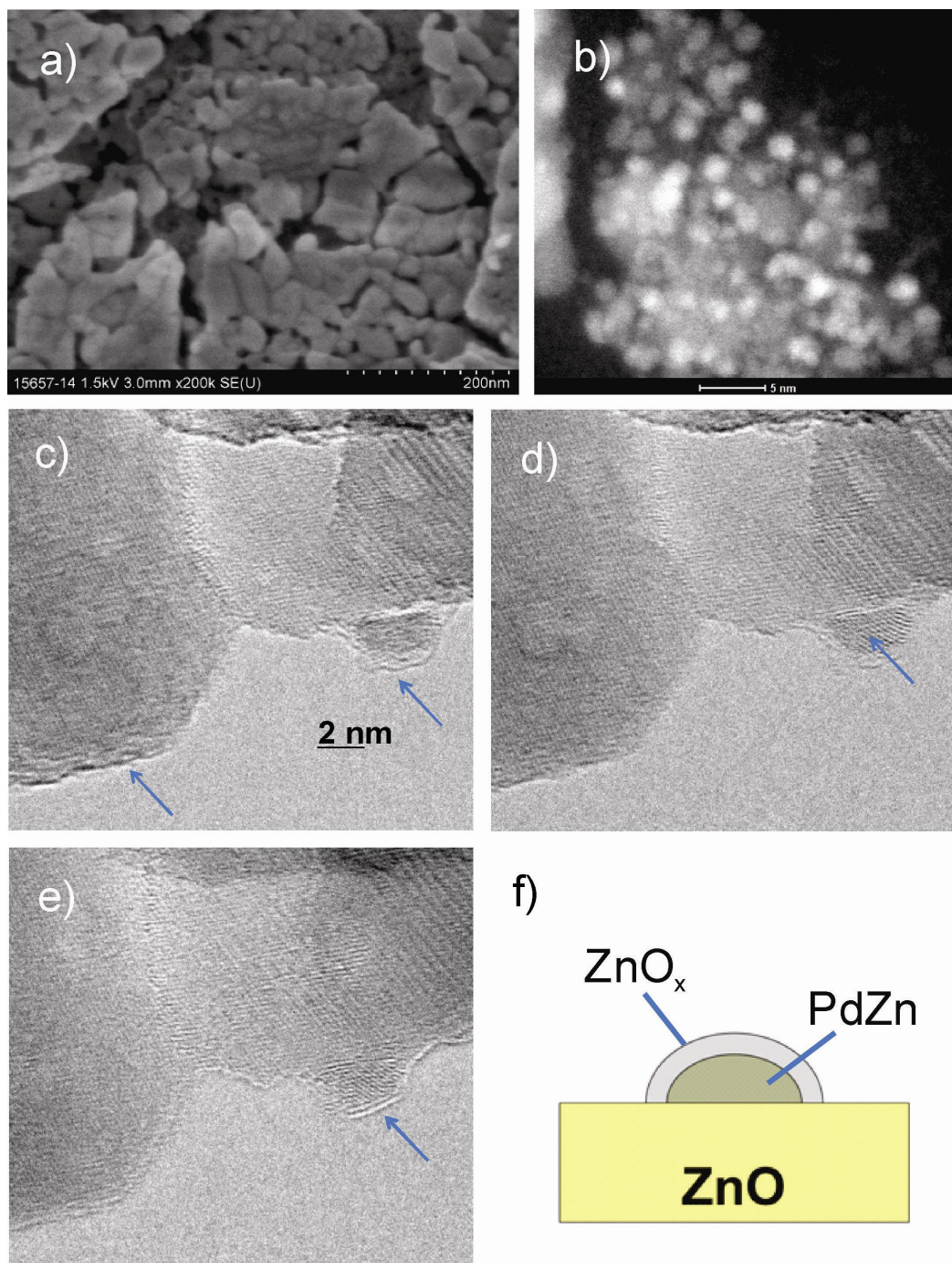


Fig. S3.5: original, uncolored version of Fig. 5. Arrows in panels c+e indicating the ZnO<sub>x</sub> overlayer. Arrow in panel d indicating the PdZn particle.

## B. Tables

Table S3.1: integrated peak area ratio of Pd3d and Zn3d after reductive treatments (normalized).

sample	conditions	signal	hv /eV	Ekin /eV	cross section <sup>1</sup>	photon flux	at.-%
16949	pre-reduced sample;	Pd3d	535	200	2.900	5.63E+10	7.6
		Zn3d	211	200	3.100	3.93E+10	92.4
	UHV, RT	Pd3d	1135	800	0.470	1.47E+11	5.1
		Zn3d	811	800	0.086	1.24E+11	94.9
16957 (2.5% Pd/ZnO in deactivated state)	0.4 mbar H <sub>2</sub> , RT	Pd3d	535	200	2.900	5.63E+10	12.7
		Zn3d	211	200	3.100	3.93E+10	87.3
		Pd3d	1135	800	0.470	1.47E+11	5.3
		Zn3d	811	800	0.086	1.24E+11	94.7
	2.5 mbar H <sub>2</sub> , 473 K, 1h	Pd3d	535	200	2.900	5.63E+10	9.3
		Zn3d	211	200	3.100	3.93E+10	90.7
	2.5 mbar H <sub>2</sub> , 473 K, 2h	Pd3d	535	200	2.900	5.63E+10	8.6
		Zn3d	211	200	3.100	3.93E+10	91.4
	0.4 mbar H <sub>2</sub> , RT	Pd3d	1135	800	0.470	1.47E+11	5.7
		Zn3d	811	800	0.086	1.24E+11	94.3
		Pd3d	535	200	2.900	5.63E+10	7.7
		Zn3d	211	200	3.100	3.93E+10	92.3
	UHV, RT	Pd3d	1135	800	0.470	1.47E+11	4.8
		Zn3d	811	800	0.086	1.24E+11	95.2
		Pd3d	535	200	2.900	5.63E+10	7.1
		Zn3d	211	200	3.100	3.93E+10	92.9
UHV, RT	Pd3d	1135	800	0.470	1.47E+11	4.5	
	Zn3d	811	800	0.086	1.24E+11	95.5	

Table S3.2: reaction parameters ( $T_{50}$ ,  $X_{425}$ ,  $E_a$ ) of the 0.75% and 2.5% sample, as determined in CO oxidation light-off measurements after different pre-reduction conditions (Fig. 3+4).

# 15657 (T red./K)	ramp no.	T50/K	X425/%	Ea/kJmol-1
fresh sample (423)	first	487	1.6	
	last	482	1.6	
same sample (523)	first	471	10	
	last	480	2	
same sample (523)	first	469	10	
	last	481	2	
same sample (623)	first	480	3.3	
	last	484	1.5	

49

#16688

reducing agent: H<sub>2</sub>

(2.5% Pd)

(last measurement: CO)

# 16688 (T red./K)	ramp no.	T50/K	X425/%	Ea/kJmol-1
fresh sample (473)	first	438	28	
	last	453	10	
same sample (473)	first	438	28	
	last	453	10	
fresh sample (573)	first	439	27	
	last	456	8	
fresh sample (723)	first	471	7	
	last	481	2.5	
				82
fresh sample (473, CO)	first	442	24.5	
	last	455	10	

### C. References

1. Yeh, J. J. & Lindau, I. Atomic subshell photoionization cross sections and asymmetry parameters:  $1 \leq Z \leq 103$ . *At. Data Nucl. Data Tables* **32**, 1–155 (1985).

## **Chapter 4: Supported Palladium catalysts in CO-oxidation and Acetylene Hydrogenation: on the role of SMSI**

Patrick Kast, Martin Kuhn, Matthias Friedrich, Ramzi Farra, Malte Behrens, Peter Claus, Robert Schlögl.

### **Abstract:**

In order to gain better understanding of the strong metal-support interaction (SMSI) phenomenon and to deliver a reference system for theoretical calculations, a series of different Pd/Fe-oxide, Pd/Zn-oxide and Pd/Ti-oxide powder catalysts was synthesized. The influence of reductive pre-treatment on the activity in catalytic CO-oxidation was compared and correlated to the reduction grade of the active metal surface area determined by CO-chemisorption measurements. The results are discussed in relation to non-reducible Pd/Al-oxide. In addition the reduction dependent selectivity changes in acetylene hydrogenation were monitored. Though we found clear evidence for reversible SMSI formation, its influence on catalytic reactions is complex due to other possible processes like alloy formation that are likely to occur at similar temperatures. The influence of electronic and geometric surface modifications with regard to CO-oxidation activity seems to strongly depend on the investigated system or pre-conditioning: CO-oxidation is found to be a promising tool to show that dynamic surface modification by SMSI can enhance or decrease catalytic activity. It could also be shown that there is no significant difference in the behavior of our systems, compared to model systems studied at much lower pressure. In selective hydrogenation, electronic modifications of the Pd in case of the zinc oxide system led to a different behavior compared to the iron oxide supported system.

### **4.1. Introduction**

The catalytic oxidation of carbon monoxide is one of the most intensively studied reactions in heterogeneous catalysis in the last decades.<sup>1,2</sup> With regard to fundamental mechanistic understanding of catalytic processes in a given (model) system, the reaction is a suitable test reaction<sup>3</sup> due to its relative simple kinetics: there is nowadays a lot of understanding of its elementary steps, it features only one rate-determining step, only one product (CO<sub>2</sub>) which easily desorbs, no intermediate/side products are formed and it is observed over 13 orders of magnitude of pressure.<sup>4</sup> Intensively studied adsorption properties on well-defined surfaces



(e.g. adsorption enthalpies, IR and other spectroscopic studies)<sup>5</sup> serve as a solid quantitative base also for realistic, technical catalysts operated under ambient and high pressure. Another benefit of CO-oxidation is that it features very similar kinetic behavior no matter if being investigated on single crystals or oxide supported nanoparticles.<sup>6,7</sup>

It is generally accepted that the reaction occurs via the Langmuir-Hinshelwood mechanism,<sup>8</sup> while both reactants, CO and oxygen are co-adsorbed at the surface, on different adsorption centers. Furthermore it is known that there is a lot of structural dynamics on the catalyst surface. There are temporal and spatial oscillations as well as reconstruction of the active sites.<sup>3,9-11</sup> For example, if performed on ruthenium, reaction-induced metal-oxide transformations (transient surface oxide formation) were observed at higher pressures,<sup>12,13</sup> but low activity was observed at lower pressures. In general, group VIII noble metals are well suitable for CO-oxidation due to their weak electron back-donation to anti-bonding CO-orbitals, while being noble enough to avoid complete oxidation.

After high-pressure STM- and SXRD studies of CO-oxidation on Pd(100) surface it was suggested that the formed surface oxide might be an active phase for the reaction.<sup>14,15</sup> On the other hand studies showed that Pd catalysts suffered deactivation during the reaction when exposed to higher O<sub>2</sub> partial pressure, due to oxide formation.<sup>6</sup> This was not the case for Pt catalysts. In general, higher O<sub>2</sub> partial pressure is discussed to be beneficial because CO inhibits oxygen adsorption more than the other way round.<sup>8</sup> CO-oxidation measurements by McClure and Goodman found, that the most active surfaces were those with minimal CO-coverage,<sup>3</sup> after comparing Pt, Pd, Rh and Ru catalysts at elevated pressures. LH mechanism was confirmed, while no “pressure gap” was found.

In case of CO-oxidation on palladium, studies were performed involving pure Pd(100)<sup>3,14-18</sup> or Pd(111)<sup>8,9,19-21</sup> surfaces as well as well-defined, supported Pd model catalysts on thin, highly ordered oxide films synthesized by impregnation or Pd evaporation<sup>19,22-24</sup> and also more realistic, co-precipitated catalysts<sup>25</sup> and resulting in a series of kinetic and thermodynamic data. For example, the adsorption enthalpy of CO on Pd-particles on Fe<sub>3</sub>O<sub>4</sub>/Pt(111) was found to be lower, the smaller the particles are (125 kJ/mol for 8 nm compared to 105 kJ/mol for 1.8 nm and compared to 145 kJ/mol for Pd(111)),<sup>19</sup> explainable by more defects and weaker CO-bonding sites on smaller clusters. In case of Pd/Al<sub>2</sub>O<sub>3</sub>/NiAl(110),<sup>22</sup> 1.8 nm particles showed a lower reaction rate but higher stability against CO-induced poisoning under steady-state conditions, compared to 5.5 nm large particles. Desorption energy decreased from 136 kJ/mol (larger particles) to 110 kJ/mol (smaller particles).

Reaction orders were confirmed to be -1 for CO and +1 for the oxygen.<sup>17</sup> With regard to the adsorption behaviour of the oxygen, a rearrangement of the oxygen ad-layer on Pd(111) was observed from a (2x2) structure ( $\Theta=0.25$ ) to  $\sqrt{3}\times\sqrt{3}$  R30° geometry ( $\Theta=0.33$ ) with increasing CO pressure and further compression until (2x1) structure. For Pd(100) catalysts under technically relevant pressures, surface oxide film structures of  $\sqrt{5}\times\sqrt{5}$  R27° were observed,<sup>26</sup> stable up to stoichiometric feeds and especially stable at higher T.

Bluhm et.al. however<sup>27</sup> observed chemisorption of oxygen in a (2x2) structure on Pd(100) during NAP-XPS oxidation, followed by a 1 layer thick surface oxide formation in  $\sqrt{6}\times\sqrt{6}$  geometry, formation of a multilayer-thick, so-called “subsurface” oxide phase until bulk PdO formation, upon time. CO-oxidation activity on noble metal catalysts like Pd, Pt or Rh was found to be increased in case of existing strong metal-support interactions between noble metal and oxidic support. This so-called SMSI-phenomenon was originally presented by Tauster et al.<sup>28</sup> and studied intensively.<sup>29–34</sup> Physically it describes noble metal particle wetting by a spreading support under reducible conditions, depending on the grade of support reducibility and leading to more or less complete decoration/covering of the metal surface and reduced chemisorption capacity. Pd/TiO<sub>2</sub> catalysts were studied intensively<sup>30,35</sup> without really resolving the nature of the reduced oxidic film cover. Recent studies of the phenomenon involved Pd and Pt on Fe<sub>3</sub>O<sub>4</sub>(111)/Pt(111) supported model-catalysts.<sup>23,36</sup> Compared to Pd, Pt exhibits a higher adhesion force and stronger SMSI. For example, thin iron oxide film-covered Pt(111) was shown to exhibit the characteristic Moiré pattern<sup>23</sup> in STM investigations and a 10 times higher activity for CO-oxidation, compared to pure platinum. Sufficient oxygen content was reported to be essential when the O<sub>2</sub> is interacting with the two-layered FeO film, formed by reduction. Due to a “lift-up” of an iron atom above the oxygen layer, the reactivity relevant e<sup>-</sup> - transfer to the oxygen occurs and the formed O<sub>2</sub><sup>-</sup> molecule reacts to an O-Fe-O tri-layer, important for CO-oxidation (ER – MvK mechanism). The present study compares kinetic data for CO-oxidation on a co-precipitated Pd/Al<sub>2</sub>O<sub>3</sub> catalyst (as a merely reducible reference) to those of impregnated Pd/TiO<sub>2</sub> and co-precipitated Pd/ZnO and Pd/Fe<sub>2</sub>O<sub>3</sub> catalysts in different reduction states to deliver a reference system for SMSI, applying surface sensitive methods like CO-chemisorption. It will further point out differences with regard to selectivity, using selective hydrogenation of acetylene.

## 4.2. Experimental

### 4.2.1. Catalyst synthesis

The catalyst precursor for the Pd/Al<sub>2</sub>O<sub>3</sub> catalyst was synthesized by a controlled co-precipitation approach. Therefore, 450 ml of a diluted (0.2 M) solution of Al(NO<sub>3</sub>)<sub>3</sub>·6H<sub>2</sub>O (Merck) which was mixed with appropriate amounts of a Pd(NO<sub>3</sub>)<sub>2</sub>-solution (8.3 wt.-% Pd-content in 10 wt.-% HNO<sub>3</sub>; Alfa Aesar) were precipitated drop-wise with 0.3 M Na<sub>2</sub>CO<sub>3</sub> solution in an automated reactor-system (Labmax, Mettler-Toledo), which contained already about 400 ml of deionized water. During the precipitation (acid solution addition rate of 6 g/min), the pH-value (pH = 6), temperature (T = 298 K) and stirring rate (r = 300 rpm) were monitored and kept constant in order to assure the most similar conditions and chemical potential for every forming crystallite and thus the best possible product homogeneity. After precipitation, the product was aged for 2 h (100 rpm, RT) while a pH increase to 7.5 could be observed. Afterwards it was filtered and washed three times (3x 1l of demin. water) until conductivity measurement of the solution detected < 0.01 mS. The solid, pale yellow product was dried in air for 24 h (298 K), mortared and calcined under controlled conditions in 20% O<sub>2</sub> – Ar atmosphere (2 h, 773 K, 2 Kpm heating rate) to yield PdO supported on γ-Al<sub>2</sub>O<sub>3</sub>. The palladium loading was calculated to yield 2.5 wt.-% Pd/Al<sub>2</sub>O<sub>3</sub>. The 1 wt.-% Pd/TiO<sub>2</sub> sample was synthesized by deposition-precipitation,<sup>37</sup> mixing TiO<sub>2</sub> (P25, Merck) with water and appropriate amounts of the Pd-solution and precipitating with 0.2 M Na<sub>2</sub>CO<sub>3</sub> at pH 4. Calcination was performed at 673 K. Synthesis of the Pd/ZnO and the Pd/Fe<sub>2</sub>O<sub>3</sub> catalysts is described elsewhere.<sup>38,39</sup> A synthesis protocol of the Pd/Al<sub>2</sub>O<sub>3</sub> sample is shown in SI (Fig. S4.1). Commercial PdO (Fluka) was used as a reference for E<sub>A</sub> measurement after RT-red.

### 4.2.2. Catalyst characterization

Elemental composition of the samples was controlled by x-ray fluorescence spectroscopy (XRF) and energy-dispersive x-ray spectroscopy (EDX, to rule out contaminations). Specific surface area was investigated by nitrogen physisorption (BET). Scanning electron microscopy (SEM) was used to check the surface morphology, whereas HR-TEM and STEM were used to investigate the Pd particle distribution and monitor structural changes after treatments or reactions. CO-chemisorption was performed to measure the active surface area and to detect support spreading/wetting (decoration of the Pd-particles). TPR measurements were applied to investigate and bulk properties during reduction.

XRF was measured in a S4-pioneer setup (Bruker) using a Rh target and boric acid pellets.

A Hitachi S-4800 SEM was used as well as a FEI Cs-corrected Titan 80-300 microscope for STEM and HR-TEM images. Samples in air-sensitive (SMSI) state (after reduction at higher temperatures) were transferred into the microscope without air contact, with the help of a glove box. An energy dispersive X-ray detector (Genesis 4000) was used for elemental mapping and composition analysis.

CO-chemisorption measurements were carried out in an Autosorb-1C chemisorption setup (Quantachrome Incorp.), equipped with a reactor for pretreatment of the sample under flow conditions. For reduction the setup was connected to a gas bottle with 5% H<sub>2</sub>-Ar mixture. Usually, the sample was reduced at 323 K for 30 min. to reduce oxidic Pd species before measuring two adsorption isotherms at 313 K and in the pressure range of 3-747 mbar, the first isotherm representing both, reversibly (weakly) and irreversibly (strongly) adsorbed CO and the second isotherm (measured after evacuation) only representing the physisorbed species. By subtracting the second from the first isotherm and extrapolating the volume to a pressure of zero, the volume of chemisorbed CO was determined. By assuming a shape-factor for the Pd-particles of 6 and further assuming that every second Pd surface atom is covered by one CO-molecule, the active surface area, the dispersion and the average diameter of the particles was calculated. Some samples were reduced at higher temperatures to generate and investigate particle decoration by the support (SMSI). After all reduction steps the sample was dried for 2 h (393 K) under He flow, before being evacuated for 2 h at the same temperature.

BET measurements were conducted in an Autosorb-6-B N<sub>2</sub>-physisorption setup (Quantachrome Incorp.) at liquid nitrogen temperature. Samples were degassed in a dynamic vacuum for 2 h at 423 K before starting the measurement. After measuring adsorption and desorption isotherms, the total surface area of the sample was calculated according to the BET method, using 11 points of the linear range of the desorption isotherm.

### **4.2.3. Catalytic testing**

CO-oxidation:

The catalytic CO-oxidation was carried out in a self-constructed catalytic reactor setup, described earlier.<sup>38</sup> Usually, 25 mg of the catalyst, diluted by 250 mg of inert SiC (particle diameter: 250-355 μm) were weighed out and reduced in 5% H<sub>2</sub>-He or in 2% CO-He (100 ml/min) at different temperatures (2 Kpm, holding time 30 min.). TPR in 5% H<sub>2</sub>-He was

performed with a heating rate of max. 5 Kpm. For CO-oxidation, normally three repeated light-off conversion cycles were measured (100 ml/min, 0.5% O<sub>2</sub>, 1% CO, 98.5 % He) from 323 to 523 K (2 Kpm heating rate, 15 min. holding time and 0.5 Kpm for cool down to 323-373 K.

Acetylene hydrogenation:

Selective hydrogenation of acetylene was performed under tail-end conditions in a fixed bed reactor, 6 mm inner diameter. About 46 mg of the catalyst (sieve fraction 250-355 μm) were diluted with 100 mg of inert α-alumina (similar sieve fraction) and fixed between α-alumina filling. The catalysts were in-situ reduced in 5% H<sub>2</sub>-Ar (100 ml/min) with a heating ramp of 2 Kpm and 30 min holding time (cool down in hydrogen mixture). The reaction gas mixture consisted of ethylene 3.0 (30.01 vol.-%), hydrogen 5.0 (0.974 vol.-%), acetylene 2.6 (1.011 vol.-%), propane 2.5 (1.005 vol.-%, internal standard) and argon 5.0 (balance). It was analyzed every 15 min by on-line GC (HP 6890 plus) equipped with a HP-PLOT Al<sub>2</sub>O<sub>3</sub> capillary column and a FID.<sup>40</sup> Calculation of conversion and selectivity was done by equations (1-2) while ethylene formation selectivity was determined indirectly by measuring ethane and C<sub>4</sub>-byproduct formation because of the ethylene excess in the feed.<sup>41,42</sup>

$$X_{C_2H_2} = \left( \frac{I_{C_2H_2,t,corr}}{I_{C_2H_2,0,corr}} \right) \cdot 100\% \quad (1)$$

$$S_{C_2H_4} = \left[ \frac{(I_{C_2H_2,0,corr} - I_{C_2H_2,t,corr}) - (I_{C_2H_6,t,corr} - I_{C_2H_6,0,corr}) - 2 \cdot (I_{C_4,t,corr} - I_{C_4,0,corr})}{I_{C_2H_2,0,corr} - I_{C_2H_2,t,corr}} \right] \cdot 100\% \quad (2)$$

### 4.3. Results and Discussion

#### 4.3.1. Comparison of the samples

For the physical parameters of the Pd/iron oxide and the Pd/zinc oxide samples, we refer to earlier publications.<sup>38,39</sup> Their actual Pd loadings were 2 % respectively 3.9%. Here we present some characteristics of the Pd/titanium oxide and the Pd/aluminum oxide sample. The nominal Pd loading of the Pd/TiO<sub>2</sub> sample was confirmed to be 1 wt.-% by XRF while the loading of the Pd/Al<sub>2</sub>O<sub>3</sub> sample was determined to 1.8 wt.-% by ICP-OES and XRF. The BET surface area of the Pd/alumina sample is 308 m<sup>2</sup>/g whereas the surface area of the Pd/titania sample is much lower with only 10 m<sup>2</sup>/g. As it can be seen in the micrographs of

the following figure 4.1 (lower row), as well as in figure S4.5 (SEM image, SI), the P25 (titania) support consists of relatively large, round crystallites, 60-300 nm in size. The STEM images of figure 4.1 show highly dispersed palladium particles distributed on the support (size 2-15 nm). Comparison of two representative images, recorded after reduction at different temperatures (323 K and 723 K), reveals that no significant particle growth due to sintering has occurred. The average Pd particle diameter was determined by CO-chemisorption measurements to 4-5 nm. Figure S4.2 (SI) shows an XRD measurement of the Pd/titania sample before and after reduction at 373 K and reveals the composition of mainly anatase, with a minor content of rutile phase as well as reduction of the palladium oxide to metallic palladium by the vanishing of the broad palladium oxide (111)- reflection at 35°. After further reduction at 773 K in the XRD-setup, no significant phase changes in the diffractogram could be observed. In case of the Pd/alumina sample, figure 4.1 (upper row) the SEM image confirms the porous structure of the support while the STEM image shows homogeneously distributed Pd particles in the size of about 2-4 nm, as confirmed by CO-chemisorption measurements (average size 2 nm). No XRD is presented in case of the Pd/alumina sample due to the low information content (no palladium visible, amorphous  $\gamma$ -alumina).

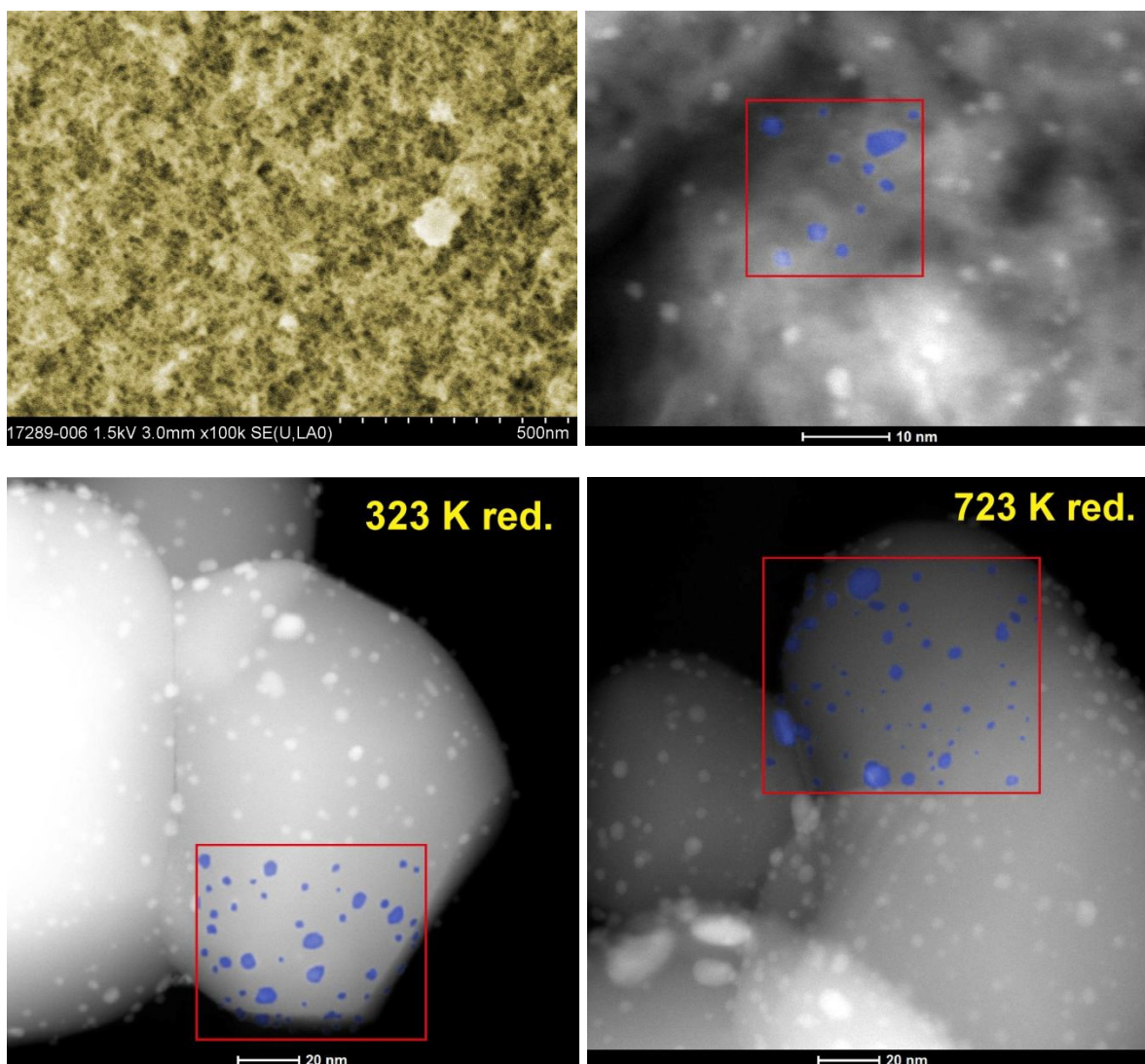


Fig. 4.1: SEM and STEM-images of Pd/Al<sub>2</sub>O<sub>3</sub> sample (upper row) and STEM images of Pd/TiO<sub>2</sub> sample after 323 K reduction (5% H<sub>2</sub>) and after 723 K reduction (lower row). Pd particles in red frame colored blue. SEM image colored yellow.

#### 4.3.2. Reduction behavior of the 1% Pd/TiO<sub>2</sub> catalyst

Similar to the earlier studied catalytic systems, thermo-programmed reduction of the impregnated 1% Pd/TiO<sub>2</sub> sample has been performed in 5% H<sub>2</sub>-He in order to initiate the formation of a support over-layer, induced by strong metal-support interaction. The according TPR measurement is presented in the following figure 4.2:

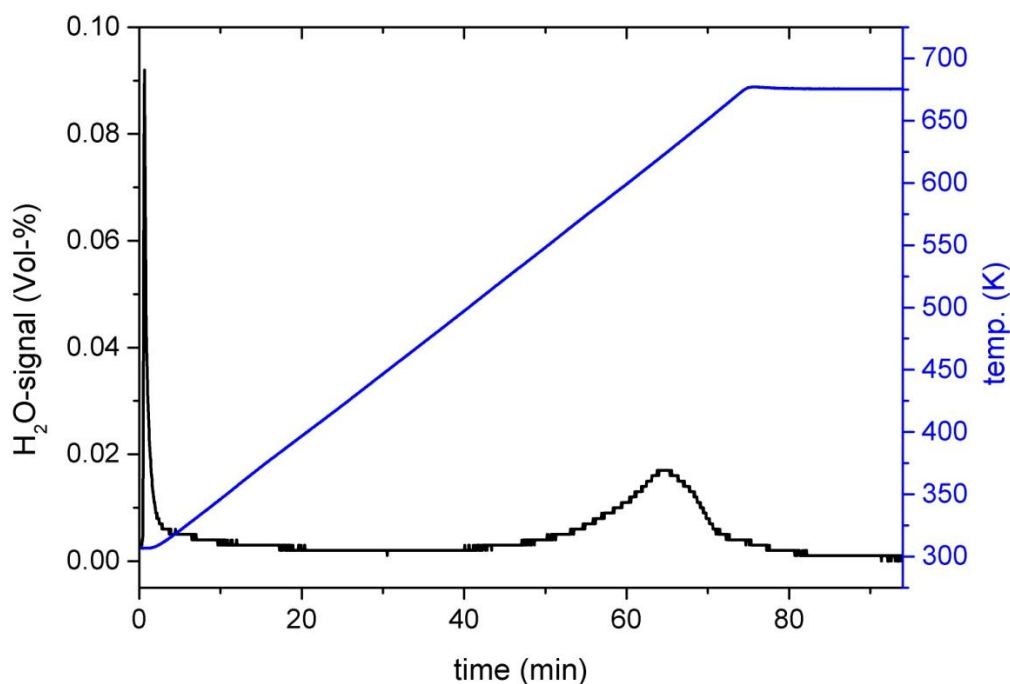


Fig. 4.2: TPR of 1% Pd/TiO<sub>2</sub> in 5% H<sub>2</sub>-He (5 Kpm, until 673 K): water formation due to PdO-reduction (RT) and partial reduction of the titania support (623 K) visible.

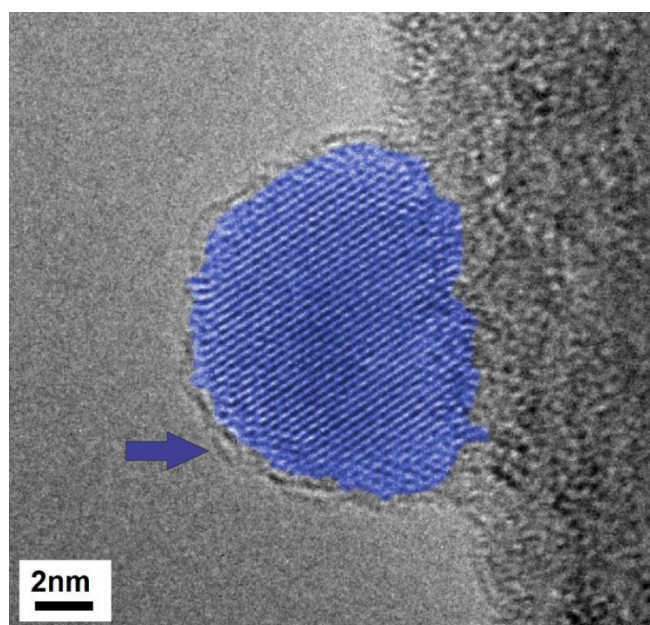


Fig. 4.3: HR-TEM image of 1% Pd/TiO<sub>2</sub> after reduction at 673 K (5% H<sub>2</sub>-He) and transfer to the microscope without air contact. Arrows indicate the formation of a partially reduced TiO<sub>x</sub> over-layer that covers the Pd particle (blue).

The first water signal in the TPR appears at room temperature and can be assigned to the reduction of palladium oxide by the hydrogen.<sup>38</sup> With increasing reduction temperature, a second water signal with an onset at 500 K and a maximum at 623 K can be detected which is about 3x as intense as the PdO reduction peak. After reduction of the sample at 673 K it was



transferred without air contact to the microscope for HR-TEM measurements. As it is indicated by the arrow in figure 4.3, an over-layer structure can be detected in that state of the catalyst, on top of the palladium particles and on the titania support. We therefore assign the observed reduction signal in the TPR to the (SMSI)-induced formation of a reduced  $\text{TiO}_x$  over-layer, as it has been observed earlier.<sup>43</sup> Further HR-TEM images were taken at a different position and within a time period of about one minute in order to exclude the deposition of carbon species that would increase with longer exposure to the electron beam and could be mistaken as induced by SMSI. Indeed, no over-layer growth with ongoing time could be detected. The thickness of the layer was stable and even decreased partially, most likely due to its volatility in the electron beam. The image series is shown in the supporting information (Fig. S4.6).

#### 4.3.3. Influence of SMSI on CO-oxidation

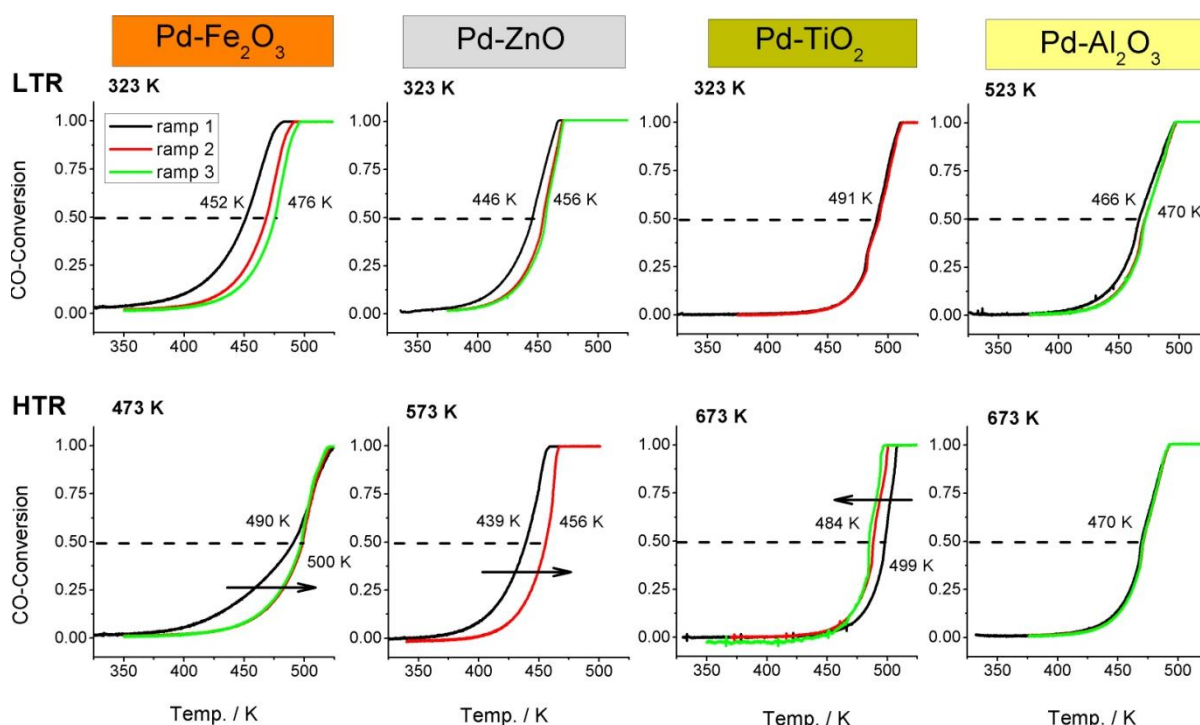


Fig. 4.4: comparison of the catalytic CO-oxidation cycles (conversion-“light-off”-curves) for the four different investigated catalytic systems, 2% Pd/ $\text{Fe}_2\text{O}_3$ , 3.9 % Pd/ $\text{ZnO}$ , 1% Pd/ $\text{TiO}_2$  and 1.8% Pd/ $\text{Al}_2\text{O}_3$ , after reduction at lower temperature (LTR, 323-523 K) and higher temperature (HTR, 473-673 K) to compare the influence of electronic and/or geometric surface modification (SMSI). Temperature of 50% conversion ( $T_{0.5}$ ) indicated for the cycles.

In order to study and compare the influence of reductive treatments on geometrical and/or electronic surface modifications like strong metal-support interaction (SMSI) and alloying, catalytic CO-oxidation was applied as a test reaction. In the study, four different supported palladium catalysts (2% Pd/Fe<sub>2</sub>O<sub>3</sub>, 3.9% Pd/ZnO, 1% Pd/TiO<sub>2</sub> and 1.8% Pd/Al<sub>2</sub>O<sub>3</sub>) were investigated after reduction at low temperature (LTR, 323 K in most cases) and at higher temperatures (HTR, between 473 K and 673 K, dependent on the system). The structure-function relationship during reductive surface processes has been thoroughly studied in our group earlier in case of the Pd/iron oxide system and the Pd/zinc oxide system and we refer to respective literature.<sup>38,39</sup> Their catalytic data are being presented in figure 4.4 (first and second column) and compared to more recent data of the Pd/titanium oxide (third column) and the Pd/aluminum oxide system (fourth column). Since the active metal surface area is crucial when talking about catalytic activities and surface changes like support over-growth, all kinetic data are cross-linked to the determined CO-chemisorption capacities of the four investigated systems and – most important – to their relative change in between the low temperature (LTR) and the high temperature (HTR) treatments (Fig. 4.5).

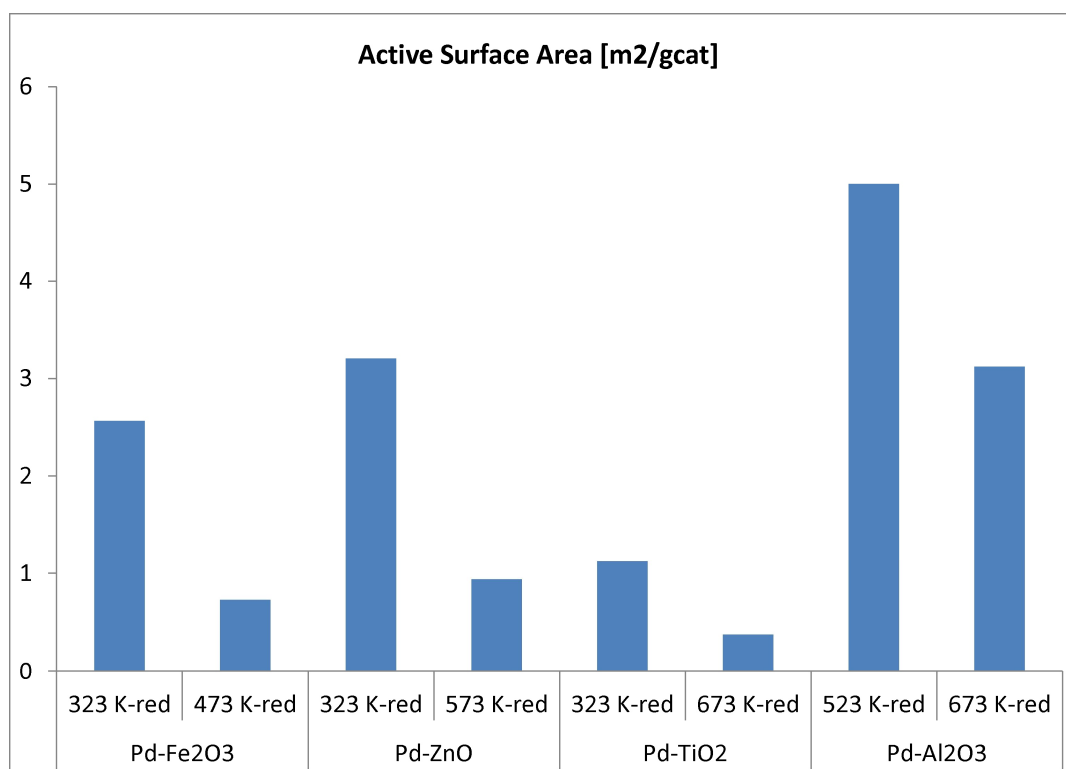


Fig. 4.5: comparison of the active metal surface areas per gram catalyst of the different catalytic systems after reduction at low temperatures (LTR) and high temperatures (HTR), in accordance with the kinetic experiments (same samples as in Fig. 4.4).

In case of the Pd/iron oxide and the Pd/zinc oxide sample, the deactivation behavior during the catalytic cycling after LTR (323 K) was described as an almost irreversible process.<sup>38,39</sup> If reduced for a second time at 323 K after the first cycling, only very low improvement of the activity could be observed (Fig. S4.4, SI). Differently, when HTR was applied (473 K for iron - and 573 K for zinc oxide), the first reaction cycle was found to be clearly more active, while the second and third cycle showed similar activities. The deactivation can be numerically expressed by an increase of the temperature of 50% conversion ( $T_{50}$ ) from 490 K to 500 K (iron oxide system) and from 439 to 456 K (zinc oxide). The activating process was explained by SMSI-induced over-layer formation in case of the iron oxide and by reversible surface alloying in case of the zinc oxide and was reported in UHV-model-studies before.<sup>23</sup> When being reduced at even higher temperatures (623 K), the zinc oxide system experienced an overall deactivation due to over-layer formation, while the first cycle was still more active.<sup>39</sup> In both systems, the active metal surface areas after HTR show an SMSI induced decrease to about 1/3 of the values after LTR. In case of the Pd/TiO<sub>2</sub> system, the relative decrease is even more pronounced (only 20% of the value after HTR, compared to LTR). According to representative STEM-images of the sample, comparing the two states (see figure 4.1), particle growth can be ruled out as the main reason for the observed behavior. Comparing the CO-oxidation behavior (third column, figure 4.4), a pronounced difference between the LTR and the HTR treatment can be observed: while the conversion cycles after LTR are almost identical ( $T_{50} = 491$  K), the first conversion cycle after HTR is less active compared to LTR and the system after HTR becomes more active with ongoing reaction.  $T_{50}$  increases from 499 K to 484 K. The surface cover (SMSI), reported for the Pd/titanium oxide system earlier<sup>44</sup> seems to have a negative influence on the CO-oxidation in that case. Probably, geometric limitation of the active sites plays the important role, while there is no sign for beneficial electronic properties here. The deactivation after HTR, probably by formation of the SMSI over-layer in case of the TiO<sub>2</sub> sample was found to be reversible by repeating the experiment. In case of the less reducible Pd/aluminum oxide system, as a reference, no change between the first and second conversion cycle could be observed in CO-oxidation (fourth column, figure 4.4) after HTR, with a  $T_{50}$  value of 470 K. No surface modifications seem to occur in that case. On the other hand, when being reduced at lower temperatures (523 K presented here), the first conversion cycle shows a slightly higher activity, while the position of the second cycle is exactly identical to the one after HTR again. 523 K was chosen as LTR temperature here in order to sufficiently dry and reduce the sample in one step. Reaction behavior after reduction at even lower temperature (423 K) however

was similar to the presented results. When compared to the chemisorption data, the  $\text{Al}_2\text{O}_3$  system also shows a decrease of adsorption capacity, which is much less pronounced however, with a decrease of 50% between LTR and HTR (Fig. 4.5). The slight difference in the activity in the first cycle after LTR could be explained by irreversible processes again. Due to the CO oxidation measurements after HTR we exclude SMSI in that state of the system.

Apparent activation energies have been determined for all the different supported catalysts. They have been measured in the stable, deactivated state after the CO-oxidation after HTR. In case of the Pd/iron- and the Pd/zinc oxide system studied recently in our group,<sup>38,39</sup> the values of the lowest loaded samples are presented in figure 6, in order to better compare to the similar loading of the titanium oxide system. The cycling behavior of these samples in the kinetic measurements is also comparable with regard to the observed qualitative differences between LTR and HTR as they are depicted in figure 4.4.

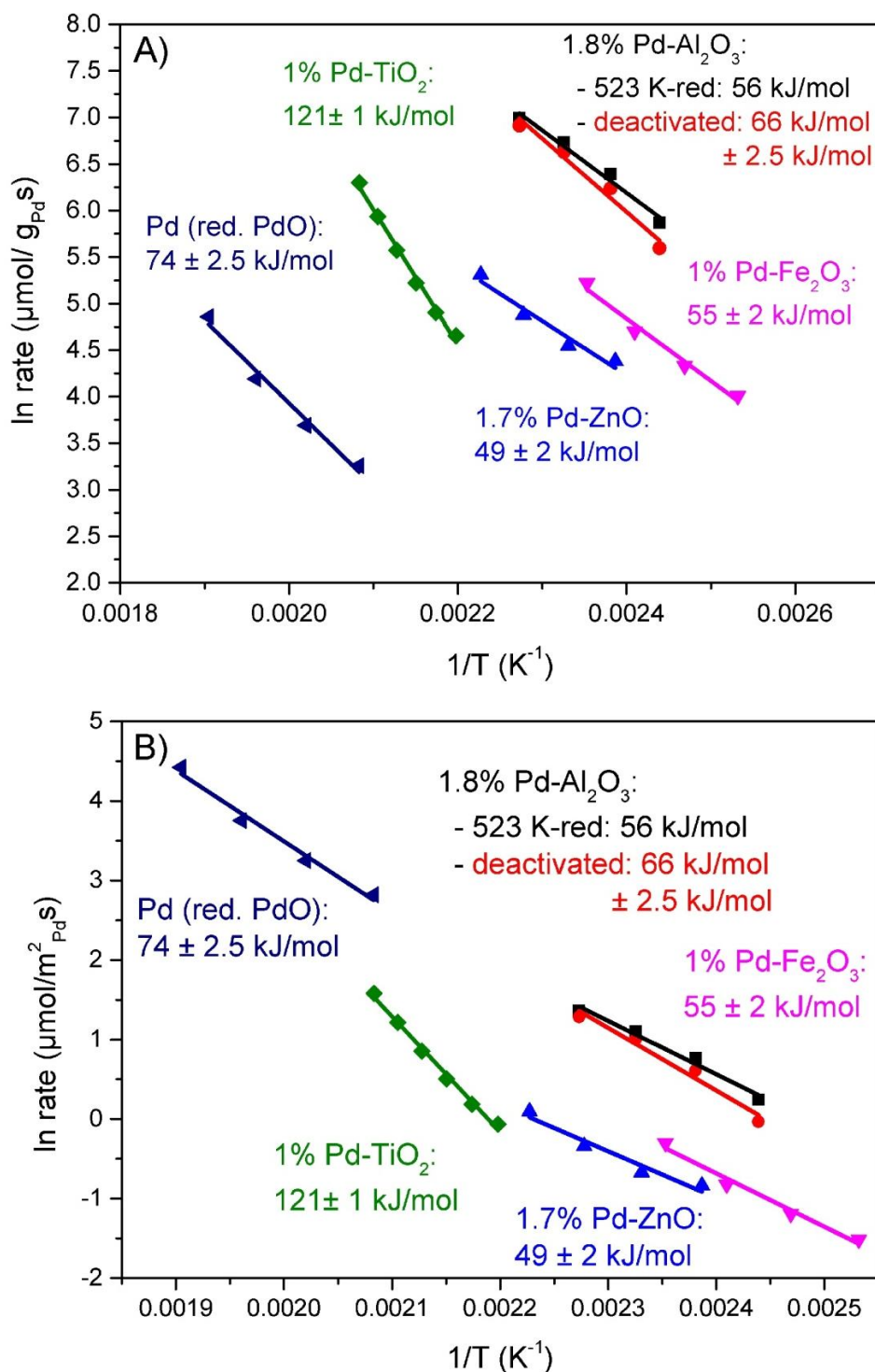


Fig. 4.6: Activation energies of 1% Pd/TiO<sub>2</sub>, 1.8% Pd/Al<sub>2</sub>O<sub>3</sub>, 1.7% Pd/ZnO and 1% Pd/Fe<sub>2</sub>O<sub>3</sub>, determined after CO-oxidation measurements. Values for pure Pd (after RT-red. of PdO) and for the freshly (523 K) reduced 1.8% Pd/Al<sub>2</sub>O<sub>3</sub> sample are included for comparison. Fig. 4.6A normalizes the activity to the mass of Pd, Fig. 4.6B to the active surface area.

The error for the activation energies has been estimated from the R-values of the linear fits. The calculated values of the zinc and iron oxide sample in the deactivated state are

comparable with  $49 \pm 2$  kJ/mol and  $55 \pm 2$  kJ/mol. The activation energy in case of the freshly reduced Pd/alumina sample was very similar with  $56 \pm 2.5$  kJ/mol, though the support is less reducible. In case of the deactivated aluminum oxide sample the value was slightly higher with  $66 \pm 2.5$  kJ/mol. The observed difference is likely due to partial re-oxidation of the palladium in case of the deactivated state, making the sample less active.<sup>9,45</sup> Values for the pure Pd sample measured after reduction of PdO at 323 K and for the deactivated Pd/titanium oxide sample were slightly higher with  $74 \pm 2.5$  kJ/mol (PdO) and twice as high with  $121 \pm 1$  kJ/mol (TiO<sub>2</sub>). Especially the high value for that latter system seems surprising due to the fact that the support is similar reducible as compared to iron or zinc oxide and might be related to the low BET surface area of the sample. The value for metallic Pd is comparable to the other values. In literature, activation energies for CO-oxidation on palladium were found to be around 135 kJ/mol both in case of nanoparticles and as single crystal,<sup>2,7,8</sup> with a wide variation, depending on the reaction conditions (e.g. 59 kJ/mol for higher CO-pressure and 105 kJ/mol for  $T > 500$  K). For Pd/CNT, 123 kJ/mol were reported by Naumann et al.<sup>25</sup> who also determined apparent activation energies for co-precipitated Pd on hematite: that system featured a lot of structural dynamics when being reduced at different T. and in accordance to a higher CO-oxidation activity in the SMSI state, the determined  $E_A$  in that state was very low with only 33 kJ/mol, but increasing with ongoing reaction (deactivation, SMSI destruction) up to 76 kJ/mol, which is slightly higher than our results. The authors also compared Pd supported on hematite in the unreduced state and found an  $E_A$  of 82 kJ/mol while re-dispersion and carbide formation was also discussed as possible reasons for the changing activity.  $E_A$  values for the 2% Pd/Fe<sub>2</sub>O<sub>3</sub> and the 3.9% Pd/ZnO samples, as depicted in figure 4.2 have also been determined in deactivated state. For the 2% Pd/iron sample, a similar value as compared to the 1% sample as obtained, namely 53 kJ/mol.<sup>38</sup> In case of the 3.9% Pd/ZnO sample,<sup>39</sup> the value was higher, with about 82 kJ/mol. In addition, further comparable CO-chemisorption measurements for the 1% Pd/iron oxide sample can be found in the respective reference,<sup>38</sup> confirming the trend depicted in figure 4.3. For the TPR experiments of the alumina system we refer to supporting information. TPR data of the other systems can be found in the respective literature as well.

The normalization of the rate to the active surface area allows identifying the generally negative trend of SMSI effects on the reactivity in a non-selective reaction like CO-oxidation. Despite this clear trend in figure 4.6B it can be seen that the SMSI effects are quite different in their function as they not only reduce the number of active sites but in some cases modify

their nature as can be seen from the different values of the apparent activation energies indicated by varying slopes. The figure underlines that generalizing statements about “the reactivity of Pd” in CO-oxidation are critical and that this reaction cannot identify the number of active sites in series of differently supported catalysts. The reaction is rather through its high sensitivity for the specific reactivity of modified Pd a chemical probe for such modifications. We conclude that the “chemical cross section” of CO-oxidation over Pd on different supports is different. This result is unexpected and limits the validity about e.g. structure sensitivity of CO-oxidation over Pd when differently supported systems are used.

#### **4.3.4. Influence of SMSI on selective hydrogenation of acetylene to ethylene**

Two different catalytic systems, previously investigated in CO-oxidation were investigated in selective hydrogenation of acetylene, namely the 2 wt.-% Pd/Fe<sub>2</sub>O<sub>3</sub> and the 3.9 wt.-% Pd/ZnO catalyst. The selective hydrogenation is a suitable complementary method to the comparison of CO conversion cycles because it is known to show higher selectivity for ethylene formation after reductive surface modification.<sup>46,47</sup> Our samples were pre-reduced at different temperatures in order to study the influence of the strong metal-support interaction induced over-layer formation and alloying on the selectivity of the hydrogenation reaction. Hereby, the iron oxide supported system has been reduced at 323 K (palladium should be in its metallic state) and at 473 K, where earlier studies found clear indications for FeO<sub>x</sub> covered Pd nanoparticles, induced by SMSI.<sup>38</sup> In case of the zinc oxide supported system, besides the reduction temperature of 323 K, the sample was reduced at 573 K (in that state PdZn alloy formation is known to have started already) and at 723 K (IR-investigations gave a hint for an existing, oxidic over-layer).<sup>39</sup> The results were compared to a merely reducible reference sample synthesized for the current work, namely co-precipitated 1.8 wt.-% Pd/Al<sub>2</sub>O<sub>3</sub> that was reduced at 523 K and should not undergo interactions between support and noble metal under these conditions. Before the hydrogenation reaction, a 10 h lasting initial break-in phase in reaction gas atmosphere for all catalysts was performed at  $p = 11$  bar and with a modified contact time  $\tau_{\text{mod}} = 17 \text{ g}_{\text{cat}} \cdot \text{h} \cdot \text{mol}_{\text{acetylene}}^{-1}$ , representing a volume stream of  $100 \text{ Nml} \cdot \text{min}^{-1}$ , in order to assure stable conversion at the beginning of the measurements. The temperature of the break-in phase was selected in a way assuring similar conversions and was in the range of 313 – 363 K, depending on the system. After the induction period, the temperature was increased step-wise until a maximum hydrogenation temperature of 483 K, with a holding

time of 1 h at each temperature. The conversion of acetylene for the two different catalysts is plotted against the temperature in figure 4.7. For all measurements, the modified contact time and the total pressure were kept constant.<sup>40,41</sup>

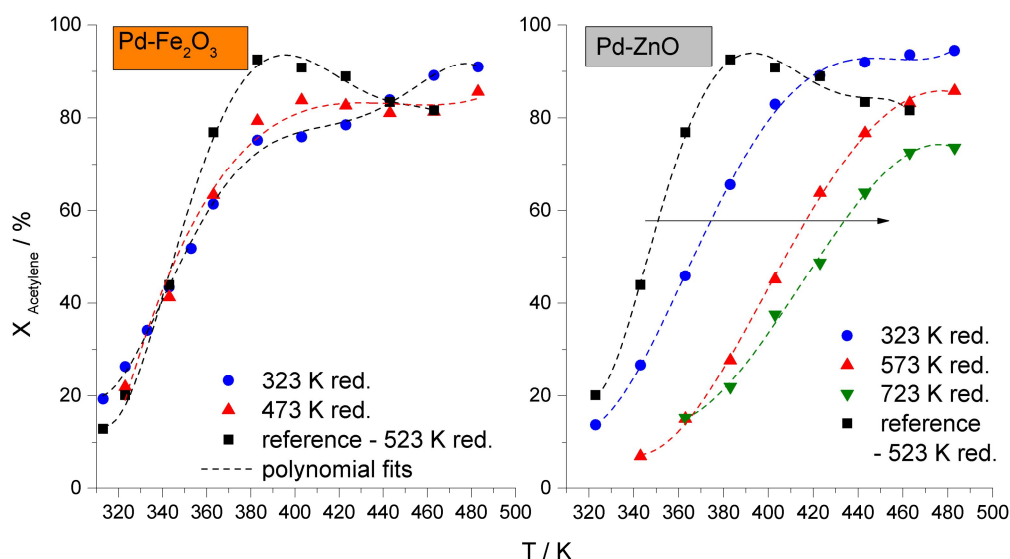


Fig. 4.7: Conversion  $X$  of acetylene vs reaction temperature for various reduced Pd/Fe<sub>2</sub>O<sub>3</sub> (left) and Pd/ZnO (right) catalysts, compared to the Pd/Al<sub>2</sub>O<sub>3</sub> reference system ( $p = 11$  bar,  $\tau_{\text{mod}} = 17 \text{ g}_{\text{cat}} \cdot \text{h} \cdot \text{mol}_{\text{acetylene}}^{-1}$ ).

It can be seen that the two supports act differently on the acetylene reactivity, despite their common nature of being “reducible”. Independent of the pre-treatment, the iron oxide system behaves rather similar to the Pd reference system, supported on non-reducible alumina. The ZnO system shows, in contrast, a differentiated reactivity evolution with changing treatment temperature of the catalyst.

Unmodified Pd exhibits its conversion maximum at a lower temperature than the iron oxide modified samples. At higher temperatures however, the consecutive reduction of ethylene becomes dominating, thus limiting the hydrogen available for the desired reaction and decreasing acetylene conversion.<sup>40,41</sup>

In case of the ZnO system, at elevated treatment temperatures, alloy formation sets in,<sup>39</sup> leading to a substantial reduction in activity. The plateau formation in the  $X$ - $T$  diagrams in figure 4.7 (right side) indicates a substantial change in the nature of the active sites caused by the formation of the PdZn alloy state that exceeds the blocking of the highly active sites on



otherwise electronically normal Pd. This mode of action may be suspected for SMSI states where an over-layer modifies the geometric access of reactants to the catalyst.

The different mode of operation of support effects leading to site blocking and to integral changes of the electronic structure of the Pd can be seen even more drastic from a plot of the selectivity to ethylene versus conversion, presented in figure 4.8:

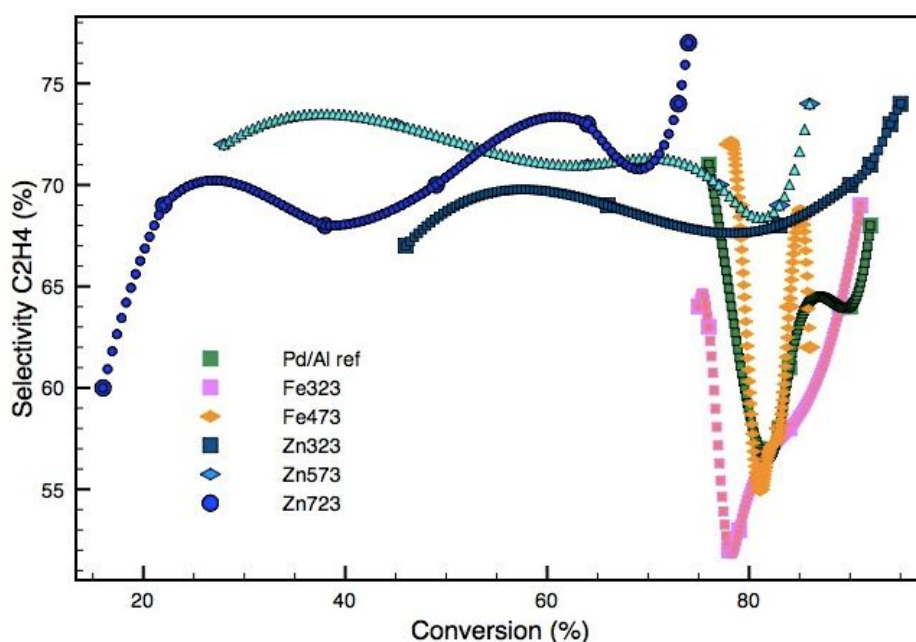


Fig. 4.8: Ethylene selectivity versus conversion for the catalysts presented in figure 4.7. Only the high-temperature range of data  $\geq 363$  K is considered. The lines are guides to the eye.

Both, the reference and the iron oxide systems exhibit a similar overall pattern of selectivity. At conversions of about 80% the blocking of unselective hydrogenation sites by strongly adsorbed acetylene is lost due to the disappearing concentration in the feed. Consequently the consecutive reactions begin to consume hydrogen, allowing carbon atoms to diffuse sub-surface. This coking behavior, in turn improves the selectivity again because larger palladium ensembles are necessary for consecutive reactions.<sup>48-51</sup> Ongoing coke and green oil formation however would decrease the selectivity towards ethylene again by pore filling and diffusion and mass transport limitation which leads to reaction of ethylene to ethane and  $C_4$  components for example.<sup>52</sup>

This behavior is a good example for the dynamic nature of the Pd in selective hydrogenation, as described recently for hydrogenation reactions involving the instable Pd/Ga system.<sup>53</sup> The

geometric SMSI of iron oxide only slightly affects these dynamics at higher conversions. However, the 323 K pre-reduced state is slightly less selective at lower conversion/reaction temperatures, compared to the 473 K reduced state (see S-T plot for the system presented in the SI, Fig. S4.7).

These observations are comprehensible since previous studies of reducible, supported noble metal catalysts, for example of palladium on titania,<sup>30,35,37,47,54–56</sup> reported that SMSI increases the selectivity for acetylene hydrogenation and other reactions, and compared to the previous results in case of the Pd/iron oxide system.<sup>38</sup>

It remains unclear, if the reaction occurs on top of the over-layer that is geometrically modified by the presence of the Pd high-energy sites (e.g. steps) or if these sites remain uncovered in the SMSI state.

The Pd/ZnO system exhibits in all three variants of SMSI and alloy states a different behavior in the plot of figure 4.8. The selectivity remains almost constant over comparable conversion levels. The dynamic response of unmodified Pd cannot be seen in any of the traces. This leads to the conclusion that the ZnO SMSI affects in all states the electronic structure of Pd such that no high-energy sites capable of unselective hydrogenation of acetylene exist. We conclude that the interaction of ZnO with the surface of Pd is more intimate irrespective of the geometric or electronic mode of SMSI. It remains speculative if this is achieved by formation of a surface alloy already with the geometric over-layer, that gradually grows into a bulk alloy or if the coverage of Pd by ZnO is more complete as in case of the iron oxide over-layer.

#### 4.4. Summary and Conclusion

The present work studied and compared CO-oxidation activity and acetylene hydrogenation activity and selectivity of a series of differently supported palladium catalysts, in various reduction states, in order to create a reference system for the structure-function relationship of strong metal-support interaction (SMSI). We were able to demonstrate a higher catalytic activity for CO-oxidation in accordance with a drastically reduced accessible active surface area, as determined by CO-chemisorption, in case of the Pd/iron oxide and the Pd/zinc oxide system. While in case of the iron oxide, a partially reduced over-layer reversibly forms already at moderate reduction temperatures, electronic modification of the surface by alloy formation was found to be responsible for the reversibly occurring observations in case of the reduced zinc oxide system. When reduced at higher temperatures however, the latter system further experienced the formation of an additional  $\text{ZnO}_x$  over-layer, leading to deactivation and counteracting the still existing electronic benefits. In contrast to these systems, reductive surface covering of the Pd/titania system did only decrease CO-oxidation activity, but still reversibly. The Pd/alumina system did not show SMSI formation by reduction. Instead, only slight differences in reactivity were detected, attributed to palladium re-oxidation.

In the selective hydrogenation studies, the behavior at higher conversions showed similarities between the aluminum oxide reference sample and the iron oxide supported samples, independent of their pre-treatment: the selectivity fluctuations resembled metallic palladium. In contrast to that, the zinc oxide supported system showed constantly high selectivity, which is an indication for alloying. At lower conversions, the samples pre-reduced at higher temperatures were slightly more selective.

Determined values for the activation energy of the deactivated systems in case of CO-oxidation reaction were comparable for most of the co-precipitated systems (iron oxide, zinc oxide), but much higher in case of the impregnated sample (titanium oxide).

In the end we were able to demonstrate that the catalytic oxidation of carbon monoxide is a suitable probe reaction for investigation of SMSI-induced surface modifications. It is specific and structure-sensitive enough to detect even small changes in the micro-structure of the catalysts. Such changes in the active sites and in the chemical potential are expressed by the specific shape and slope of the conversion curves. There apparently is not only one general activity for CO-oxidation on Pd but it depends on many factors as it can be also seen

regarding the wide variation of the Arrhenius parameters. Due to the complex behavior of the systems, involving electronic and geometric phenomena, both, increasing and decreasing activity in the surface-covered state were observed in CO-oxidation. Furthermore it was shown that the SMSI phenomenon could be reasonably studied by CO-oxidation in our “real” powder catalysts. Apparently no fundamental difference (due to a pressure-gap) to the high-vacuum studies of model catalysis exists. The same reversible surface phenomena and the same catalytic influence as for model-systems have been found.<sup>23,45</sup> The only difference between the systems could depend on pressure-dependent processes like surface-reconstructions.<sup>9,48</sup>

### Acknowledgement:

Maïke Hashagen, Wiebke Frandsen, Norbert Pfänder, Frank Girgsdies and Achim Klein-Hoffmann are acknowledged for their work (BET, SEM, TEM, XRD and XRF measurements).

### 4.5. References

1. Langmuir, I. The mechanism of the catalytic action of platinum in the reactions  $2\text{CO} + \text{O}_2 = 2\text{CO}_2$  and  $2\text{H}_2 + \text{O}_2 = 2\text{H}_2\text{O}$ . *Trans. Faraday Soc.* **17**, 621–654 (1922).
2. Freund, H.-J., Meijer, G., Scheffler, M., Schlögl, R. & Wolf, M. Die CO-Oxidation als Modellreaktion für heterogene Prozesse. *Angew. Chem.* **123**, 10242–10275 (2011).
3. McClure, S. M. & Goodman, D. W. New insights into catalytic CO oxidation on Pt-group metals at elevated pressures. *Chem. Phys. Lett.* **469**, 1–13 (2009).
4. Somorjai, G. A. & Rioux, R. M. High technology catalysts towards 100% selectivity: Fabrication, characterization and reaction studies. *Catal. Today* **100**, 201–215 (2005).
5. Ertl, G. *Reactions at Solid Surfaces*. (John Wiley & Sons, 2010).
6. Berlowitz, P. J., Peden, C. H. F. & Goodman, D. W. Kinetics of carbon monoxide oxidation on single-crystal palladium, platinum, and iridium. *J. Phys. Chem.* **92**, 5213–5221 (1988).
7. Libuda, J. *et al.* The CO oxidation kinetics on supported Pd model catalysts: A molecular beam/in situ time-resolved infrared reflection absorption spectroscopy study. *J. Chem. Phys.* **114**, 4669–4684 (2001).
8. Engel, T. & Ertl, G. A molecular beam investigation of the catalytic oxidation of CO on Pd (111). *J. Chem. Phys.* **69**, 1267–1281 (1978).

9. Vogel, D. Local reaction kinetics of CO oxidation on heterogeneous platinum, palladium and palladium oxide surfaces. (TU Wien, 2012).
10. Over, H. *et al.* Atomic-Scale Structure and Catalytic Reactivity of the RuO<sub>2</sub>(110) Surface. *Science* **287**, 1474–1476 (2000).
11. Böttcher, A., Conrad, H. & Niehus, H. Reactivity of oxygen phases created by the high temperature oxidation of Ru(0001). *Surf. Sci.* **452**, 125–132 (2000).
12. Lee, H.-I. & White, J. M. Carbon monoxide oxidation over Ru (001). *J. Catal.* **63**, 261–264 (1980).
13. Böttcher, A., Conrad, H. & Niehus, H. Characterization of oxygen phases created during oxidation of Ru(0001). *J. Chem. Phys.* **112**, 4779–4787 (2000).
14. Hendriksen, B. L. M., Bobaru, S. C. & Frenken, J. W. M. Bistability and oscillations in CO oxidation studied with scanning tunnelling microscopy inside a reactor. *Catal. Today* **105**, 234–243 (2005).
15. Ackermann, M. D. & others. Operando SXRD: a new view on catalysis. (Leiden Institute of Physics, Faculty of Science, Leiden University, 2007). at <<https://openaccess.leidenuniv.nl/handle/1887/12493>>
16. Szanyi, J. & Goodman, D. W. CO oxidation on palladium. 1. A combined kinetic-infrared reflection absorption spectroscopic study of Pd (100). *J. Phys. Chem.* **98**, 2972–2977 (1994).
17. Cant, N. W., Hicks, P. C. & Lennon, B. S. Steady-state oxidation of carbon monoxide over supported noble metals with particular reference to platinum. *J. Catal.* **54**, 372–383 (1978).
18. Lundgren, E. *et al.* Kinetic Hindrance during the Initial Oxidation of Pd(100) at Ambient Pressures. *Phys. Rev. Lett.* **92**, 046101 (2004).
19. Fischer-Wolfarth, J.-H. *et al.* Particle-size dependent heats of adsorption of CO on supported Pd nanoparticles as measured with a single-crystal microcalorimeter. *Phys. Rev. B* **81**, 241416 (2010).
20. Reuter, K. & Scheffler, M. First-principles kinetic Monte Carlo simulations for heterogeneous catalysis: Application to the CO oxidation at RuO<sub>2</sub>(110). *Phys. Rev. B* **73**, 045433 (2006).
21. Matsushima, T. & Asada, H. Kinetic studies on the CO oxidation on Pd(111) with low energy electron diffraction (LEED) and angle-resolved thermal desorption. *J. Chem. Phys.* **85**, 1658–1668 (1986).

22. Hoffmann, J., Meusel, I., Hartmann, J., Libuda, J. & Freund, H.-J. Reaction Kinetics on Heterogeneous Model Catalysts: The CO Oxidation on Alumina-Supported Pd Particles. *J. Catal.* **204**, 378–392 (2001).
23. Lewandowski, M. Scanning Tunneling Microscopy Study of Iron Oxide based Model Catalysts. (Technische Universität Berlin, 2011). at <<http://opus4.kobv.de/opus4-tuberlin/frontdoor/index/index/docId/3060>>
24. Ertl, G. & Freund, H.-J. Catalysis and Surface Science. *Phys. Today* **52**, 32–38 (1999).
25. Naumann d'Alnoncourt, R. *et al.* Strong metal–support interactions between palladium and iron oxide and their effect on CO oxidation. *J. Catal.* **317**, 220–228 (2014).
26. Rogal, J., Reuter, K. & Scheffler, M. CO oxidation on Pd(100) at technologically relevant pressure conditions: First-principles kinetic Monte Carlo study. *Phys. Rev. B* **77**, 155410 (2008).
27. Bluhm, H. *et al.* In Situ X-Ray Photoelectron Spectroscopy Studies of Gas-Solid Interfaces at Near-Ambient Conditions. *MRS Bull.* **32**, 1022–1030 (2007).
28. Tauster, S. J., Fung, S. C. & Garten, R. L. Strong metal-support interactions. Group 8 noble metals supported on titanium dioxide. *J. Am. Chem. Soc.* **100**, 170–175 (1978).
29. Vannice, M. A., Wang, S. Y. & Moon, S. H. The effect of SMSI (strong metal-support interaction) behavior on CO adsorption and hydrogenation on Pd catalysts: I. IR spectra of adsorbed CO prior to and during reaction conditions. *J. Catal.* **71**, 152–166 (1981).
30. Sá, J., Bernardi, J. & Anderson, J. A. Imaging of low temperature induced SMSI on Pd/TiO<sub>2</sub> catalysts. *Catal. Lett.* **114**, 91–95 (2007).
31. Dandekar, A. & Vannice, M. A. Crotonaldehyde Hydrogenation on Pt/TiO<sub>2</sub> and Ni/TiO<sub>2</sub> SMSI Catalysts. *J. Catal.* **183**, 344–354 (1999).
32. Uchijima, T. SMSI effect in some reducible oxides including niobia. *Catal. Today* **28**, 105–117 (1996).
33. Colmenares, J. C. *et al.* Influence of the strong metal support interaction effect (SMSI) of Pt/TiO<sub>2</sub> and Pd/TiO<sub>2</sub> systems in the photocatalytic biohydrogen production from glucose solution. *Catal. Commun.* **16**, 1–6 (2011).
34. Galloway, H. C., Benítez, J. J. & Salmeron, M. The structure of monolayer films of FeO on Pt(111). *Surf. Sci.* **298**, 127–133 (1993).

35. Bennett, R. A., Stone, P. & Bowker, M. Pd nanoparticle enhanced re-oxidation of non-stoichiometric TiO<sub>2</sub>: STM imaging of spillover and a new form of SMSI. *Catal. Lett.* **59**, 99–105 (1999).
36. Schalow, T. *et al.* Oxygen-induced Restructuring of a Pd/Fe<sub>3</sub>O<sub>4</sub> Model Catalyst. *Catal. Lett.* **107**, 189–196 (2006).
37. Shen, W.-J., Okumura, M., Matsumura, Y. & Haruta, M. The influence of the support on the activity and selectivity of Pd in CO hydrogenation. *Appl. Catal. Gen.* **213**, 225–232 (2001).
38. Kast, P. *et al.* CO oxidation as a test reaction for strong metal-support interaction (SMSI) in nanostructured Pd/FeO<sub>x</sub> powder catalysts. *Appl. Catal. A*, submitted (2015).
39. Kast, P. *et al.* Strong Metal-Support Interaction and alloying in Pd/ZnO catalysts for CO-oxidation. *Catal. Today*, submitted (2015).
40. Herrmann, T. Selektivhydrierung von Acetylen unter industriellen tail-end Bedingungen. (TU Darmstadt, 2014). at <<http://tuprints.ulb.tu-darmstadt.de/3951/>>
41. Pachulski, A. *Evaluierung der Eigenschaften von industriellen Selektivhydrierkatalysatoren [Elektronische Ressource] / vorgelegt von Axel Pachulski.* (2009). at <<http://nbn-resolving.de/urn:nbn:de:tuda-tuprints-14101>>
42. Kuhn, M., Lucas, M. & Claus, P. Advanced Temkin Reactor: Testing of Industrial Eggshell Catalysts on the Laboratory Scale. *Chem. Eng. Technol.* **38**, 61–67 (2015).
43. Logan, A. D., Braunschweig, E. J., Datye, A. K. & Smith, D. J. Direct observation of the surfaces of small metal crystallites: rhodium supported on titania. *Langmuir* **4**, 827–830 (1988).
44. Li, Y. *et al.* The effect of titania polymorph on the strong metal-support interaction of Pd/TiO<sub>2</sub> catalysts and their application in the liquid phase selective hydrogenation of long chain alkadienes. *J. Mol. Catal. Chem.* **216**, 107–114 (2004).
45. Schalow, T. Bildung und katalytische Aktivität partiell oxidiertes Pd-Nanopartikel. (Technische Universität Berlin, 2006). at <<http://opus.kobv.de/ubp/volltexte/2007/1474/>>
46. Ota, A. *et al.* Intermetallic Compound Pd<sub>2</sub>Ga as a Selective Catalyst for the Semi-Hydrogenation of Acetylene: From Model to High Performance Systems†. *J. Phys. Chem. C* **115**, 1368–1374 (2011).
47. Kang, J. H., Shin, E. W., Kim, W. J., Park, J. D. & Moon, S. H. Selective Hydrogenation of Acetylene on TiO<sub>2</sub>-Added Pd Catalysts. *J. Catal.* **208**, 310–320 (2002).

48. Teschner, D. *et al.* The Roles of Subsurface Carbon and Hydrogen in Palladium-Catalyzed Alkyne Hydrogenation. *Science* **320**, 86–89 (2008).
49. Teschner, D. *et al.* Understanding Palladium Hydrogenation Catalysts: When the Nature of the Reactive Molecule Controls the Nature of the Catalyst Active Phase. *Angew. Chem. Int. Ed.* **47**, 9274–9278 (2008).
50. Teschner, D. *et al.* Alkyne hydrogenation over Pd catalysts: A new paradigm. *J. Catal.* **242**, 26–37 (2006).
51. Shao, L. *et al.* Improved Selectivity by Stabilizing and Exposing Active Phases on Supported Pd Nanoparticles in Acetylene-Selective Hydrogenation. *Chem. – Eur. J.* **18**, 14962–14966 (2012).
52. Asplund, S. Coke Formation and Its Effect on Internal Mass Transfer and Selectivity in Pd-Catalysed Acetylene Hydrogenation. *J. Catal.* **158**, 267–278 (1996).
53. Wowsnick, G. *et al.* Surface dynamics of the intermetallic catalyst Pd<sub>2</sub>Ga, Part II – Reactivity and stability in liquid-phase hydrogenation of phenylacetylene. *J. Catal.* **309**, 221–230 (2014).
54. Kim, W. Effect of potassium addition on the properties of a TiO<sub>2</sub>-modified Pd catalyst for the selective hydrogenation of acetylene. *Appl. Catal. Gen.* **268**, 77–82 (2004).
55. Weerachawanajak, P. *et al.* Effect of strong metal–support interaction on the catalytic performance of Pd/TiO<sub>2</sub> in the liquid-phase semihydrogenation of phenylacetylene. *J. Catal.* **262**, 199–205 (2009).
56. Li, Y. *et al.* Strong metal-support interaction and catalytic properties of anatase and rutile supported palladium catalyst Pd/TiO<sub>2</sub>. *Chem. Phys. Lett.* **372**, 160–165 (2003).



## Supplementary Information

1. “Labmax” co-precipitation synthesis protocol for Pd/Al<sub>2</sub>O<sub>3</sub> sample:

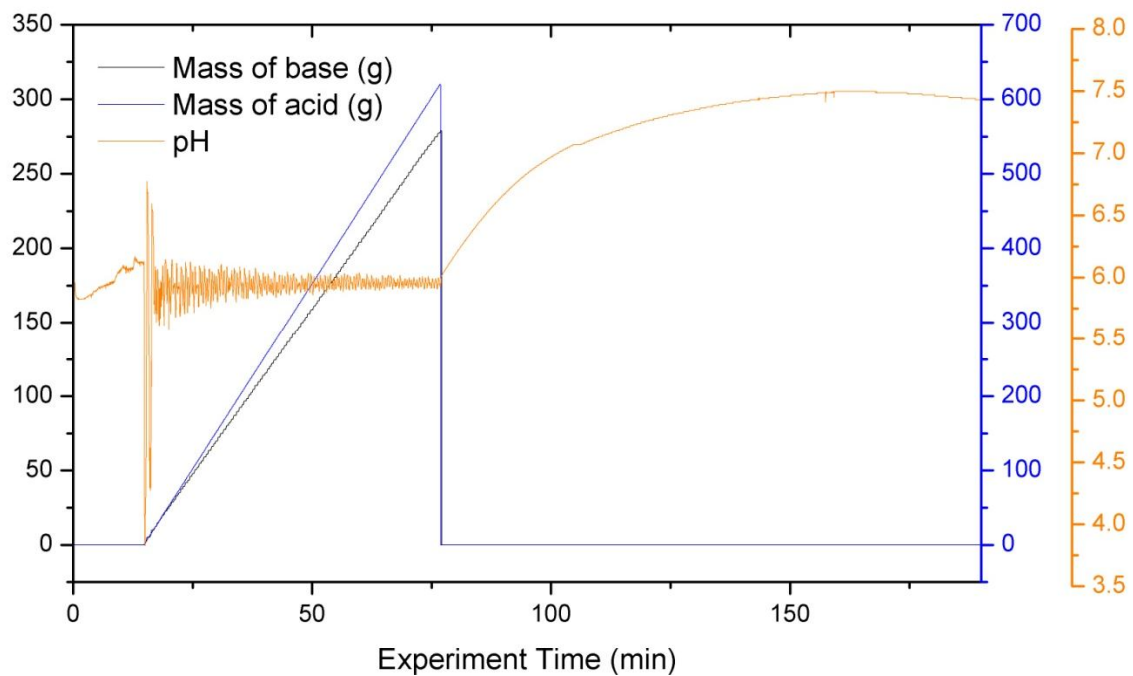


Fig. S4.1: Synthesis protocol of the Pd/Al<sub>2</sub>O<sub>3</sub> reference sample: co-precipitation of metal nitrates with sodium carbonate solution and 2h ageing afterwards.

## 2. XRD of Pd/TiO<sub>2</sub> sample before and after 373 K reduction:

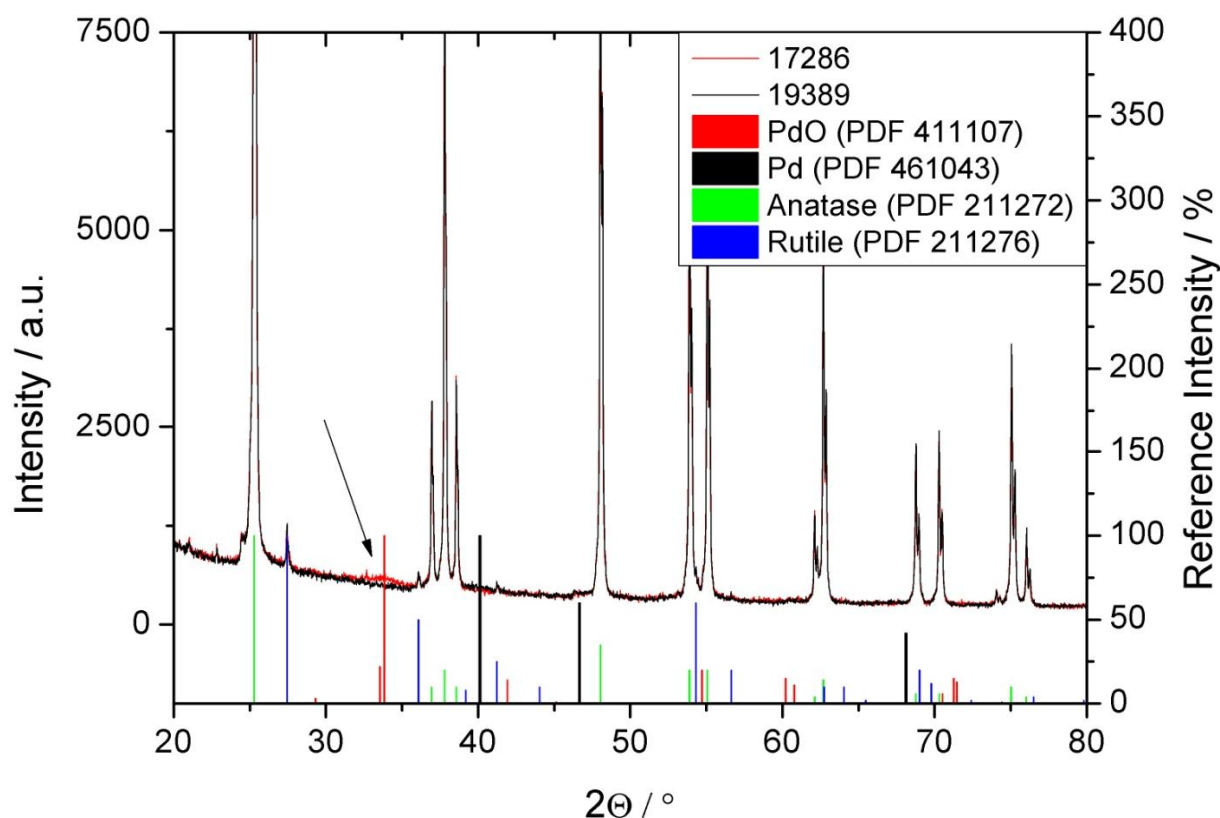


Fig. S4.2: XRD of the 1% Pd/TiO<sub>2</sub> sample before (17286, red curve) and after reduction at 373 K in 5% H<sub>2</sub>-Ar (19389, black curve). Reference bars for PdO (red), Pd (black), anatase (green) and rutile (blue) included from the PDF database.

As it can be seen, the support consists of P25 that represents a mixture of anatase (major content) and rutile TiO<sub>2</sub> polymorph (minor content). The broad (111)-reflection for palladium oxide is visible shortly before 35 °, as indicated by the arrow. It diminishes after reduction at 373 K (5% H<sub>2</sub>-He, 19389) to form metallic palladium, together with a slight increase of intensity at 40 ° (Pd-111 reflection). Sample 17286 has been further reduced at 773 K (5% H<sub>2</sub>-He) in the XRD set-up afterwards. When measured for a second time at room temperature, the diffractogram showed no significant changes compared to the one after 373 K reduction. No signs for alloy species formed upon reduction could be detected, but the loading is not sufficient to exclude such a possibility completely.

The XRD measurements were performed in Bragg-Brentano geometry on a Bruker AXS D8 Advance theta/theta diffractometer equipped with a secondary graphite monochromator (Cu K<sub>α1+2</sub> radiation) and scintillation detector. The sample powder was filled into the recess of a cup-shaped sample holder, the surface of the powder bed being flush with the sample holder edge. The XRD data were analyzed by full pattern fitting according to the Rietveld method in conjunction with the fundamental parameter approach for the instrumental and double-Voigt approach for the sample contribution to the peak profiles as implemented in the TOPAS

software (Bruker, version 4.2). The XRD setup was equipped with an in situ reactor cell. Reaction gases were mixed by means of mass flow controllers (Bronkhorst).

3. TPR of Pd/Al<sub>2</sub>O<sub>3</sub> sample in He (drying until 523 K, switch to 5 % H<sub>2</sub>-He for 30 min):

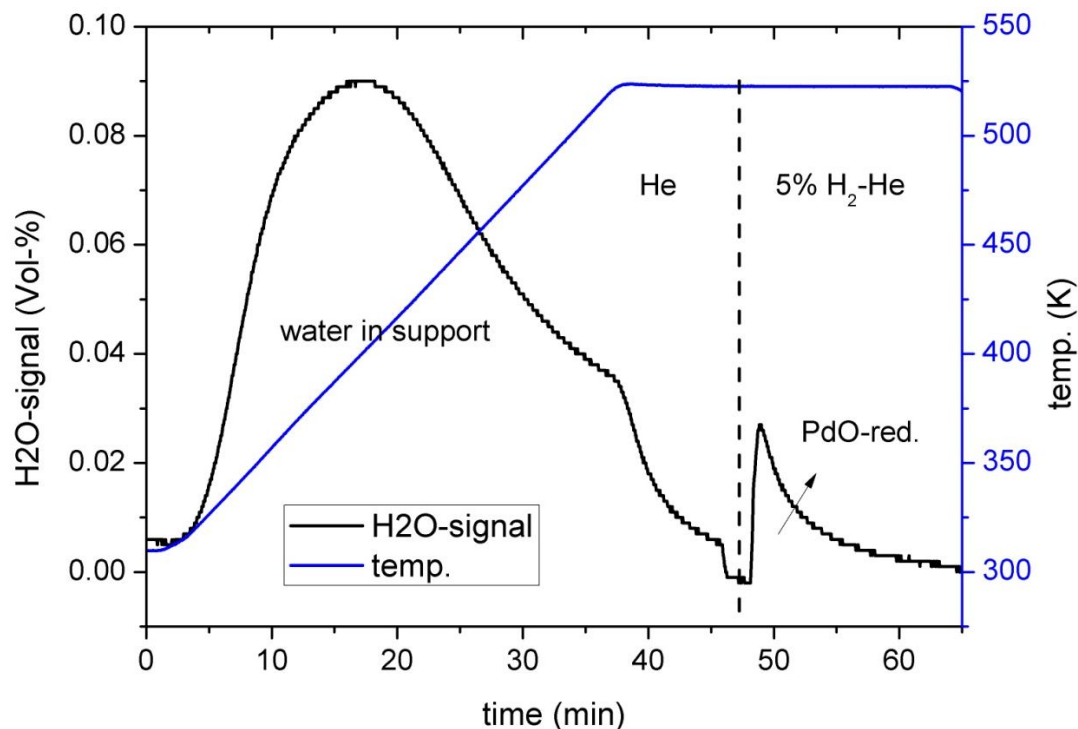


Fig. S4.3: TPR of 1.8% Pd/Al<sub>2</sub>O<sub>3</sub> sample in He (5 Kpm, until 523 K). Switch to 5% H<sub>2</sub>-He at 523 K to distinguish between drying effect of the support and PdO reduction.

4. Repeated CO-oxidation cycles after 323 K reduction of the 3.9% Pd/ZnO sample:

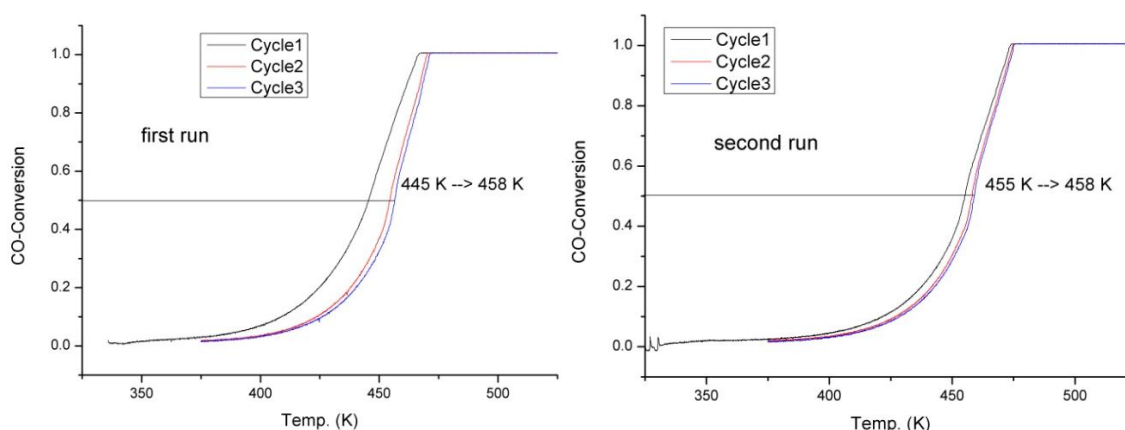


Fig. S4.4: CO-oxidation runs of 3.9% Pd/ZnO sample after repeated reduction at 323 K: the effect of possible re-oxidation of the palladium during the CO-oxidation is minor. The higher activity in the first cycle of the first run should be due to irreversible effects.

5. SEM micrograph of 1% Pd/TiO<sub>2</sub> sample directly after calcination:

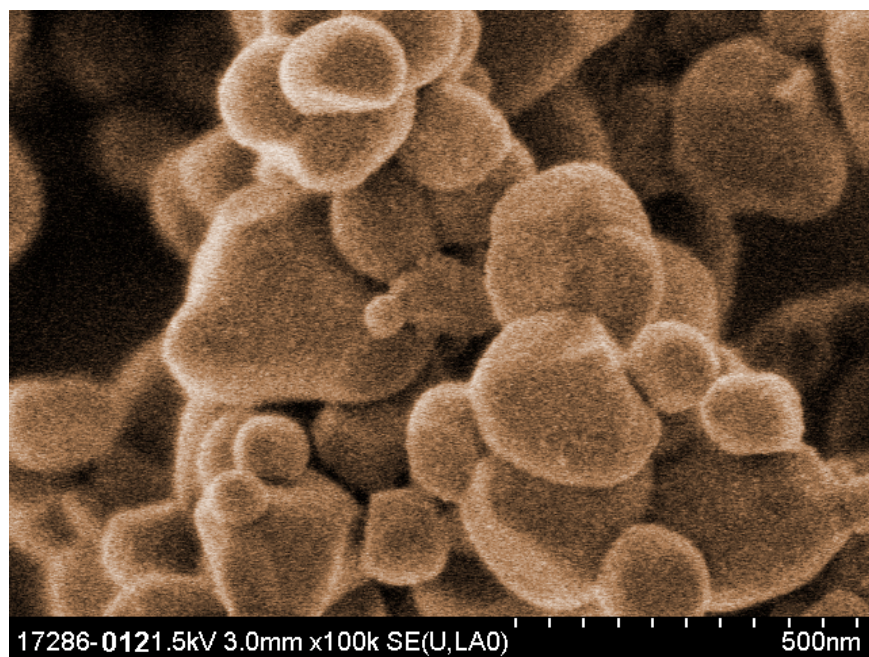


Fig. S4.5: SEM image of 1% Pd/TiO<sub>2</sub> sample (colored orange).

6. HR-TEM image series

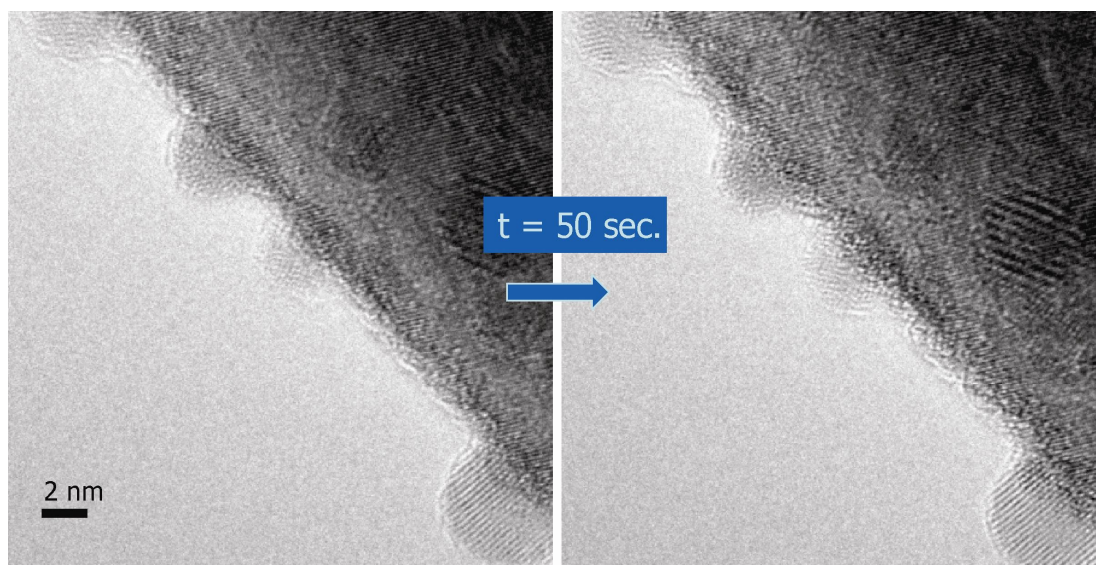


Fig. S4.6: HR-TEM image series of 1% Pd/TiO<sub>2</sub> sample after 673 K reduction – after 50 s in the electron beam, no carbon deposition can be detected.

7. S-T-plot of the Pd/iron oxide system in acetylene hydrogenation:

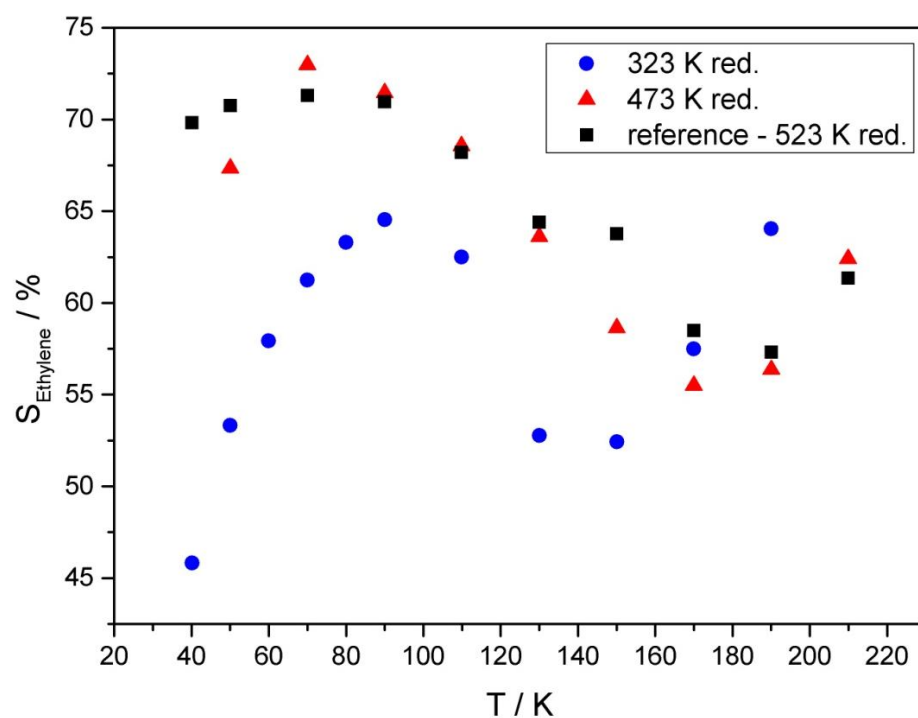


Fig. S4.7: S-T-plot of the Pd/iron oxide sample during selective acetylene hydrogenation after pre-reduction at 323 K (blue circles) and 473 K (red triangles). Reference system (Pd/alumina) after 523 K reduction presented for comparison (black squares).

## Chapter 5: Summary and Conclusion of the thesis

The present study tried to investigate the nature of strong metal-support interaction by comparing the structural and electronic changes of a series of variously loaded, co-precipitated and impregnated palladium powder catalysts during reduction at different temperatures and in different reducing atmospheres. Moreover, the influence of the structural changes in the bulk and on the surface on the catalytic activity of the samples was studied at ambient pressure by CO oxidation as a well-established, comparably simple catalytic test reaction. This so-called structure-function relationship has been further studied by means of selectivity changes in the selective hydrogenation of acetylene.

In chapter 2, a series of iron oxide supported palladium catalysts with homogeneous particle size distribution has been investigated. By DRIFTS, TEM, CO-chemisorption and XPS measurements we were able to clearly verify surface decoration by an oxidic over-layer that was forming upon reduction at 473 K, independent of the reducing agent, diluted hydrogen or diluted carbon monoxide. The catalysts in this decorated, so-called SMSI-state showed higher activity for CO oxidation that proved to be a suitable test-reaction. Furthermore the SMSI state was proven to be unstable, with smaller palladium particles increasing the instability compared to larger ones. The formation of the SMSI induced over-layer was found to be reversible and independent of phase transformations in the bulk or possible alloy formation or even formation of  $\alpha$ -iron, induced by reduction at higher temperatures. After several CO oxidation reaction cycles (light-off curves), the deactivated state of the catalyst, after decomposition of the SMSI over-layer, was found to be relatively stable, with little further deactivation by formation of carbon species. The palladium in that state was shown to be partially re-oxidized. Activation energies in that state were comparably low with about 55 kJ/mol.

The co-precipitated palladium/zinc oxide catalysts presented in chapter 3 were also studied with regard to their structure-function relationship. In detail, the electronic and structural surface properties after reduction in H<sub>2</sub> or CO containing media had a remarkably influence on CO oxidation activity whereas the latter atmosphere was found to be more suitable for setting and distinguishing certain reduction states. Earlier beginning of (surface and bulk) alloy formation as compared to the iron oxide support was detected by XRD but also by surface sensitive methods like XPS, CO-chemisorption and infrared measurements. The

beneficial effect of PdZn alloy formation at the surface on CO oxidation was proven as well as the reversibility of that process. Further reduction of the lowest loaded sample at higher temperatures was able to generate additional surface decoration by a ZnO<sub>x</sub> over-layer, as it could be identified by HR-TEM images in combination to further decrease of the CO uptake determined by CO-chemisorption and DRIFTS measurements. This additional surface modification by SMSI was proven to lead to a deactivation of CO oxidation activity, though the catalyst during the first reaction cycle, directly after the reduction was still more active than during the succeeding ones. In contrast to the iron oxide samples, clearly both, electronic (alloying) and structural (over-layer formation) surface modifications played a role in a quite narrow reducing temperature regime and were hard to distinguish. The size of the palladium particles as well as the reducing atmosphere was found to influence the surface modifications as well, with activation energies determined after CO oxidation cycling in the range of 55-82 kJ/mol.

In chapter 4, the influence of surface decoration of different supported, similar loaded Pd catalysts on the catalytic properties in CO oxidation as well as on selective hydrogenation of acetylene was compared. In addition to the iron - and zinc oxide supported systems, an impregnated Pd/titania catalyst and a co-precipitated Pd/alumina catalyst have been investigated. While no characteristic surface modifications or influence of reduction on the CO oxidation activity that could be ascribed to such SMSI-induced effects could be detected in case of the Pd/alumina system, the Pd/titania system showed surface decoration by SMSI after 673 K reduction, as proven by HR-TEM images, in combination with CO-chemisorption and TPR investigations. That state was found to be reversibly destroyed and re-formed, similar to the other easily reducible systems. But this time, the effect on the activity in catalytic oxidation of carbon monoxide was negative, with the higher activity being restored after decomposition of the SMSI induced over-layer. Alloying effects in that case could not be detected. While the activation energy determined again after three CO oxidation cycles was comparably high in case of the titania support, with about 121 kJ/mol, the activation energy of the Pd/alumina sample was found to be in a similar range to the other systems, with about 66 kJ/mol, not far away from the determined value of 74 kJ/mol for pure, unsupported palladium that was tested after reduction of commercial PdO. The alumina sample was additionally applied as reference sample for comparison of the modified acetylene hydrogenation selectivity in dependence on the reducing temperature, compared to the iron oxide and the zinc oxide sample. As expected, the acetylene conversion as well as the

ethylene selectivity in case of the alumina sample decreased at higher conversions due to hydrogen consuming competitive and consecutive reactions in case of the metallic palladium particles present. At higher conversion, coking improved selectivity again. The behavior of the iron oxide samples was similar: the geometric SMSI only slightly affected the dynamic nature of Pd at higher conversion. In contrast to that, the zinc oxide samples showed a different behavior, irrespective of the pre-treatment and existing alloying or SMSI. However, the samples reduced at higher temperatures showed slightly higher selectivity for acetylene formation. At lower conversions, especially the iron oxide sample pre-reduced at higher temperatures was more selective, whereas the selectivity in case of the one pre-reduced at lower temperatures increased with increasing reaction temperature, probably due to in-situ SMSI formation in the hydrogen containing feed. Surface decoration is known to prevent follow-up reactions as they happen on pure palladium.

In conclusion, the present work could help to get better insight in the phenomenon of strong metal-support interaction (SMSI) and to decouple its structural and electronic surface influences from phase transformations or bulk alloying processes, potentially happening simultaneously or under slightly different conditions, depending on the investigated system. In case of the reduced Pd/iron oxide system, the activity for catalytic CO oxidation was clearly enhanced in the surface-decorated state, while no alloying in the investigated temperature regime could be observed. In case of the Pd/zinc oxide system, reversible surface alloying processes beneficial for the CO oxidation activity were detected already at comparably low reduction temperatures, while additional surface decoration by reduced  $\text{ZnO}_x$  species occurred at higher reduction temperatures, leading to an over-all loss of catalytic activity. The process of reversible surface decoration in case of the impregnated Pd/titania sample (SMSI-induced) occurred at slightly higher temperatures compared to the pre-mentioned systems. While SMSI was proven to decrease the catalytic activity for CO oxidation without detectably alloy formation in that case, the merely reducible Pd/alumina system showed no signs for surface decoration or alloying in the investigated temperature regime at all and could be used as an “inert” reference system for the catalytic activity of supported palladium. The selectivity behavior for acetylene hydrogenation at higher conversions in case of the iron oxide sample resembled that of metallic palladium, irrespective of SMSI. In contrast, the zinc oxide system showed a different, alloy-like behavior.



In addition, it could be demonstrated that the catalytic oxidation of carbon monoxide is a suitable test reaction for investigation of SMSI-induced surface modifications in general. Though the instability of the SMSI state will prohibit its application in sustained CO oxidation, the reaction helped to conveniently study the effects of SMSI on reactivity and stability and decouple SMSI from the other mentioned processes like alloying, sintering or re-oxidation of Pd or formation of carbon species.

Due to the complex behavior of the systems, involving electronic and geometric phenomena, both, increasing and decreasing activity in the surface-covered state could be observed in CO oxidation. Furthermore it could be shown that the SMSI phenomenon could be reasonably studied by CO oxidation in “realistic” powder catalysts and under ambient pressure. Apparently no fundamental difference (due to a pressure-gap) to the high-vacuum studies of model catalysis exists. The same reversible surface phenomena and the same catalytic influence as for model-systems have been found. The only difference between the systems could depend on size- or pressure-dependent processes like surface-reconstructions for example.

The CO oxidation reaction is, according to the present study not structure-insensitive in general, as described for example by Ertl et al for single crystal surfaces. In the contrary it is very specific and capable to detect even small changes in the micro structure of the investigated system. These changes in the active sites and in the chemical potential are expressed by a specific shape and slope of the CO conversion ramps. However since they depend on many factors it is not possible to generalize certain observed behaviors. The changes are no measurement artefacts as they appear reproducibly as long as being studied in sufficiently high precision.

There is not “the one” activity of palladium in CO oxidation as also indicated by the large variation in the Arrhenius parameters determined both in this study and described previously by other authors.

## Appendix:

### List of abbreviations

BET	Brunauer, Emmet, Teller adsorption isotherm model
BJH	Barrett-Joyner-Halenda (pore size distribution analysis)
CVD	Chemical Vapor Deposition
DRIFTS	Diffuse Reflectance Infrared Fourier Transform Spectroscopy
EDX	Energy Dispersive X-ray spectroscopy
ER	Eley-Rideal reaction mechanism
fcc	face-centered cubic
FID	Flame Ionization Detector
FWHM	Full Width at Half Maximum
GC	Gas Chromatography
HAADF	High-Angle Annular Dark-Field
(HR-) TEM	(High-Resolution) Transmission Electron Microscopy
HTR	High-Temperature Reduction
IC	Combined Isotherm
ICSD	Inorganic Crystal Structure Database
ICP-OES	Inductively-Coupled Plasma Optical Emission Spectroscopy
IMC	Inter-Metallic Compound
IR	Infrared
IS	Strong Isotherm
IW	Weak Isotherm
LEIS	Low-Energy Ion Scattering
LH	Langmuir-Hinshelwood reaction mechanism
LTR	Low-Temperature Reduction
MCT	Mercury-Cadmium-Telluride (detector)
MFC	Mass-Flow Controller

MSR	Methanol Steam Reforming
MvK	Mars-van-Krevelen reaction mechanism
NEXAFS	Near Edge X-ray Absorption Fine Structure
PROX	Preferential Oxidation
QMS	Quadrupole Mass Spectrometer
RT (-R)	Room Temperature (-Reduction)
SEM	Secondary Electron Microscopy
SMSI	Strong Metal-Support Interaction
STEM	Scanning Transmission Electron Microscopy
STM	Scanning Tunneling Microscopy
TG-DSC	Thermo-Gravimetry coupled with Differential Scanning Calorimetry
TPO	Thermo-Programmed Oxidation
TPR	Thermo-Programmed Reduction
UHV	Ultra-High Vacuum
XAS	X-ray Absorption Spectroscopy
(NAP-) XPS	(Near Ambient Pressure-) X-ray Photoelectron Spectroscopy
(S-) XRD	(Surface-) X-Ray Diffraction
XRF	X-Ray Fluorescence

## List of publications:

- 1.) P. Kast, G. Kucerova, R.J. Behm  
*„On the nature of the active Au species: CO-oxidation on cyanide leached Au/TiO<sub>2</sub> catalysts”*  
Catalysis today, corrected proof, available online since 28.7.2014
- 2.) P. Kast, M. Friedrich, D. Teschner, F. Girgsdies, T. Lunkenbein, R. Naumann  
d’Alnoncourt, M. Behrens, R. Schlögl  
*“CO-oxidation as a test reaction for Strong Metal-Support Interaction in nanostructured Pd/FeO<sub>x</sub> powder catalysts”*  
Submitted to Applied Catalysis A, 31.1.2015
- 3.) P. Kast, M. Friedrich, F. Girgsdies, J. Krönert, D. Teschner, T. Lunkenbein, M. Behrens, R. Schlögl  
*“Strong Metal-Support Interaction and alloying in Pd/ZnO catalysts for CO-oxidation”*  
Submitted to Catalysis Today, 7.2.2015
- 4.) P. Kast, M. Kuhn, M. Friedrich, R. Farra, M. Behrens, P. Claus, R. Schlögl  
*„Supported Palladium catalysts in CO-oxidation and Acetylene Hydrogenation: on the role of SMSI“*  
To be submitted to Catalysis Letters.
- 5.) R. Arrigo, M. Schuster, Z. Xie, Y. Yi, G. Wowsnick, L. Sun, K. Hermann, M. Friedrich, P. Kast, M. Hävecker, A. Knop-Gericke, R. Schlögl.  
*"The nature of the N-Pd interaction in nitrogen-doped carbon nano-tube catalysts"*  
Submitted to ACS catalysis, 19.1.2015

## List of poster presentations:

- 1.) Patrick Kast, Raoul Naumann d'Alnoncourt, Malte Behrens, Robert Schlögl  
„Strong Metal-Support Interaction (SMSI) of Pd/FeO<sub>x</sub>”  
45. Jahrestreffen Deutscher Katalytiker, Weimar, März 2012
- 2.) Patrick Kast, Malte Behrens, Robert Schlögl  
„Synthesis of Pd on Fe<sub>2</sub>O<sub>3</sub>, Al<sub>2</sub>O<sub>3</sub>, ZrO<sub>2</sub> and CNTs for SMSI-studies“  
46. Jahrestreffen Deutscher Katalytiker, Weimar, März 2013
- 3.) Kast P., Friedrich M., Teschner D., Behrens M., Schlögl R.  
„Strong Metal Support Interactions (SMSI) studied by XPS on Pd/FeO<sub>x</sub> and Pd/ZnO”  
5. Joint BER II and Bessy II User Meeting, HZB, Dezember 2013
- 4.) Patrick Kast, Matthias Friedrich, Malte Behrens, Robert Schlögl  
„Strong Metal-Support Interaction studied on Pd/ZnO and Pd/FeO<sub>x</sub>”  
47. Jahrestreffen Deutscher Katalytiker, Weimar, März 2014

# Lebenslauf

## zu meiner Person

Patrick Kast

geboren am 12.11.1984 in Füssen

ledig, keine Kinder

## schulische Ausbildung

1991 – 1995

Grundschule Seeg

1995 – 2004

Gymnasium Füssen

Mathematisch-Naturwissenschaftlicher Zweig  
mit Abschluss der Allgemeinen Hochschulreife

## Hochschulausbildung

10/2005-10/2010

Chemiestudium an der Universität Ulm

02/2010-10/2010

Diplomarbeit am Institut für Oberflächenchemie  
und Katalyse, Prof. Dr. R.J. Behm, Universität  
Ulm. Titel: „CO-oxidation on Au<sup>0</sup>-free Au/TiO<sub>2</sub>  
catalysts“

02/2011-02/2015

Promotion in Chemie (TU-Berlin), angestellt  
beim Fritz-Haber-Institut der Max-Planck-  
Gesellschaft in Berlin (Prof. Dr. R. Schlögl,  
Abteilung Anorganische Chemie). Titel der  
Dissertation: „Structure-function relationship of  
Strong Metal-Support Interaction studied on  
supported Pd reference catalysts“

## Eidesstattliche Versicherung und Erklärung zur Promotionsordnung

Hiermit versichere ich eidesstattlich, dass ich die vorliegende Dissertation selbstständig angefertigt und nur die im Literaturverzeichnis aufgeführten Quellen verwendet habe.

Die geltende Promotionsordnung der Fakultät für Mathematik und Naturwissenschaften der Technischen Universität Berlin erkenne ich an.

Patrick Kast

Berlin,